Republic of Iraq

Ministry of Higher Education and Scientific

Research University of Babylon College of Engineering

Mechanical Engineering Department

Experimental Study of Flame Characteristics for Different Liquefied Petroleum Gas / Ammonia Blends

A Thesis Submitted to the

College of the Engineering / University of Babylon in Partial Fulfillment of the Requirements for the Degree of Master of Science in Engineering /Mechanical Engineering /power

By

Ruwaida kassid Eesa Al sultani B.Sc. (Mech.Eng. 2008)

Supervised By

Assist Prof. Dr. Samer Mohammed Abdulhaleem

2022 A.D. *1443A.*

وَوَصَّيْنَا الإِنسَانَ بِوَالِدَيْهِ إِحْسَانًا حَمَلَتْهُ أُمُّهُ كُرْهًا وَوَضَعَتْهُ كُرْهًا وَحَمْلُهُ وَفِصَالُهُ ثَلاثُونَ شَهْرًا حَتَّى إِذَا بَلَغَ أَشُدَّهُ وَبَلَغَ أَرْبَعِينَ سَنَةً قَالَ رَبِّ أَوْزِعْنِي أَنْ أَشْكُرَ نِعْمَتَكَ الَّتِي أَنْعَمْتَ عَلَيَّ وَعَلَى وَالِدَيَّ وَأَنْ أَعْمَلَ صَالِحًا تَرْضَاهُ وَأَصْلِحْ لِي فِي ذُرِّيَّتِي إِنِّي تُبْتُ إِلَيْكَ وَإِنِّي مِنَ الْمُسْلِمِين

صدق الله العظيم

سورة الاحقاف اية ﴿15﴾

Certification

I certify that the thesis entitled **Experimental Study of Flame Characteristics for Different Liquefied Petroleum Gas/Ammonia Blends**

was prepared by **"Ruwaida kassid Eesa"** under my supervision at the University of Babylon in partial fulfillment of the requirements for the degree of Master of Science in Mechanical Engineering (Power Engineering).

I recommend that this thesis be forwarded for examination in accordance with the regulation of the University of Babylon.

Signature

Assist Prof.Dr. Samer Mohammed Abdulhaleem

Department of Mechanical Engineering College of Engineering/University of Babylon

Dedication

I dedicated this work to My great family who offered me immense support encouragement and throughout my work:

My dear husband Gaffer

My children Rami Naya Elia

My father and My mother

My brothers

Ruwaida 2022

Acknowledgments

This thesis would not have been possible without expressing my gratitude and thanks to ALLAH (be glorious) for all the blessings upon me.

I would like to express my heartfelt thanks and gratitude to my supervisor, ***Assist prof. Dr. Samer Mohammed Abdulhaleem*** *for his guidance, invaluable instruction, help, and unwavering encouragement throughout the preparation of my study. I'd like to express my gratitude to the head of the mechanical engineering department* ***Assist prof. Dr. Samer Mohammed Abdulhaleem*** *for constructive contribution to this work. My thanks are also extended to the the staff of mechanical engineering Department, at Babylon College of Engineering.*

Ruwaida 2022

ABSTRACT

This study investigates experimentally the laminar flame speed and burning velocity of premixed flames for different Gases.

A centrally ignited constant volume chamber has been designed and constructed to investigate experimentally the stretched flame speed (S_n), laminar burning velocity (S_u), Markstein length (L_b), The combustion process is recorded by a high-speed camera using schlieren technique. The experiments have been conducted using constant volume chamber.

Ammonia and liquefied petroleum gas are mixed in a combustion chamber with a constant volume of cylindrical shape and volume (0.04899 m^3), inner diameter 395 mm, and length 400 mm, containing the combustion chamber on the flange with a thickness of 12 mm diameter 407 mm and 570 mm both side made by Stainless steel to resist external conditions (Ammonia gas - liquefied petroleum gas - air) in specific proportions (10% - 20% - 30%) and using a central ignition spark , and imaging system using a high-speed camera and initial pressures (100 - 200 - 300) kPa and equivalence ratios (0.8 - 1 - 1.3) and a temperature of 298 K.

The experimental study uses a combustion chamber of constant size and central ignition showed that the increase the initial pressure, the decrease the laminar flame speed, the Markstein length, and the laminar burning velocity. It also showed at an equivalence ratio of 0.8, an initial pressure of 100 kPa, a concentration of ammonia %10, and a flame radius of 20 mm reaches the laminar flame speed 1.3 m/s When the same initial pressure is 100 kPa and ammonia concentration 30%. The laminar flame speed reaches 1.52 m/s.

The results showed that gradual increase of ammonia gas to the mixture at an equivalence ratio of 0.8, which increases the laminar flame speed. The concentration of ammonia gas is 30% and the flame radius is 25 mm. The value of the laminar flame speed is 1.19 m/s.

At the same conditions, at a concentration of 30% and an initial pressure of 200 kPa, the laminar flame speed is 1.10 m/s. The results showed an increase in the initial pressure and reduction in the value of the flame speed, The Experimental results showed the effect of the increase Gradual ammonia gas on the Markstein length values at an initial pressure of 100 kPa, at equivalence ratio of 0.8, ammonia gas concentration 10%, and the Markstein length value reaches 6.3 .

It The same conditions, an initial pressure of 100 kPa and a concentration of ammonia 30% reaches a value of 5.6, The results showed that the increase in the initial pressure decreases the value of Markstein length at an initial pressure of 100 kPa and a equivalence ratio of 0.8 and ammonia concentration of 30% that reaches a value of 5.6 At the same conditions the initial pressure of 200 kPa reaches 4.6. The effect of the initial pressure on the laminar burning velocity, which is decreased with the increase in the initial pressure. At a pressure of 100 kPa, an equivalence ratio of 0.8, and a concentration of ammonia 30%, it became a value of 24.5 cm/s.

During the same conditions and with initial pressure of 200 kPa, the value of the laminar burning velocity reaches 19.6 cm/s The results showed that the gradual increase of ammonia gas reduces the combustion speed, at an initial pressure of 100 kPa , equivalence ratio of 1 and ammonia gas concentration 10%, the combustion velocity becomes 39.3cm/sec, and at the same conditions and an initial pressure of 100 kPa the ammonia concentration 30%, the burning velocity reaches 34.9 cm/sec.

List of Contents

Contents

Nomenclature

Symbol	Definition	Unite
A	Flame Surface Area	m^2
d	Diameter	mm
e	Number of Mole of Component,	mol
J	Ammonia Volume Fraction	
L_b	Markstine Length	
Le	Lewis Number	
M	Mol Mass	kg/mol
P	Pressure	kPa
R	Specific Gas Constant	J/kg.K
r	Radius	mm
$R_\circ$	Universal Molar Gas Constant	J/ mol.K
S_g	Gas Velocity Ahead of the Flame Front	m/s
S_b	Stretched Laminar of the Flame Speed	m/s
T	Temperature	K
t	Time	s
S_u	Laminar Burning Velocity	m/s
V	Volume	liter
x	Mol fraction	

Greek Symbols

Symbol	Definition	
Ø	Equivalence Ratio	
α_T	Temperature Stretch Rate	
β_P	Pressure Dependent Parameter	
ε	Flame Stretch Rate	1/s
ρ	Density	kg/m^3

Abbreviation

Symbol	Definition
CPM	Constant Pressure Method
CVC	Constant Volume Method
DIB	Diisobutylene
dil	Diluent
ext	Extensional
LBV	Laminar Burning Velocity
LPG	Liquefied Petroleum Gas
Mix	Mixture
Ref	Reference
Sch	Schlieren image

CHAPTER ONE

INTRODUCTION

CHAPTER ONE

INTRODUCTION

1.1 General

Global warming results from increased greenhouse gas concentration (GHG_S), in particular, carbon dioxide (CO_2) in the atmosphere. This atmospheric accumulation of greenhouse gases is largely the result of fossil fuel combustion and other human activities.

Many possible reforms were suggested to address this study, and the search for fossil-fuel replacements is a significant task for society. Various researches were conducted to evaluate alternative fuel's energy efficiency and environmental impact. The use of ammonia gas represents a possible solution for the storage of intermittent renewable energy.

Ammonia is considered more suitable for storage and transportation compared to Hydrogen gas because the tanks in which ammonia is stored is light, not expensive and its storage is also safer due to the low pressure.

The ammonia energy storage system has great advantages over a wide range and less restriction of geographical conditions compared to many other conventional energy storage method **[1]**.

1.2 Ammonia Fuel

The ammonia NH3 product might be made from biomass, fossil fuels, or other renewable sources like photovoltaic cells and wind, Ammonia is carbon-free, has no direct effect on GHG, and might be produced utilizing a carbon-free process employing renewable energy sources. Approximately 180 million tons of NH3 are generated as well as transported each year, The Ammonia and LPG combustion characteristics, are shown in Table (1.1)

Table (1.1) characteristics of Ammonia and LPG

Specifications / unit	LPG [2],[10]	NH_3 [11]
LHV MJ/Kg	45.5	18.8
HHV MJ/Kg	49.3	22.5
Density Kg/m^3	0.536	0.37
Octane number	106 -110	130
Minimum ignition temperature K MIT	683-853	930
Boiling point ˚C	-18	-33.34
Flashpoint ˚C	-40	132

1.2 LPG Fuel

Iraqi Liquefied petroleum gas (LPG), which consist primarily of propane(C_3H_8) and butane (C_4H_{10}), with minor unit's other materials acquired a byproduct petroleum refining. (C_2H_6) and (C_5H_{12}) the vapor pressure at 37.8 ˚C ranging from (8.4-8.6 kg/cm^2), and the density at 15.6 ˚C ranges from (0.537- 0.541) throughout the month. Specifications for LPG have been obtained from Hilla Gas Depot and the laboratory.

LPG is mixture of propane and butane, and other materials in small amounts, and it's cooled to a low temperature or high pressure. When being liquefied, the mixture size is 260 times comparison with the gaseous phase. LPG is a fuel similar to petroleum. It has an Heating value of 45MJ.kg^{-1}**,** Due to LPG efficient combustion characteristics and low emissions it is widely used as an alternative fuel in automobiles [2].

LPG is heavier compared with air in gaseous form and contains less water as a liquid. The mixture of butane and propane is colorless, and the smell of LPG can be detected by sniffing it. In terms of using LPG as a fuel, the value regarding its octane number is highly essential; this number (106 - 110) it is higher compared to the octane number for C_6H_6 but lower than the octane number for ammonia , As a result, greater resistance to explosions are provided **[2].**

1.4 The Importance of Ammonia flame in Industrial Application: -

Ammonia can be defined as a colorless gas that has a distinctively unpleasant odor. Power engineering, industrial, and agriculture processes all use it. As a hydrogen energy carrier and a carbon-free fuel, ammonia has a low cost and high efficiency.

For internal combustion engines, ammonia is presented as a viable substitute for fossil fuels, because ammonia has a low flame temperature and a high-octane rating of 130, it may be used at high compression ratios without producing a lot of NOx because it doesn't contain carbon. It can't result from burning carbon monoxide hydrocarbon or silly compared to hydrogen because fuel ammonia is more energy-efficient and the production and storage of hydrogen as ammonia will be less expensive than compressed and cold hydrogen **[3]**.

Since just nitrogen and water are produced from total combustion, ammonia is considered one of the sustainable –carbon-neutral electricity fuels like hydrogen (H_2). When compared to hydrocarbons or hydrogen, ammonia has a lower flame temperature, a narrower burning range, and lower flammability.

Due to such factors, ammonia was not thoroughly investigated. In comparison with hydrogen, ammonia offers a few advantages. Ammonia, for instance, might be stored at room temperature under moderate pressure (0.8

MPa), resulting a low storage costs. In spite of the advantages of ammonia as a fuel, numerous drawbacks such as toxicity and low heating value have previously been identified.

In the 1960s, the studies of New shall, and Stark Mann and Pratt have shown that because of the slower interactions of ammonia, the friction system designed for fuel must be twice as big as possible **[4].**

Ammonia can be produced from Renewable source and is one of the most productive chemicals worldwide with a huge production history **[5].** Ammonia may be quickly liquefied and stored at 8.5 bar at room temperature, cooled to -33˚ Celsius, and stored at ambient pressure. Ammonia storage is far less expensive compared to hydrogen storage, which needs around 350-700 bar and - 252 Celsius for storage as a liquid at ambient pressure **[6].**

Ammonia is considered a power carrier that can also be utilized to store renewable energy and for a variety of other applications. Ammonia, for instance, could be utilized as a precursor to other chemicals, such as cleaning products, in the production of explosives and fertilizers.

Approximately 80%of produced ammonia is utilized to make fertilizers like ammonium nitrate (8%), urea (48%), and ammonium phosphate (7%), which are utilized for direct application (4%) or other fertilizers (14%) **[7].**

As a result, agriculture has the best possibility of producing sustainable ammonia. In agriculture, ammonia derived from renewable energy can reduce emissions from this industry. Actually, fertilizer production emits 1.2% of world greenhouse gas emissions, **[8].**

1.5 The Aim of the Present Work

The use of ammonia as fuel is a practical approach to have the way towards allowing a carbon economy. Ammonia consists of approximately 18% of hydrogen in mass and is accepted as an enabling factor for the combustion of hydrogen with current transport and storage infrastructure.

Liquefied gas petroleum is a good catalyst for ammonia gas during the combustion process due to the high flame speed of LPG compared to ammonia gas, the Boiling point for ammonia equal (-33.34 ˚ C), and the Boiling point for LPG equal (- 44 ˚C).

The fuel (ammonia and LPG) and air with pre-calculated data into the combustion chamber, an ignition system, consisting of a coil, electronic push-button, and two opposite electrodes are used to ignite fuel/air mixtures and

used in this optical study technique, Schlieren photography, and high- speed camera.

The experiment conducted with different initial pressure (100 – 200 – 300 kPa) and initial temperature of (298K). Besides, the tested equivalence ratios range (0.8, 1, 1.3) .

CHAPTER TWO
LITERATURE REVIEW

CHAPTER TWO

LITERATURE REVIEW

2.1 Introduction

The current chapter reviews prior research on the combustion chamber of constant volume and flame speed of Ammonia and LPG fuels. As well as methods and procedures for measuring the properties of laminated flames, such as laminar flame speed. The Available experimental formulae focus on the link between laminar flame speed and factors such as the initial pressure and equivalence ratio. The difference of adding Ammonia NH_3 fuel to LPG varies with flame speed and laminar burning velocity.

2.2 Combustion and Shaping of Flame

The combustion system often involves two reactants, a fuel, and an oxidant; The activities of these two reactants must be merged and blended at the molecular level prior to the reaction manner of combustion might be flame or non-flame.

Processes that occur in a knocking sparks ignition engine can indicate how a flame differs from a non-flame.

Fuel and oxidizing premixed and non-premixed flames are the two most common forms of flames.

Each of these types is further distinguished in terms of fluid motion, which is classified as laminar or turbulent **[13].**

Non-premixed flames: -The fuel and oxidizing mixing rate is controlled by a slow mixing rate.

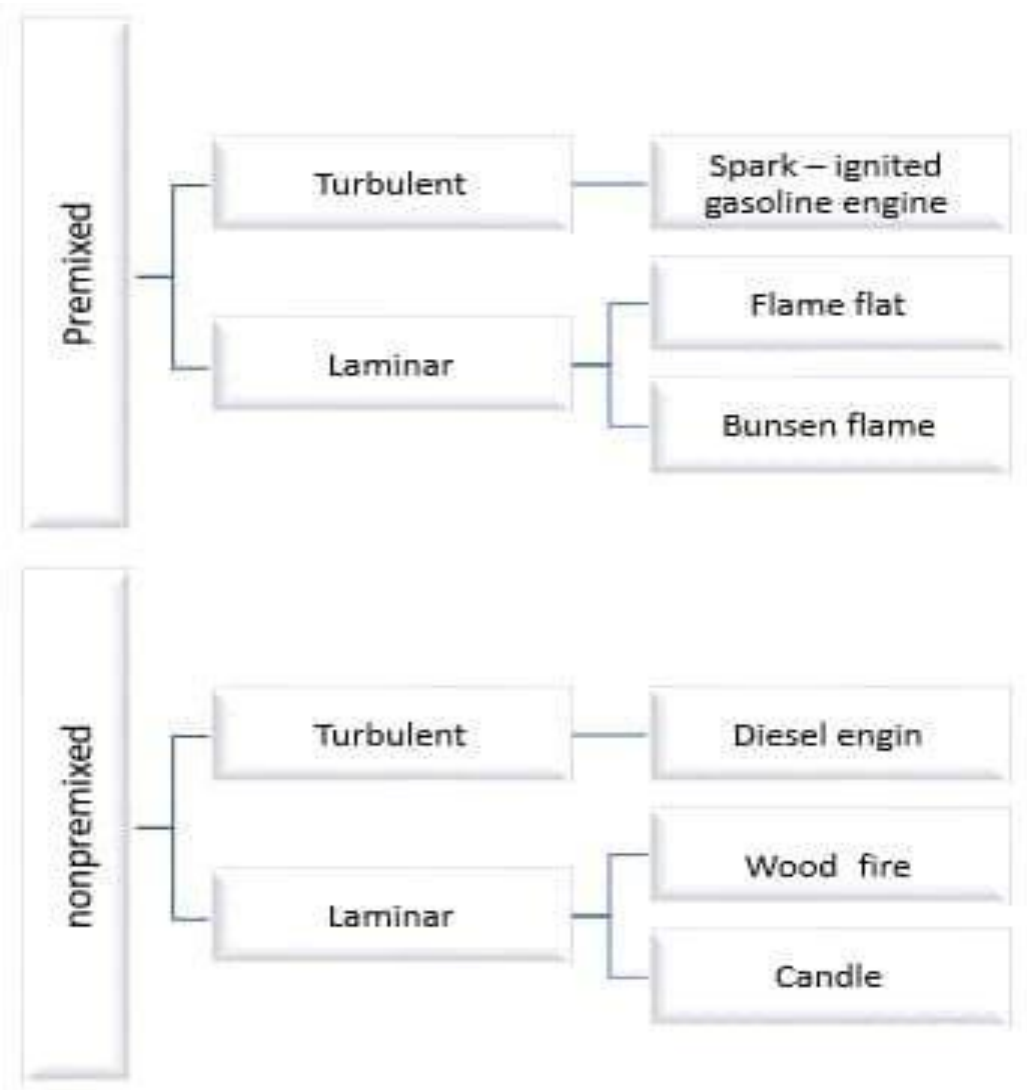

Figure (2.1) schematic classification of flame type [12]

Premixed flame: If an ignition source applied locally raises the temperature significantly or creates a high concentration of radicals to form a flame that will propagate through the gaseous mixture, the fuel and oxidizer are mixed with molecular levels before ignition .

2.3 Laminar Flame Speed and Laminar Burning Velocity

Laminar flame speed has been defined as a highly fundamental characteristic of a combustion mixture. Flame speed has been defined as the speed at which an adiabatic un stretched premixed planar flame propagates relative to the unburned mixture. Laminar flame speed (Sn**)** contains physical and chemical information about the spread, interaction, and heat emission of the mixture **[15].**

Many mixed flame phenomena can be described in advance, such as extinction back fluidity and explosion by (**Sn)** as a reference factor **[14].**

The spherical flame may be spread either externally (Sn positive) or internally ($\mathbf{S_n}$ negative) plus it may spread into space and display the speed of the flame or constant ($\mathbf{S_n}$ Zero). The externally spread flame is ignited or burst centrally.

Internally diffuse flames or internal explosion is the immediate ignition around a spherical outer limit. The fixed inward-oriented flame is practically more feasible and may be created by external unburned gas flow from a porous ball stove is an important combustible mix restriction, due to the fact that it includes required information concerning its reactivity, exothermicity, and diffusivity. In addition to that, the velocity of the unburned gas is dependent upon the temperature of the flame, and can be obtained by two methods according to the period of analysis **[16].**

Constant Pressure Period in the pre-pressure combustion period, the burned mass fraction (the mass fraction burnt represents the ratio between cumulative heat release to the total heat release and is used to describe the amount of heat released as a function of crank angle) is low enough for temperature and pressure to not be significantly increased. This is why they may be considered to be equal to the value of the initial pressure. This provides the user with the ability for getting the data of the burning velocity for certain conditions of interest.

Constant volume period, laminar burning velocity may be obtained from pressure history within the bomb. The constant volume approach uses the full combustion bomb approach benefit, however, more detailed and complex equations are required than for the constant pressure approach. Laminar burning velocity $\boldsymbol{u}_l$ has been more accurately defined as the velocity at which the unburned gases move through a wave of the combustion in a direction which is normal to the wave surface, as can be seen in Figure (2.2) **Marshall S. P. [17].**

Laminar Burning Velocity can be defined as a physio-chemical characteristic describing the reactance movement toward the zone of reaction which includes mixing and reaction whereas the speed of the flame presents the flame front movement that is a two compound of the chemical reaction and temperature that increases in the same direction.

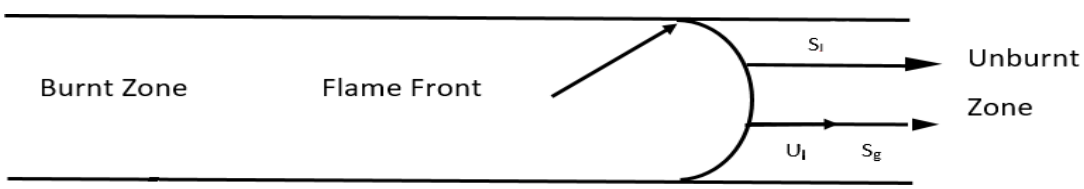

Figure (2.2) premixed flame in a Tube

This definition assumes a one – dimensional (1D) upstretched flame

$$S_l = u_l \pm S_g \quad (2.1)$$

Where

u_l = Unstretched Laminar burning velocity

S_l = Unstretched laminar flame speed

S_g = Unburned gas velocity right before the flame

2.4 Measurements of Laminar Burning Velocity

Measurement methods are classified into two main types according to the type of flame **Stationary flame and non-Stationary flame** in this study deal with non- Stationary flame.

2.4.1 Stationary Flames

In this category, a flow of premixed combustible mixture flows into a constant flame with a speed equivalent to Su. It can be created by flowing a continuous combustible mixture into a burner at a constant velocity. It is attached at the burner rim, from which burning velocity can be taken. There are many measuring techniques used for this type of flame **.**

2.4.1.1 Bunsen burner method

2.4.1.2 Flat flame burner method

2.4.1.3 Slot burner method

2.4.1.4 Nozzle burner method

2.4.1.5 Annular step-wise and diverging channel method

2.4.1.6 Stagnation flame method

2.4.2 Non-stationary flame

this category, the flame propagates through a quiescent combustible mixture. Many techniques are available to study the flame propagation speed.

2.4. 2. 1 Tube Method

This approach can be defined as a very early approach where a flame propagates through the tube's length. On the other hand, this approach has been found easier, tube approach suffers from related issues, like the loss of heat to pipeline walls, and the tube is opened at one of the ends and closed at the other one.

estimated burning velocity by capturing the flame photos at specified time intervals and utilizing them for the purpose of measuring the burned gas volume per time unit as well as the flame area **Marshall S. P 2010 [17].**

This method is one of the earliest used. The tube is opened at one end closed at the other is filled with fuel-air mix and ignited at the free end. Photos have been captured for the flame to travail along the tube **Almarcha et al , C 2015 [18].**

There has been a difference in the velocity of the burning among different diameter tubes. The difference in the measured values depends upon whether or not the flame has propagated upwards, downwards, or horizontally. On the other hand, the key issue has been the effect of wall interaction **Konnov, A. A., 2018[19].**

However, the main issue has been the effects of wall interaction, which has resulted in **Garforth & Rallis (1980) [20]** concluding the fact that this approach is not satisfactory.

2.4.2.2 Constant Volume Bomb Method (spherical flame method)

Hopkinson reported B. (1906) [21] about the first experimentation of spreading the flames within a fixed container through the ignition with the central electric spark at different temperatures and the position of the flame measured by placing fine platinum wires across the vessel at various radii and measuring their resistance.

These wires melted and so had to be replaced after each experiment, The speed was calculated from the time taken for the flame to pass from one wire to another.

Flame and Mache (1917) [23] proposed a correlation between the amount of burned mix and the pressure of the spherically expanded flame. This approach remains affected by a number of factors, despite the simplicity of experimental formation and the geometry of the flame, including spark ignition, radiant heat loss, flame instability, chamber confinement, and flame stretch.

Fiock et al. (1940) [24] developed the technique by using a glass window with a (10") diameter bomb to film the combustion through a slit onto a rotating drum Burning velocity can be calculated in a number of ways.

One method is to mount a fast response pressure transducer on the outer wall of the Bomb. This provides a pressure trace as the flame grows. A computer model is then used to calculate the burning velocity from this pressure record. Secondly, schlieren photography can be used to visualize the flame**.**

The flame radius can then be measured from these photographs. Photographic drums and high–speed cameras have been later replaced by high–speed digital video. The whole bomb can be placed inside a heated chamber to allow studies with elevated initial temperature the constant volume design can be a spherical interior or cylindrical chamber.

A bomb can be defined as a pressure vessel inside which is homogeneous cylindrical or spherical fuel/air mix is introduced into the vessel and ignited by two opposing thin metal electrodes that produce a spark in the spherical vacuum center and after that, the flame grows out spherically**.**

Kwon, *et al* (2002) [21] It has been referred to as the spherical flame method as well. Which has been widely implemented to measure the speed of combustion $\mathbf{S_n}$ with reliable empirical results.

In this way, a confined vessel that contains a pre-mixed combustible mixture at specified conditions is ignited at the chamber center and propagates spherical flame propagates via combustion mixture as in Figure **(2. 3)**

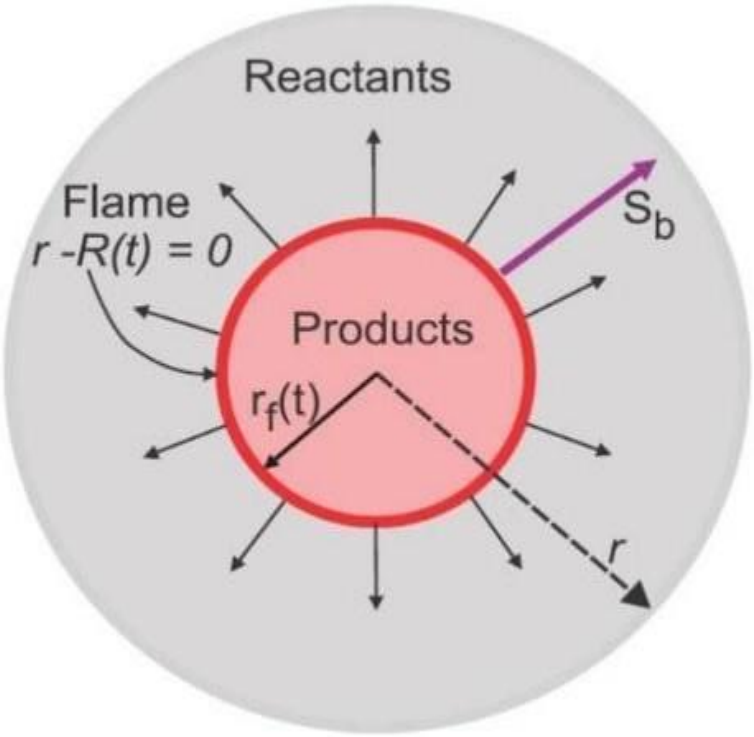

Figure (2.3) outwards expanding spherical flames **[19]**

The dimensions of the constant volume chamber changed from one apparatus to another. **Johnston, R.J. Farrell, J.T. (2005) [25]** used stainless steel vessel with a (165mm) diameter spherical with the volume of (2.4 L) with four windows.

Chenglong Tang (2008) [26] used a cylindrical type combustion chamber in experimental work with an inner diameter of (180 mm) and a length of (210mm).

Hu et al (2009) [27] used a cylindrical type combustion chamber in experimental work with an inner diameter of (180mm) and volume (5.5 L)**.**

Egolfopulos *et al* 2014 [28], Chan *et al* 2015 [29] , and Lipatinikov *et al* 2015 [30] for the purpose of achieving accurate measurements of S_n the impacts of the factors that have been mentioned above on the flame spread have to be minimized carefully. The constant volume chamber's interior design may be a spherical or cylindrical cavity with dimensions that vary from one apparatus to the other**.**

Saleh and AL- Fattal 2006 [31] used the vessel of a cylindrical shape with an inner diameter and length of 305 mm and thick 11 mm as a result, by increasing the initial pressure of a propane – air mixture, the flame speed decreases and vice versa **.** **Glamiche *et al*.2011 [32]** have carried out their experimentations in stainless steel cylindrical vessels that had an inner volume of 24.32L**.**

Stone and Hinton 2014 [33] utilized a spherical chamber of combustion with a 160 mm internal diameter.

Manaa *et al* 2015 [34] used a spherical Stainless steel combustion vessel that has an internal diameter of 330mm.

Yasiry and shahad 2016 [35] used a cylindrical constant–volume combustion vessel that is 250mm long with a 190mm internal diameter. Experimental results have been shown that the effect of hydrogen addition Becomes noticeable when the hydrogen blend is larger than 60%. When hydrogen blending is 80%, adiabatic flame temperature increases by about (40 K), the laminar flame speed of LPG also increases from (2.2-4.75 m/s) and laminar burning velocity from (31-59.5 cm/s)**.**

Bao *et al* 2017 [36] used cylindrical constant–volume combustion vessels with 350mm inner diameter**.** The maximum laminar burning velocity of cyclopentanone is 0.82 m/s; for gasoline, it is 0.72 m/s and for ethanol it is 0.86 m/s, at an initial temperature of 423 K and pressure of 0.1 MPa**.**

Duva *et al* (2020) [37] used a cylindrical constant–volume combustion vessel that has a 305mm internal diameter, and 89mm thick wall for resisting 130bar at 523 K . Experimental results show that the laminar flame speed values of methane/ air mixtures diluted with actual combustion residuals are between those of N_2 and H_2O dilution, whereas the laminar burning velocities of methane flames diluted with CO_2 are considerably slower. The effects of different combustion residuals on the burned gas Markstein length were not found to be significant.

Laminar burning velocity can be obtained in constant volume vessel in two ways, which are: the constant pressure method (CPM) that has been suggested first by **Ellis 1928 [38],** and the constant volume method (CVM) has been proposed first by **Lewis B, 1934 [39].**

At CPM experimentations have been carried out with the use of Schlieren and high – a speed camera. The structure of the flame may be checked for seeing when flame cells and their instability happen with the use of the Schlieren photos.

The most prominent rates the flame expansion takes place through the early diffusion of the flame, which causes the difference between the derived burning Velocities in the previous study **(Bradly *et al* 1996) [17]** Extension corrections were linear and nonlinear data induction of zero expansion conditions.

It was shown that non–linear induction was more accurate than linear induction, which may cause increased prediction of upstretched burning velocity, particularly at a high ratio of equivalence.

The extrapolation method is still considered an investigation issue and uncertainty associated with CPM.

Tahtouh 2010 [40] and **Z. Chen 2011[41]** has resulted in advancements in the calculation of laminar burning velocity without the use of the mix characteristics.

In the constant volume method (CVM) the laminar burning velocity is estimated as combustion pressure function and burned gas fraction (X**)** **Lewiss, 1934 [39]** suggested the laminar burning velocity calculated in this way includes some theories, therefore it has the tendency of being less precise compared to that estimated with the use of the CPM**.**

Xu *et al* 2020 [42] studied the flame of the spherical proliferation of biofuels in the constant vessel at an initial temperature of 358K - 418K, equivalence ratio of 0.70-1.40, and initial pressure 1 of 4 bar. They have shown that the laminar burning velocity difference between static size and static pressure method has been 15% except for conditions in which flame cell accrued.

While the technique used for measuring the speed of the flame and the velocity of the burning the area of the reaction is typically referred to as the lame front or the reaction wave. In this area, the reactions take place quickly, typically emitting light **(K. Kuo, 1986) [43].**

2.5 Techniques of Measuring Laminar Flame Speed and Burning Velocity

The reaction region is often called a reaction wave or flame front. In this region, reactions occur rapidly and usually light is emitted from it. A particular technique is needed to measure flame speed by detecting the flame wave along a specific space. Hence, several researchers worked extensively to get various techniques to measure flame speed and burning velocity.

For flame speed, the techniques used are explained below:-

- **Visual technique: -** Which represents the simplest and oldest technology to measure the speed of the flame, utilizing the transparent channels to see flames, and by recording the time that it takes to pass

the flame front between two points, the speed of the flame may be estimated. The visual technique has been utilized by **Zaid (1982) [44]**, and Krestschmer ***et al*** **(1985) [45].**

- **Optical techniques:** There is a variety of optical technique types, which can be summarized as**:** -
  - **a-** Shadow zone photograph: Which is a simple method it is the least favorable method as it is considered unreliable suggested avoiding using this method for flame speed measurements **Halter 2009 [46] , Wang et al 2018 [1] .**
  - **b-** Schlieren photograph, which is dominated used approach burning experimentation, due to the fact that it shows a higher accuracy compared to the other approaches, **Zhang *et al* 2013 [47]. Yasiry and shahad 2016 [35], Duva, *et al* (2020) [37]** used this approach**.** The technique uses Schlireen photograph.
  - **c-** Visible Zone photographs: -which represents the technology that shows lower accuracy compared to the other where it's difficult to determine the visible are accurate**. R. Sreeni Vasan et al. (2012) [48].**

- **Thermocouple technique:** in this technique, the flame propagates inside the combustion vessel and passes over many thermocouples, which will sense the flame front since it had the highest temperature among that of burned and unburned gases. This technique was used by Saleh and AL-Fattal 2006 [31].

- **Ionized probe technique:** in this technique, the flame front will be detected since the ionization level is very high at the flame front. This technique cannot predict the actual location of the flame front since the levels of ionization stay high behind it. Li et al. [9] used this technique.

While the methods used to get the burning velocity are:

- **Density ratio method:** this method used equation to calculate the burning velocity:

$$Su = S_l \frac{\rho b}{\rho u} \quad (2.1)$$

where ρb is the density of the burned gases, and ρu is that of the unburned gases. Yasiry and Shahad [35] , Okafor et al [ ] used this method.

-**Pressure measurement method**: it is used in combustion in a constant volume method, where the change of pressure with the radius of the flame front leads to determining burning velocity using equation Xu et al. [3]

$$Su \propto \frac{dp}{drf} \quad (2.2)$$

2.6 Factors Affecting Flame Speed and Burning Velocity

The mean factors attend in flame speed and burning velocity and type of fuel, Initial Temperature and Initial Pressure.

2.6.1 Fuel Type

The flammable mixture includes the air as the maximal part, therefore the molecular weight fuel has a low effect upon burning velocity **[49] 2021.**

As well the fuel molar mass does not have a strong impact on the velocity of the burning, due to the fact that most mixture is considerably more significant. The air is the thermal content of fuel combustion because this affects the temperature of the adiabatic flame where the temperature has maximum impact in relation to burning velocity.

The motility of oxidation reactions is also important and can explain the reason for the difference in burning velocity of some of the fuels that have an adiabatic flame, Temperature **Marshall, 2010 [18].**

In general, the velocity of the burning for the hydrocarbon fuel types is decreased in the case where the atoms of the carbon in molecular fuel are increased **Kuo, 2005 [50].** Research has discovered the Laminar burning velocity is distressed by increasing the number of the carbon atoms in the hydro-carbon in fuel **Saleh, and AL-Fattal 2006[31].**

Marshall et al. (2011) [51] Laminar burning velocity screening for n-heptane and iso-octane toluene ethyl-benzene and ethanol on a broad variety of the primary pressure temperature and equivalence ratio along with tests using combustion residues**.** A 12 – term correlation for the burning velocity has been fitted to the data.

2.5.2 Initial Temperature

The most important aspect that affects the variety of the burning velocity in general, is the temperature raising of unburning gas increasing laminar burning velocity, and allowing the flame to spread in a more stable manner. The most common that represents the initial temperature and pressure effect is

$$S_l = S_{l.ref}\left(\frac{T_u}{T_{u.ref}}\right)^{\gamma}\left(\frac{P}{P_0}\right)^{\beta} \qquad (2.3)$$

Where the subscript (ref) represents the reference conditions (Typically $T_{u,\,ref}$ = 298 K, P_{ref} =1 bar).

The exponent's power for pressure β and temperature ɣ has been discussed in detail by **Konov *et al* (2018) [19]** varying as the fuel type function, oxidizer, and ratio of equivalence.

The temperature has been considered the largest aspect that is involved in the change of the velocity of burning. The dependencies of the temperature of the laminar burning velocity and flame thickness could be calculated as:

$$Sl = \left(-2\alpha(v+1)\frac{m^{\circ}f}{\rho_u}\right)^{0.5} \qquad (2.4)$$

$$\delta = \frac{2\alpha}{Sl} \tag{2.5}$$

Recognizing the following approximate scaling of the temperature for simplicity use T_b for the estimation of $\dot{m}_f$ the pressure dependencies have been indicated also by:

$$\alpha \propto Tu\, T^{1.75} P^{-1} \tag{2.6}$$

where exponent (n) represents general reaction order and T= 0.5 (T_u + T_b) through the combination of the scaling above, the result would be **[13].**

$$S_l\, \alpha\, T^{-0.875} T_u^{-0.5}\, T_b^{\frac{-n}{2}}\, e^{\left(-\frac{-E_A}{2R_u T_b}\right)} P^{\frac{n-2}{2}} \tag{2.7}$$

$$\delta \propto T^{-0.875} T_u^{-0.5}\, T_b^{\frac{-n}{2}}\, e^{\left(-\frac{+E_A}{2R_u T_b}\right)} P^{\frac{n-2}{2}} \tag{2.8}$$

Sharma et al (1981) [52] found that for natural gas (95% methane) that the temperature effect is: -

$$u_l = Q \times \left(\frac{T}{300}\right)^n \tag{2.9}$$

Where Q is the burning velocity at 300 K and n= 168 $\sqrt{\emptyset}$.

Keck and Metghalchi (1982) [53] characterized experimentally the laminar flame speed for different fuel-air mixtures for different initial conditions (T, P, and Ø) and they suggested the following correlation.

$$S_l = S_{l,ref} \left(\frac{T_u}{T_{u,ref}}\right)^{\gamma} \left(\frac{P}{P_{ref}}\right)^{\beta} (1 - 2.1 Y_{dil}) \tag{2.10a}$$

Where

$$\gamma = 2.18 - 0.8\,(\emptyset - 1) \tag{2.10b}$$

$$\beta = -0.16 + 0.22\,(\emptyset - 1) \tag{2.10c}$$

$$S_{l,ref} = B_M + B_2\,(\emptyset - \emptyset_M)^2 \tag{2.10d}$$

Where reference conditions defined by $T_{u,ref}$ = 298 K, P_{ref} = 1atm.
While B_M, B_2, and $Ø_M$ depend on fuel type. Y_{dil} represents the mass fraction of the diluent that presents in the air-fuel mixture.

2.6.3 Initial Pressure

The first pressure impact verification on the laminar burning velocity has been shown by **Ubbelohde (1916) [54]** with the use of the following power – law pressure dependence that has been applied for a range of the pressure of (1bar - 4bar).

$$S_u = S_{u,o} \left(\frac{P}{P_0}\right)^{\beta_1} \quad (2.11)$$

Understanding the equation above has some specific basics in the initial flame speed theories. **Mallard (1983) [55],** indicated negative dependence of S_u with the pressure by heat and mass balance only**. Daniell (1930) [56], Nusslet, *et al* (1915) [57]** expanded the theory through the introduction of the rate of total reaction ($\dot{w}$) explicitly. **Zoldovich 1938 [58]** developed the theoretical approach viewing that mass burning rate $\dot{w} = \rho S_u$ has been directly proportionate to the square root of the rate of the total reaction $\dot{w}$. Another pressure dependence relation.

$$S_u = S_{u,o} [1 + \beta_2 \, log \, (\frac{P}{P^\circ})] \quad (2.12)$$

It has been proposed first **by J.T. Agnew 1961 [59] with β_2** = - 0.206 for a stoichiometric methane mix **Sharma et al 1981 [52]** explained their measurements with the use of eq. **(2.3**) and proposed that the coefficient β_2 value is close to (-0.20) for the equivalence ratio of (0.80-1.20)
Andrews *et al* 1972 [65] reviewed available experimental data before 1972 and suggested the following correlation:

$$u_l = 43 / \sqrt{P} \text{ cm/s} \quad (2.13)$$

Where P represents the pressure atmosphere unit for the stoichiometric mixtures at a level of the pressure that is higher than 5atm. **Stone and Hinton**

2014 [33] researched the laminar burning velocity of the bio-gas over a broad variety of pressures and temperatures.

2.6.4 Equivalence Ratio

The correlation between the burning velocity and the equivalence ratio followed between laminar burning velocities except for vibrant fuel-air mixtures. So, it is maximum at slightly more than stoichiometry.

Andrew *et al* (1972) [65] studied flames for CH_4 / air mixture and showed that laminar burning velocity peaked at Ø = 1.08**.**

Hayakawa *et al* (2015) [66] showed that maximum laminar burning velocity for the NH_3 /air flames at all of the initial mixture pressures that have been reached the peak values Ø = 1.10**.**

Kumar *et al* 2020 [67]**,** utilized diverging mesoscale channel with externally heated to measure the velocity of the laminar burning for the mix at a temperature that is higher than its auto-ignition for the pre-mixed n-heptane – air mixtures it was found that maximum laminar burning velocity value has been obtained for Ø that approximately equals 1.10 at all of the temperature degrees that have been examined.

Kim *et al* (2020) [68] showed that the velocity of laminar burning of Diisobutylene (DIB) is one such alternative biofuel for use in vehicles and can be promising alternative jet fuel because of its excellent properties. DIB – air mixtures at 428K and 1atm have been at their greatest at a 1.07 equivalence ratio. Equivalence ratio (Ø) is the ratio of the actual fuel-air ratio to the stoichiometric fuel-air ratio.

$$\boldsymbol{Ø} = \frac{(F/A)_{act}}{(F/A)_{stoich}} \qquad (2.14)$$

lekseev et al 2015[69] used an updated mechanism to study the effect of temperature on the burning velocity of hydrogen flames for different equivalence ratios and validated the mechanism with many researchers and

found that slightly richer than stoichiometric is the region of the maximum laminar burning velocity.

Liu Xu et al 2019 [3] also found carbon-neutral fuel and hydrogen energy carrier, ammonia has been expected as a promising carrier of energy

and will be widely utilized in the industry, laminar flame speed, length of Markstein, the thickness of laminar flame, and the half of the critical radius for the beginning of experimental and numerical instability of the flares were examined.

Used in a static size room and a high-speed digital imaging system have used from Schlieren to study the laminar burning velocity of $NH_3 – O_2 –$ air. The thickness of the flames has been decreased with an increase in initial pressure. In general, the value of Markstine length was increased with the increase in the equivalence ratio, whereas it was decreased with the increase in the value of the initial pressure**.**

Okafor et al 2018 [5] used an updated mechanism for studying the effects of the concentrations on the burning Velocity of Ammonia flames for a variety of the equivalence ratios and validated the mechanism with a high number of researches and discovered that linear and non-linear correlations, is the maximum laminar burning velocity region at Stiochmetric.

2.6.5 Oxygen enrichment

In some modern advancement of combustion techniques, fuel is not burned in the air but with Oxygen Enrichment Combustion (OEC) or oxy-fuel fuel combustion Wang et al. [1] studied the outward propagation flames for ammonia at various initial temperatures, equivalence ratios, and oxygen fractions. The results showed that increasing oxygen fraction and initial temperature led to an increase the laminar burning velocity, and the maximum value of Su reach 125.05 cm/s at the pure oxygen and normal temperature 303K

2.6.6 Diluents

The dilution of different combustible mixtures with chemically inert species led to enhance the characteristics of flame control and quenching, and control the emissions of combustion process because of increased the specific heats, variations in transport properties and chemical path-way of fuel oxidation The advantages of using inert additives are fire safety and nitrogen oxides emission control. On the other hand, it influences the flame reactivity, which causes problems of flame stability in combustion processes. It requires a knowledge of the influence of diluents on flame propagation behavior.

Many investigators studied the effects of the inert additives to the unburned mixture such as Duva et al. [37] concluded that utilizing one or mixture of two of the major exhaust gases cannot precisely simulate real combustion residuals since the chemical reactivity and thermodynamic properties of the combustion residuals can vary extremely with pressure, temperature, equivalence ratio, and dilution ratio. So, the effect of dilution of methane/air mixture with actual flue gas content on laminar burning velocity and Markstein length (L_b) values were measured at 473 K and 1 bar over a broad range of Ø. The results showed that the Su was reduced by additions of actual flue gases.

Chan et al. [29] used kinetic model and experimental study to investigate the influence of CO_2 dilution on the laminar flame speed for CH4/air mixture. Experiments were conducted using a flat-flame burner method at 298 K and 1atm pressure over the equivalence ratio range of (0.8- 1.4). The results showed the laminar burning speed was inversely proportional to increasing CO_2 dilution.

Increasing carbon dioxide led to reduce concentrations of reactants and reduce the net reaction rate, which caused a reduction in flame speed. Also, the presence of CO_2 is considered a heat sink, which results in a reduction in the temperature of reaction and therefore reduces the capability to overcome the energy of activation for reactions to take place.

2.6.7 Fuel Blends

Real fuel is typically a mixture of a number of chemicals. **Wheeler & Paymann 1922** have suggested an equation for the prediction of the burning velocity of fuel of more than a single component.

$$S_{u\cdot mix} = \sum \zeta x_i \, S_{u.i} \qquad (2.15)$$

ζ_i represents the volume fraction of a mixture of a component fuel its oxidant with respect to the entire mixture **Marshall (2010) [18]**

$$\zeta x_i = \frac{volume\ of(fuel\ i + corresponding\ oxidant)}{volume\ of(total\ oxidants + total\ fuels)} \qquad (2.16)$$

which has been considered as the simplest base of mixing. Fuel blends indicates that the mixture burning velocity is equal to burning velocity values of components, which have been weighted by the respective volume ratio.

On the other hand, **Yumlu (1967) [72]** showed that the rule doesn't fit experimental data quite well, due to the fact that it doesn't take into consideration variations in the temperature of the fuel flame of the mixture with the concentration changes. Hence, the alternative has been suggested by **Spalding 1956[73]:**

$$S_u^2{}_{,mix} = = \sum \zeta_i \, S^2{}_{u.i} \qquad (2.17)$$

Hence ζ_i relates to a mass fraction and assumed that the components' burning velocity values all correspond to the mixture flame temperature.This expression assumed as well a random oxidant allocation between the fuels.

Yumlu (1967) [72] showed that this equation is a much better fit, especially if the equivalence ratio is taken to be the same for each fuel i.e. the fuels have an equal share of available oxygen and explain that this makes a theoretical sense by assuming the heat release rate.

Okafor et al 2018 [83] studied the velocity of the laminar burning of the NH_3 - CH_4 -air premixed flame experimentally and numerically studied over a broad variety of the ratio of the equivalence and concentration of the ammonia. The concentration of the Ammonia in the fuel, which has been represented based on NH_3 heat fraction in fuel has been ranged between 0 and 0.30 Whereas the ratio of the equivalence has ranged between 0.80 to 1.30.

Experimentations was carried out with the use of a constant volume chamber at 298K and 0.1Mpa laminar burning velocity has been reduced with the increase in the concentration of the ammonia.

Ichikawa et al 2015 [74] have numerically and experimentally investigated the velocity of laminar burning of the ammonia/ hydrogen/air premixed flame at increased pressure (1-5) bar in a constant chamber. Results have shown that laminar burning velocity is nonlinearly increased with increasing hydrogen blends and reduced with increases in initial mixture pressure.

Okafor, et al 2019 [5] Studied NH_3 - CH_4 -air flames' laminar burning velocity at high pressure with the use of the reduced mechanism of the reaction, experimentations were carried out in a chamber of constant volume the ratio of equivalence that ranges between 0.70 and 1.30 and mixture pressure ranging between 0.1MPa and 0.50MPa, laminar burning velocity has been reduced with increasing the concentration of the ammonia E_{NH3} in fuel and mixture pressure, found that at high pressure the flames, and increased with increasing E_{NH3} for the rich flame. A mechanism of the reduced reaction Has advanced and optimized with the data from the literature as well as the present measurements.

Hayakawa *et al* 2015[66] researched laminar burning velocity of ammonia- air premixed flame at various pressure values, up to 0.5 MPa which propagate in the constant volume combustion chamber, it has found that laminar burning velocity has decreased by the increase of initial mixture pressure.

Liao et al 2004 [61] measurements of burning velocity for LPG - air mixture. The laminar burning velocity depended on the initial pressure, temperatures, and Equivalence ratio, and the laminar burning velocity decreased as increasing in initial values of the temperature and pressure**.**

2.7 Factors affecting Flame Speed Measuring Accuracy in CVC Method

2.7.1 Energy of Ignition

The discharge of the spark results in causing a shock wave, which is succeeded by a slower heatwave. As there is a difference in the voltage between the electrodes the air in the gap is ionized and a spark is generated. This energy might result in increasing the mixture temperature and then the speed of the flame.

For the energy of ignition that is lower Compared to minimal power of ignition, the speed of the flame had dropped quickly to 0. The energy values are slightly higher than minimum ignition energy .

The flame speed drops to a minimal value, and then Increases when the flame is created as mentioned in **Bradly *et al1996* [17], Kwon *et al* 2002 [60]** found that burning velocity changed little with spark energy and gap wide for hydrogen and propane mixture in the combustion chamber.

while **Liao *et al* 2004 [61]** found that the burning velocity increases with the energy of the spark because the radius of the flame is less than 6mm utilizing the ignition system energy of (25MJ, 45MJ, and 65MJ) for igniting the natural gas samples .

Huang et al 2006 [62] mentioned that the flame speed became independent of the ignition energy when it exceeds the flame radius of 6 mm.

Bradley et al. 1996 [17] also summed it up that spark ignition impact may be disregarded in the case where the radius of the flame has been more than 6mm.

The critical radius is dependent upon the energy of the ignition, Lewis number (Le), flame thickness, the ratio of Equivalence Ø.

Table (2.1) List of initiation and end radius for obtaining the S_u for several researches

Year	r_{ini}(mm)	r_w (mm)	r_{end}(mm)	Investigators
2009	6	50	15	Burke *et al* (2009) [64]
2010	10	180	60	Qiao L *et al* (2010) [70]
2011	6	90	25	Wu X *et al* (2011) [71]
2011	8	152.50	46	Lowry WB *et al* (2011) [75]
2012	6.50	100	25	Galmiche B, *et al* (2012) [77]
2013	6.50	42.50	19	Varea E, *et al* (2013) [78]
2016	5	95	35	Yasiry and Shahad2016 [35]
2019	10	135	20	Okafor et al [5]
2020	6	152	37	Duva et al [37]
2022	5	197.5	65	Present research

Bradly *et al* 1998 [63] and **Burke *et al* 2009 [64]** experimentally discovered that the radius of the critical initiation has been varied within a range between (10.5mm and 13.5mm) for the n-decane / air mixture at a high Lewis number (1.46 - 3.10), results have shown that critical initiation radius is decreased with the pressure and increased with Lewis number value.

2.7.2 Flame instabilities

In constant volume bomb experiments, the flame propagation speed can be enhanced by thermal – diffusive and hydrodynamic instabilities Compared to the constant volume method, the constant pressure method has the advantage of visualizing the propagating flame such that the instability that might develop

on the flame front during its propagation can be revealed. Therefore, the upper flame radius should be properly chosen to make the flame propagation speed devoid of the instability effect.

Thermo-diffusive flame front cellular instability develops for mixtures with negative Markstein length or sub-unity Lewis number, while the hydrodynamic instability usually develops as the ratio between flame thickness and flame radius decreases (e.g. at high pressure) **[49]**.

2.7.3 Buoyancy

The flame is exposed to buoyancy impacts due to the large density difference between the burned and unburned gases. Kim et al [68] reported that buoyancy effects on measuring the S_u are considered to be weak in cases with S_u > 15 cm /s and hence its effect decreased with reducing the initial pressure

2.8 Flame Stretched Rate and Markstein Length

In combustion, flame extends amount measuring the surface of the flame as a result of the curvature and outer velocity field strain the flame extension concept has suggested first **in 1953** by **Garlosvitz. G**. **Markstine** researched the flame extent through the treatment of flame surface as a hydrodynamic break (which has been referred to as the flame front).

The flame extension has been explained as well by B. Lewis and G. von Elbe in a book. All of those discussions have dealt with the disruption of the flame as flow speed impact.

However, as a result of the fact that flame bowing there for definition required a more generalized formulation and its exact definition has suggested first by Forman. as the change rate ratio of the flame surface area to an identical area **Flamm et al 1917 [76].**

$$\alpha = \frac{1}{A}\frac{dA}{dt} \qquad (2.18)$$

For outward-propagating spherical flames, the stretch rate of the flame may be obtained by:

$$\alpha = \frac{1}{A}\frac{dA}{dt} = \frac{2}{ru}\frac{dru}{dt} = \frac{2}{ru}Sn \quad (2.19)$$

The rate of the flame stretch α pointed out the flame area expanding rate for the spherically expanding flames. The expression of the flame stretch rate, concerning the curvature of the flame as well as the flow local characteristics, for the present tensor expression, regarding the strain rate tensor α_s and stretch rate as a result of the curvature of the flame, α_c Is that.

$$\alpha = \alpha_s + \alpha_c \quad (2.20)$$

Throughout pre-pressure periods, there's a linear correlation between the speed of the flame propagation and the rate of the stretch (α); which is

$$S_l - S_n = L_b \alpha \quad (2.21)$$

The unstretched propagation speed (S_l) may be obtained as a junction value at α= 0, in the Sn vs. chart. The length of burning gas Markstein, L_b, represents the negative slope of the Sn-α installation curve, Markstine length then may be characterized as a reduction decrease in the burning velocity per the unit stretch.

2.8 Summary

The unstretched flame speeds (S_l) and laminar burning velocities (S_u) had been previously studied as mentioned for different fuels at different initial conditions. It was noticed that there is a lack in studying the effect of CC geometry on these two parameters. It is achieved by studying the same conditions in more than one CC with different volumes. Table (2.2) shows the results for some cited studies according to their references.

In this study, a new experimental setup facility is fabricated and tested. It consists of a centrally-ignited cylindrical constant volume combustion chamber. S_n and S_u are studied for different condition.

In addition to investigating the Markstein length (L_b) Tests are performed for different fuel (ammonia, LPG , air) initial pressures (100, 200 , and 300kPa), and initial temperatures (298 K) at different equivalence ratios (0.8, 1.0, and 1.3).

The study will include the following aspects.

1. Study the effect of initial pressure on laminar burning velocity, and effect with equivalence ratio and ammonia gas percentage.
2. Validating the experimental L.B.V for NH_3 – LPG – air .

Table (2.2) Comparison and practical results between Other researchers

Researchers	Ichikawa et al 2015 [74]	Hayakawa 2015 [66]	Okafor E C. et al 2019 [5]	Ahmed sh. Haroun Shahad2016 [35]	Duve et al 2020[37]
Vessel shape	Cylindrical	cylindrical	cylindrical	cylindrical	cylindrical
ID (mm)	270	270	270	190	305
Length mm	410	410		250	130
Mixing gasses	NH_3 - H_2 – air	NH_3 - air	NH_3 - CH_4– air	LPG/hydrogen /air	CH_4 – air
Initial pressure	0.1- 0.3 - 0.5 Mpa	0.1-0.3-0-5Mpa	0.1-0.3-0.5Mpa	1-2-3 bar	1 bar constant pressure
Conclusion	The upstretched laminar burning velocity increases non- linearly with increasing hydrogen ratio. In the case of the same hydrogen ratio, the upstretched laminar burning velocity decreases with increasing initial mixture pressure	The maximum laminar burning velocity reaches its peak value around an equivalent ratio of 1.1 for all examined initial mix- true pressure conditions. Uunstretched laminar burning velocity of ammonia/air premixed flames decreases with an increase in The initial mixture pressure. That tendency is the same as that of hydrocarbon fuels	The upstretched laminar burning velocity decreased with an increase in ammonia concentration in the fuel And mixture pressure. It was found that at high pressures the Markstein length decreased with an increase in ENH3 for the lean Flames and increased with an increase in ENH3 for the rich flames. A reduced reaction mechanism was developed and optimized the present 22measuremen ts and data in Literature.	LBV increase exponentially with the increase of hydrogen blends and they decrease exponentially with the increase of initial Pressure .	the laminar burning velocity of methane/air mixtures diluted with actual combustion residuals always lie between the ones for N_2 and H_2O dilutions, the S_L values of methane flames diluted with CO2 are considerably slower .

CHAPTER THREE
EXPERIMENTAL SETUP AND PROCEDURE

CHAPTER THREE

EXPERIMENTAL SETUP AND PROCEDURE

3.1 Introduction

A description of the experimental rig the chamber and measuring instruments used to investigate experimentally the effect of ammonia blending ratio with LPG on combustion system safe operation and flame stability are presented. All experiments are conducted in the Mechanical Engineering Department Laboratories at the University of Babylon. The complete setup rig is shown in figure (3.1) . It consists of the following units:

i-Combustion chamber unit

ii- Ignition system and Control unit

iii-Mixture Preparing Unit

iv-Capturing Unit

and A schematic layout of the facility is shown in figure (3.2).

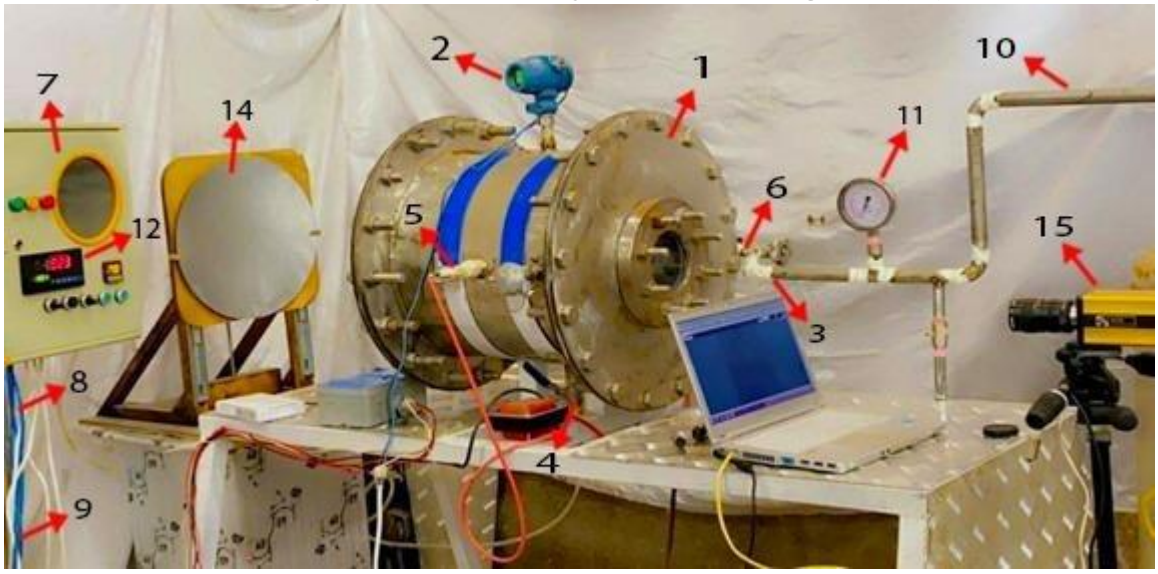

Figure (3.1) photograph of the experimental rig used in the study

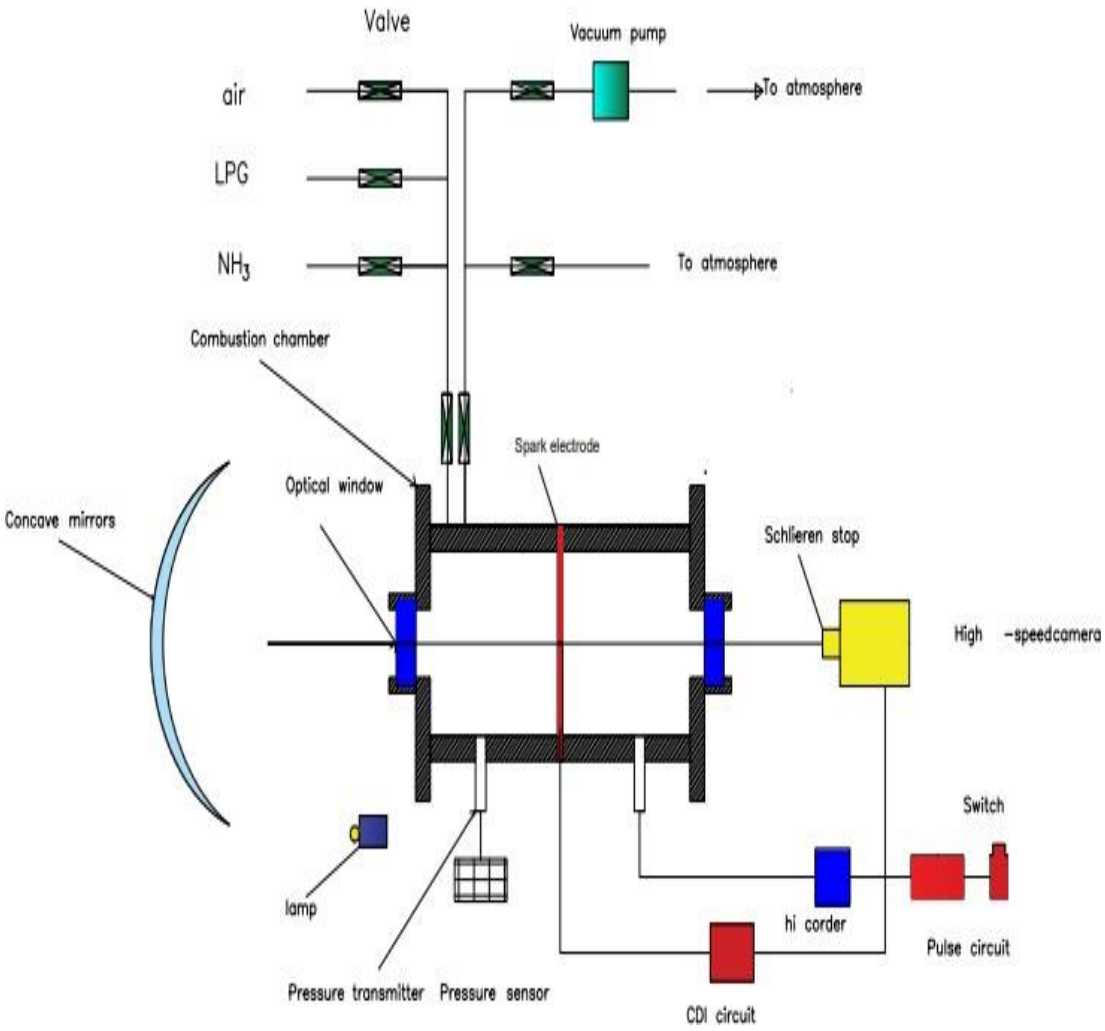

Figure 3.2: A schematic diagram for the experimental rig setup

Each of the units mentioned above consists of many components:

i-Combustion Chamber Unit: - (1) Combustion chamber, (2) Pressure transmitter, (3) Safety Valve, (4) Vacuum pumps

ii-Ignition Unit: (5) Electrodes (6) Ignition system (7) Control system and Switch

iii-Mixture preparing Unit: - (8) Air Compressor (9) LPG Storage Tank (10) Ammonia Storage Tank (11) Pressure Gage ammonia (12) Initial and Total Pressure Gauges

iv-Capturing Unit (13) Light Source (14) Concave Mirror (15) High – Speed Camera.

3.2The Expermerimental Rig: -

The Experimental rig consists of the following units:

3.2.1The Constant Volume Unit: -

3.2.1.1 Combustion Chamber

A cylinder with a fixed size made of stainless steel that is resistant to

experimental conditions, material type Stainless – steel type 304, and its thickness is 12 mm and contains six holes with a diameter of 15 mm, and the volume of the cylindrical chamber is (0. 04899 m^3) with an inner diameter of 395 mm, length 400 mm.

Two flanges with 12 mm thick lower and upper flanges with diameters of 407mm and 570 mm respectively, which have been made of stainless steel in order to resist the external conditions.

These flanges have been joined with the combustion chamber by sixteen of the hex bolts type 12.1 for every one of the flanges. The resister–pressure quartile windows of (100 mm, 140 mm) size have been installed on two combustion chamber sides by the flanges for the purpose of allowing the processes of combustion to be accessible optically.

The cylinder was provided with two electrodes that was connected centrally to the system of the ignition as shown in figure (3.3). A pressure gauge of type QYBO2 SERIES PRESSURE AND DIGITAL PANAL METER – SERIES has been installed in the combustion chamber as shown in figure (3.4).

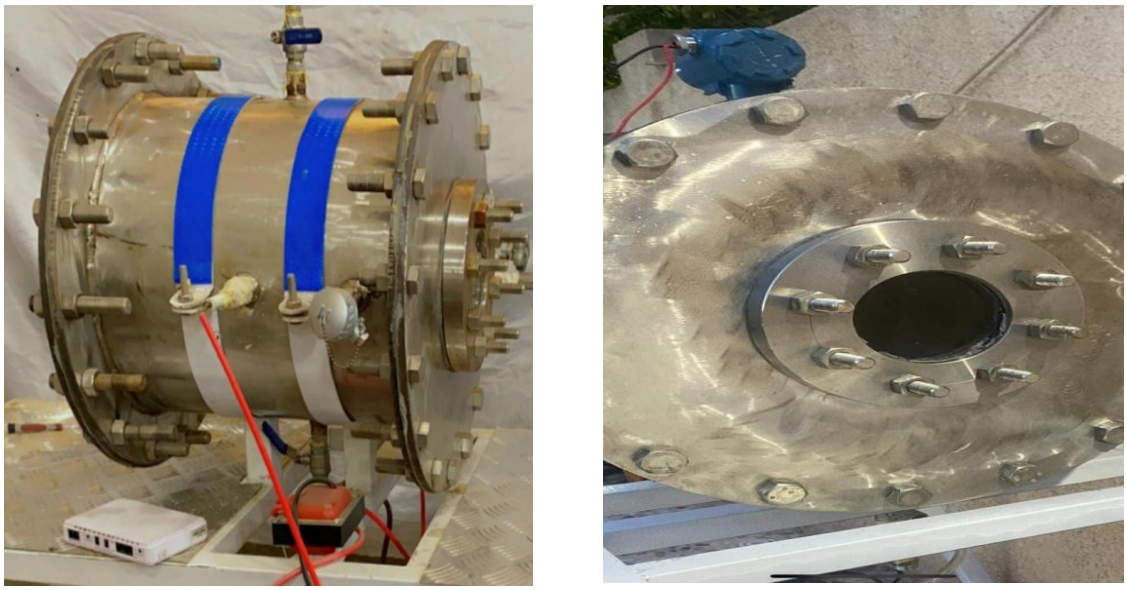

Figure (3.3) Photograph of the Combustion Chamber Unit.

3.2.1.2 Pressure Gauge Transmitter: -

This series of products is suitable for petroleum, chemical, metallurgy, electric power, water conservancy, scientific research, environmental protection, and other various enterprises and institutions, to realize the measurement of fluid pressure and is suitable for various occasions all-weather environment and all kinds of corrosive fluid**.**

- Features

1. Multi measure range selection
2. Digital LCD display
3. Convenient debugging for zero range
4. Intrinsically safe explosion-proof
5. High performance-price ratio
6. High precision & stability

-Specifications

Measure range	-0.1 - 100 MPa	Precision	0.2 % - 0.5%
Overload	Output	Output	wi h
Stability	<0.1% /year	Power supply	
Display	5 – digit LCD	Display range	-
Operating temperature	-	Relative humidity	<80%
Thread	M20 * 1.5	Interface material	Stainless steel

Figure (3.4) QYB102 Pressure Transmitter

3.2.1.3 Thermal Gasket: -

To get the required scaling for the combustion chamber and to make sure that no leakage between the flanges. Two thermal gaskets are utilized for every one of the flanges of (1.5). The gasket has made of material thermal asbestos gasket, which is partly yielding such that it can be deformed and fill spaces that they have been designed.

3.2.1.4 Safety Valve: -

A safety Valve is installed in the lower edge of the combustion chamber for the prevention of any extreme increase of the pressure, which results from the burning procedure within a chamber, and is seized for opening at a high level of the pressure (i.e. 60 bar) for the purpose of avoiding explosions or damage of cylinder.

3.2.1.5 Vacuum pump

The chamber of the combustion is emptied from the products of the combustion and then cleaned by the air after every process of combustion utilizing by using vacuum pump type an ¼ HP, 220V-50HZ.

3.2.2 Ignition Circuit: -

For the purpose of producing a strong spark, an electronic circuit has been utilized for providing power to the electrodes as shown in Figures (3.5 a and b) A continuous current energy source is produced from a current–line converter (220 VF). The transformer (2*5000 V) HOSEL) is 10 KV at peak.

The electronic circuit is utilized for controlling the spark duration, it is placed in front of the transformer for the production of on/off for the initiation of spark in the chamber of the combustion.

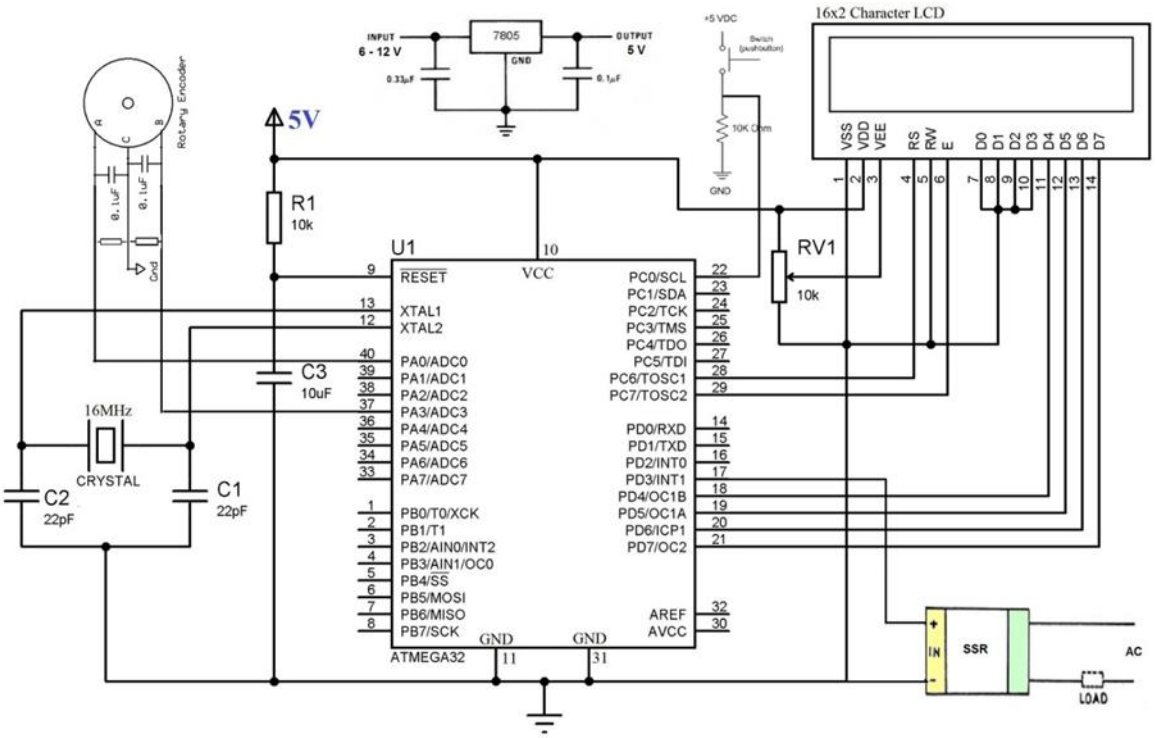

Figure3.5a: Schematic Diagram of Electronic Circuit for The Ignition Unit.

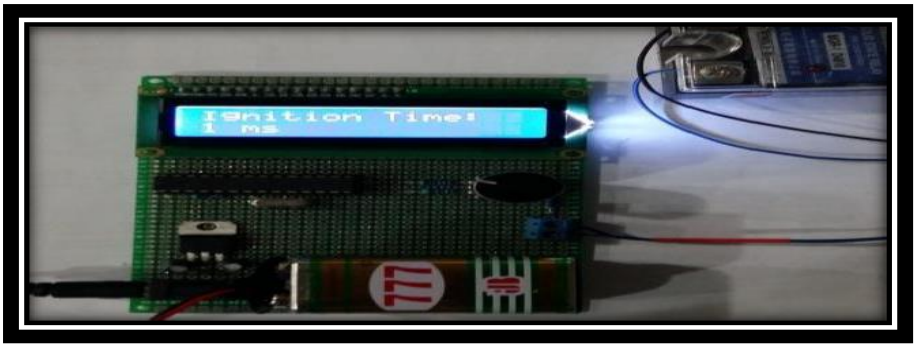

Figure 3.5 b: Photograph of The Electronic Circuit Controlling the Duration of Ignition. (CDI)

Figure 3.5c Photograph of Transformation Type

Ignite the mixture at appointing along the central axis of cylindrical with the use of intensive discharge flaring (CDI). The spark electrode diameter is 2.0 mm and the spark gap is fixed at 1.5mm. electro-static energy that is charged in the CDI circuit capacitor

Figure (3.6) Modified Electrode Used in the combustion chamber

3.2.3 Mixture Preparing Unit: -

The mixing process is based on Gibbs – Dalton law of partial pressures for each component depending on the blend, equivalence ratio, and the total mixture pressure. The preparation of the mixture is done inside the combustion chamber in the following steps:

a) The recalculated volume of liquid is injected by syringe to the combustion chamber through the liquid fuel injection valve. the required volume of the fuel is calculated from its vapor partial pressure according to the ideal gas law PV=mRT

b) The required gaseous fuel is admitted from its tank to the combustion chamber according to its partial pressure, while opening the inlet and pressure transmitter valves, and closing the other valves.

c) Evacuated the gaseous injection unit, and the tube which connects it to the combustion chamber, because it contains a gaseous fuel from step (c). This process takes place by turning the switch of vacuum pump on, while closing the inlet valve.

d) Air is admitted to the combustion chamber until reaches the required total pressure, by turning the switch of the air compressor on, while opening the inlet and pressure transmitter valves, and closing the other valves.

e) The mixture is left for 5-6 minutes to ensure perfect mixing before igniting the mixture.

3.2.3.1 Air Compressor: -

One compressor (od DARI type, DEC 720/520HP4 40068, IT., 2002) has been utilized for providing air at high pressure to the unit of the mix-preparation. The capacity of the compressor is (270 Liter), works at (1160 RPM), and maximal working pressure is (10.50 bar) as shown in Figure (3. 7).

Figure (3.7) Photograph Air Compressor

3.2.3.2 NH_3 Storage Tank: -

The ammonia fuel tank is a cylindrical bottle with a capacity of 40 kg a height of 1.20 m and a diameter of 30 cm, It contains a high-pressure valve with a value of 100 bar and is resistant to acid corrosion, and is connected to 1/2-inch stainless steel tubes, and these tubes are connected to each other by welding and connected to the ammonia gas pressure gauge.

To control more precisely the ammonia gas entering the combustion chamber, the operation is carried out by placing A valve before the combustion chamber before the position of the ammonia pressure gauge, as the ammonia gas needs a pressure gauge of a special type within the required quantity.

3.2.3.3 LPG Storage Tank: -

The LPG Storage Tank is a cylindrical bottle with a capacity of 30 kg and connected with a gas regulator that controls the amount of gas leaving the fuel tank. This regulator is connected with the control unit through high-pressure plastic tube that withstand 6 bar pressure.

Note that the pressure of a fuel tank during the opening of the fuel tank valve and regulating the flow rate using the second regulator, the gas flows to the control unit for the purpose of entering the gas into the combustion chamber,

The switch for the LPG gas is opened from the control unit, which in turn opens the celluloid from closed to open to allow the passage of gas towards the combustion chamber to complete the injection process, the main valve of the combustion chamber is closed.

3.2.3.4 Ammonia Gauge Pressure: -

Ammonia gauge Regulator, Dial size: 4" (100mm), connection: ½ ", range (-1 to 12 bar) the gauge gives the gas pressure before entering the combustion chamber. Also, a pressure gauge was used to control the amount of entering the combustion chamber. as shown in Figure (3.8).

3.2.3.5 LPG Pressure Regulator: -

A pressure gauge was used to control the amount of LPG in the model AW40 and port size ¼, 3/8, ½, set pressure range 0.05 to 0 .85 Mpa, Drain capacity (cm^3) 45, and Mass (kg) 0.72 to prevent the occurrence of ignition or Gas leakage because the regulating meter has the property of non-leakage and non-return of gas in the opposite direction as shown (3.9).

Figure (3.8) Photograph of Ammonia Gauge Pressure

Figure (3.9) Photograph of the LPG Pressure Regulator

3.2.4 Control Unit: -

The control unit is an electric board. It contains a three-way solenoid valve in order to control the type of gases entering the combustion chamber type Festo, so It is in a closed state in the normal position and linked to an open and close switch to control the flow of gases entering the combustion chamber.

The control unit, as shown in figure (3.10) contains a transformer for the purpose of operating the solenoid valve. It is operated on 24 volts, and the transformer converts the current from 220 volts to 24 volts. The control unit is equipped with two display screens, one of which helps to display pressure readings during the injection process, and the other displays the temperature before conducting the experiment. The main purpose of the control unit is to control the gases entering the combustion chamber during the charging process and to measure the temperature of the laboratory during the experiment.

This unit is equipped with pipes connected with solenoid valves, and these pipes are equipped with two valves on both ends of the control unit. The function of one of these valves is to prevent gas from returning in the opposite direction during the injection process. The second valve and its function are to empty the pipes from the previous gas for the purpose of injecting the next gas.

The switch for the LPG gas injection is opened, as the gas begins to flow into the combustion chamber at a rate of (0.06 - 0.16 m^2/ sec) as well as for the air. The remaining gas is disposed of in the pipes after closing the combustion chamber valve and opening the gas outlet valve for the purpose of unloading the pipes from the previous gas, where the values and quantities of materials inside.

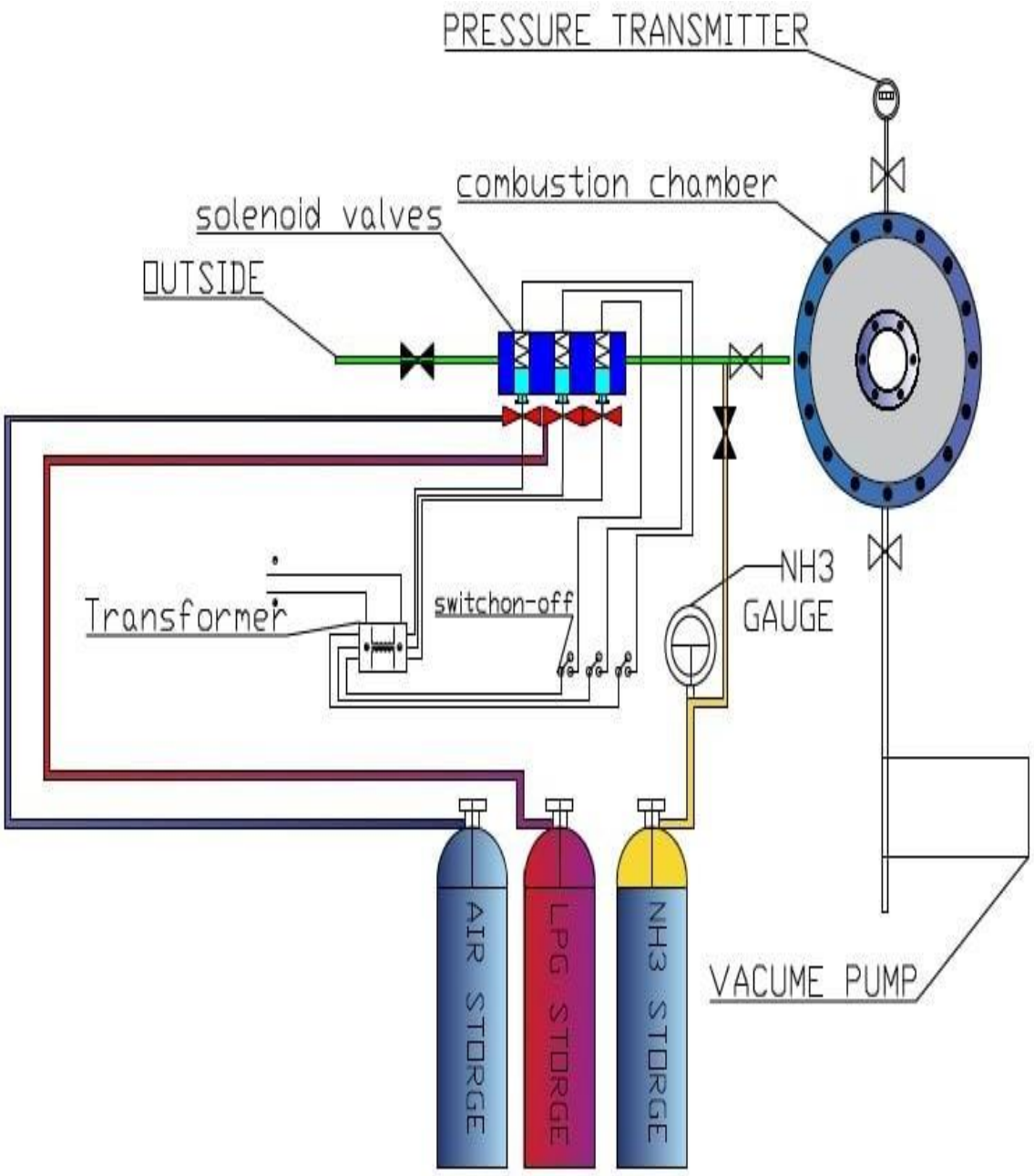

Figure (3.10) Schematic Diagram of the Operation of the Control Unit

3.2.5 Capturing Unit: -

An optical system has been utilized for the visualization and recording of flames and flame flashback process with a camera of high-speed. A source of light and a concave mirror is depending on Schlieren photography from **Bunjong et al. (2018) [80].**

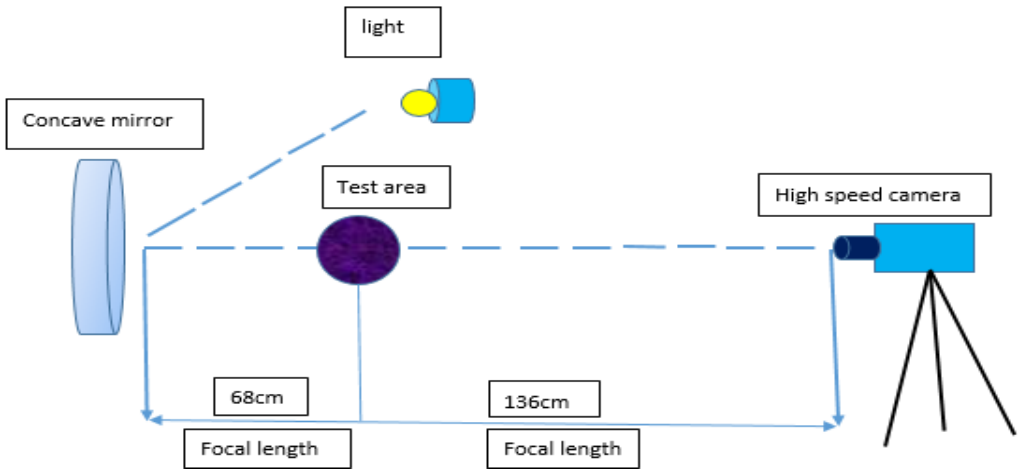

Figure (3.11) Schematic diagram for capturing unit

3.2.5.1 Concave Mirror

A concave mirror is used for the generation of virtual as well as real object images. Parabolic shape focuses the parallel ray's o one point. The mirrors focal length was 68 cm and its diameter 40.5 cm. This mirror is shown in Plate (3.12)

Figure (3.12) Concave mirror

3.2.5.2 Camera and Light Source: -

The high-speed portable camera type (AOS-Q-PRI) with high accuracy of the picture (3 MPixel) and an inner memory of 1.3 GB and 16000 fps. Is used for the purpose of measuring the spread of the flames as can be

As seen from Figure (3.11) the preparation that used in the experiment was 576x500 lams for 4,000 tyros/sec., the total time for recording was 1.10 seconds, and 10% of the time designated as pre-operating for the purpose of ensuring

The fact that all of the operations were recorded in the case of operating the operators, the ignition unit and the camera. A NE-2 Narrator with a size of 5 mm (continuous current 12-volt energy) was placed in a closed box with one exit; a lens (5 mm) focal length placed before the lamp to assemble and then disperse light, then scatter it out.

Figure 3.13: AOS -Q PRI High-Speed Camera.

3.3 Test Procedure: -

The mixing process relies on the Gibbs - Dalton Law for partial pressure of each component of the mixture to obtain a precise parity ratio. The mixture was prepared within the mixing combustion chamber. the total absolute pressure (5bar) per test by: -

3.3.1 Combustion Chamber Preparation Processes

To make a homogenous mixture for exact equivalence ratio Ammonia – LPG – air blending, there are steps to prepare the mixing chamber.

3.3.1.1 Cleaning Process

The outer flanges are opened and then the rig lining is cleaned with a clean cloth to get rid of the soot generated after the explosion process if any, as well as cleaning the windows quartize.

3.3.1.2 Vacuum Process

The vacuum process takes place by closing all the valves except the valves of the vacuum pump and the vacuum gauge so that the pump can sufficiently clarify the combustion chamber from any previous air until its pressure reaches approximately (-0.95 bar). After the unloading process, leave the rig for five minutes, noting the pressure transmitter and tracking the pressure to make sure that there is no leakage of the mixture during the injection process inside the combustion chamber.

3.3.1.3 Mixing Process inside the Combustion Chamber

The gases are admitted into the combustion chamber after it is completely emptied from the air. Ammonia gas is injected, then liquefied petroleum gas, and then air from the special storage tanks for each gas. The mixture enters into the

combustion chamber at required initial pressure, and after that, it closes all the fuses and waits for a period of 10 minutes prior to the ignition for the purpose of stabilizing the mixture, obtaining laminar flame, and sustaining a mixture free of the eddies and turbulence.

3.3.2 Combustion and Recoding Processes: -

The homogeneous mixture was prepared in the preceding steps thereafter.

a) The **i**nitial values of the temperature and pressure shall be adjusted on the initial status of the test**.**

b) The electronic transformer of pressure begins recording the pressure of combustion.

c) Determine the ignition duration (5-second ml).

d) High – Speed camera have to size at the time of formation (1.2) seconds with 10% pre – operability and the illuminating system begins to lighten

e) Both the ignition logging operators and the camera are moved.

f) The data is recorded and photos are captured. Step (a) has been repeated with a variety of initial conditions.

3.4 Analysis Assumption

Laminar burning velocity can be calculated through a series of calculations, from the Schlieren photographs taken during each test. To make use of data from the bomb, many assumptions need to be made. These have been developed by many authors**.** **Huzayyin et al 2008 [60]** which include

1- The non–burned regular gas is in a state of rest in principle .

2-The total mass and volume of the contents of the receptacle are preserved

3-Pressure is supposed to be regular through flame during combustion analysis

4-The mixture is burning in the middle of the pot with a small temperature entrance.

5-The preface of flame extends to the outside spherically and remains the smooth flame speed is fast enough to buoyancy is negligible

6-The flame front itself is an external heat constant system

7- The flame front is infinitely thin

8- No chemical reaction and no dissociation occur in the unburned gas.

9- There is no heat transfer between the zones

3.5 Mixing Ratio and Combustion Processes: -

A MATLAB program was written to calculate the induction pressures of mixing for Ammonia, LPG fuel, and air according to the blend of ammonia. LPG is a mixture of many types of hydrocarbons (Ethan, propane, butane, and pentane)

The volume percentage of a component of LPG is shown in table (3.1). Analysis of LPG components provided from Hilla Gas plant shown in Appendix (B).

Table (3.1) LPG composition

Composition	C_2H_6	C_3H_8	C_4H_{10}	C_5H_{12}
Volumetric fraction %	0.95	66.01	32.42	0.62

The general form of chemical combustion equation

$$JNH_3 + (1\text{-}J)\sum a_I C_{ni} H_{mi} \left[\frac{x}{\emptyset}\right](O_2 + 3.76\, N_2) \rightarrow e_2 H_2O + e_1 CO_2 + e_3 CO + x_1 O_2 + e_4 N_2 \quad (3.1)$$

While:

$$\sum a_I C_{ni} H_{mi} = a_1 C_2H_6 + a_2 C_3H_8 + a_3 C_4H_{10} + a_4 C_5H_{12}$$

Where :

Table (3.2) Symbols Definition

Symbols	Meaning
J	Ammonia volume fraction
Ø	Equivalence Ratio
n_i	Equivalent No. of carbon atoms
m_i	Equivalent No. of Hydrogen atoms
e_2	NO. of moles of H_2O in products
e_1	NO. of moles of CO_2 in products
e_3	NO. of moles of CO in products
e_4	NO. of moles of N_2 in Products
x	NO. of moles of O_2 in reactant
x_1	NO. of moles of O_2 in products

n_i: Equivalent NO. of Carbon atoms= 3.327

m_i: Equivalent NO. of Hydrogen atoms =8.6542

$$x = \frac{J}{2} + (1 - J) * (n + \frac{m}{4}) \quad (3.2)$$

Ammonia fraction J is calculated as: -

$$J = \frac{V_{NH3}}{V_{NH3} + V_{LPG}} \quad (3.2a)$$

Where V_{LPG} and V_{NH3} are the volumes of LPG and Ammonia respectively.

overall equivalence ratio for duel fuel calculated using the equation :-

$$\emptyset = \frac{\left(\frac{F}{A}\right)}{\left(\frac{F}{A}\right)_{st}} \quad (3.3)$$

Daltons Law of partial pressures indicates that the ratio of the partial pressure of the fuel and the air is equal to their molar ratio : -

$$P_f = \left(\frac{nf}{nf + nair}\right) p_{mix} \quad (3.4a)$$

For per unit mole of fuel from equation (3.2)

$$P_f = \left(\frac{1}{1 + (4.76 * x)}\right) p_{mix} \quad (3.4b)$$

For a non – stoichiometric mixture, this is modified to:

$$P_f = \frac{1}{1 + \left(\frac{4.76 * x}{\emptyset}\right)} p_{mix} \quad (3.4.c)$$

While partial pressure for air is calculated from equation (3.4a) the partial pressure of each constituent of the blend can be calculated by the same method

$$P_f = P_{NH3} + P_{LPG} \quad (3.4e)$$

$$P_{NH3} = J + P_f \quad (3.4f)$$

$$P_{LPG} = (1 - J) * P_f \quad (3.4.g)$$

This should be done at a fixed temperature to obtain the best accuracy, although changes in temperature can be compensated in proportion to the temperature accuracy measured before and after each gas added to the mixture, the mixture of NH_3/LPG is prepared in the ratio indicated in table (3.3) volumetric fuel is adjusted to represent the composition.

Table (3.3) tested Fuel Blends

NH3 %	C_2H_6	C_3H_8	C_4H_{10}	C_5H_{12}	Stiochmetric air / fuel ratio (Vol)
0	0.95	66.01	32.42	0.62	14.240
0.1	0.855	59.409	29.178	0.558	15.226
0.2	0.76	52.808	25.936	0.496	16.358
0.3	0.665	46.207	22.694	0.434	17.672

3.5.1 Stoichiometric Mixture are tested and the calculation for each test are shown below

Ideal combustion, where fuel is ideally burned as equal combustion, full combustion is the burning of the air and fuel mass ratio leading to full fuel combustion [81]. Stoichiometric Combustion for LPG gives: -

$$e_1 = (1-J) \cdot \sum a \; n_i \quad (3.5a)$$

$$e_2 = \frac{3J + (1-J) \cdot \sum a \; m}{2} \quad (3.5b)$$

$$e_3 = 0 \quad (3.5c)$$

$$e_4 = 3.76 \frac{x}{\emptyset} \quad (3.5d)$$

$$x_1 = 0 \quad (3.5e)$$

$$x = e_1 + 0.5\, e_2 \quad (3.5f)$$

3.5.2 Rich Mixture are tested and the calculation for each test are shown below

The rich mixture occurs when the amount of air available is lower than the stoichiometric quantity , which means that there is not enough air to burn all available fuel . It is supposed that the hydrogen combines completely with the oxygen and the rest of oxygen does not have sufficient carbon to be burned completely to produce carbon dioxide . This results in partial oxidation of part of the carbon to carbon monoxide .

$$e_1 = 3\frac{x}{\emptyset} - J - (1 - J)\sum a \ (n + \frac{m}{2}) \quad (3.6\ a)$$

$$e_2 = \frac{3J + (1 - J).\sum a \ m}{2} \quad (3.6b)$$

$$e_3 = 3\frac{x}{\emptyset} - e_2 - 2\, e_1 \quad (3.6c)$$

$$e_4 = 3.76 \frac{x}{\emptyset} \quad (3.6d)$$

$$x_1 = 0 \quad (3.6e)$$

$$x = e_1 + 0.5\, e_2 \quad (3.6f)$$

3.5.3 Lean Mixture are tested and the calculation for each test are shown below

A lean mixture means excesses in the available air , where the reaction kinetics and dissociation are neglected . This excess air traverses the process without participating in combustion . However, although it does not react chemically, it has a consequence on the combustion process basically because it reduces the temperature due to its capacity to absorb energy **[81]** The equation for the combustion of a lean mixture is :

$$e_1=(1-J)\,.\,\sum a\ \ n_I \tag{3.7a}$$

$$e_2 = e_2 = \frac{3J+(1-J).\sum a\ \ m}{2} \tag{3.7b}$$

$$e_3 = 0 \tag{3.7c}$$

$$e_4 = \ 3.76\,\frac{x}{\emptyset} \tag{3.7d}$$

$$x = e_1 + 0.5 \tag{3.7 e}$$

$$x_1 = x * (1/\emptyset - 1) \tag{3.7f}$$

3.6 Density Calculations

The density of the burning mixture to the non-burn mixture density is recognized as the density ratio calculated assuming adiabatic equilibrium of burning gases .

Applying ideal gas law for the initial and final state to get ,

$$P_i = \rho\ R\ T_i \tag{3.8}$$

$$R = \frac{R_\circ}{M_w} \tag{3.9}$$

Where R specific gas constant. From equations (3.8 and 3.9) then,

$$(\rho_u)_i = \frac{P*M_{w,i}}{R\circ T} \quad (3.10)$$

The unburned gas density (ρ_u) is computed by using the following equation that derived from Dalton's law :

$$\rho_u = X_{air.}\rho_{air} + X_{fuel.}\rho_{fuel} \quad (3.11)$$

Where X is the mole fraction for each component . This equation can also be used to find the density of burnt mixture at adiabatic flame temperature . The initial and final temperature, the pressure, the components of fuel affect the density ratio and equivalence ratio and density ratio will be: -

$$Density\ Ratio = \frac{\rho_b}{\rho_u} \quad (3.12)$$

3.7 Flame Propagation Analysis

The density ratios obtained from the GASEQ program to be used with the experimental data obtained from analysis of the Schlieren photos to complete the analysis of the process.

3.7.1 Stretched Flame Speed Analysis

The density gradient appears inside the combustion chamber when the flame radius is measured directly by Schlieren photography , the radius of the flame may be in the shadow image, unlike the actual image because the photographic image does not display the edge of the flame directly.

Flame radius is measured from Schlieren photography , the laminar flame speed (S_n) from the radius – time of flames.

$$Sn=\frac{drsch}{dt} \quad (3.13)$$

The stretched flame speed is calculated using software (Tracker version 4.87) to collect the Cartesian coordinates , by observing the front of the flame for each subsequent frame, then the film is recorded by the high-speed camera and the output data would be (S_n, r, and t) the table (3. 4) shows the setup of the Tracker Software and how to measure the speed of the flame.

$$S_n = \frac{dr}{dt} = \frac{rj+1-rj}{tj+1-tj} \quad \rightarrow \quad (3.14)$$

The mean radius is assumed to be the radius that corresponds this speed.

$$R_{(j+1/2)} = \frac{rj+1+rj}{2} \quad \rightarrow \quad (3.15)$$

The data are necessary as a result of this method, the data is dispersed, making it impossible to see a distinct pattern, because of averages of four half–diameters for time per direction to calculate the speed of the flame given by.

$$S_n = \frac{dr}{dt} = \frac{\left((r_{i,j+n+1} - r_{i,j+n+2}) + (r_{i,j-n-1} - r_{i,j-n-2}) + (r_{i+n+1,j} - r_{i+n+2,j}) + (r_{i-n-1,j} - r_{i-n-2,j})\right)/4}{t_{j+1} - t_j} \quad (3.16)$$

The only advantage of the average technique with the tracking software is particularly sensitive to small elevations compared to the endpoints. Large radius effect becomes apparent due to the consequences of the thickness of the electrical code and this increase the error due to a lack of the clarity in the photograph on film and could arise from multi-sources.

Table (3.4) Setting of Tracker Software that Measuring Flame Speed.

Clip Setting	
Start frame	**Changeable**
Step size	**5(frame)**
End frame	**Changeable**
Start time	**Changeable**
Frame rate	**4000f/s**
Frame dt	**2.50E-4s**

3.7.2 Flame Stretched Rate and Markstein Length

A general stretch at any point on the surface of the flame is defined as the Lagrangian time derivation of the logarithm of area (A) of any small element on the surface [35].

$$\alpha = \frac{d(lnA)}{dt} = \frac{1}{A}\frac{dA}{dt} \qquad (3.17)$$

For the outwardly propagating spherical flame, the flame stretch rate can be deduced in the following form .

$$\alpha = \frac{1}{A}\frac{dA}{dt} = \frac{2}{ru}\frac{dr}{dt} = \frac{2}{ru}\,Sn \qquad (3.18)$$

The flame stretch rate α points out the expanding rate of the area of flame for spherically expanding flame. Flame stretch rate expressions, regarding the purposes an appropriate unified tensor expression, regarding .

the strain rate tensor α_s and the stretch rate due to flame curvature, α_c that is

$$\alpha = \alpha_s + \alpha_c \quad (3.19)$$

During the pre-pressure period, there exists a linear relationship between the flame propagation speed and the stretch rate: that is

$$S_l - S_n = L_b \alpha \quad (3.20)$$

The unstretched propagation speed, $S_{l,}$ can be obtained as the intercept at $\alpha=0$ value in the plot of S_n against α. The burned gas Markstine length L_b, is the negative slope of the $S_n - \alpha$ fitting curve **[35].** Markstine length can be defined as the decrease in burning velocity per unit stretch .

3.8 Laminar Burning Velocity

In the initial stage of flame propagation, the total volume of the burned gases is around 0.5% of the volume of the combustion chamber , the unstretched laminar burning velocity, u_l, is related to S_l through the mass conservation across the flame front.

$$A \rho_b S_l = A \rho_u u_l \quad (3.21)$$

Where A is the flame front area, $\rho_{u,}$ and ρ_b are the unburned and burned gas densities respectively. The unstretched laminar burning velocity can be get from equation (3.22), **[82]**.

$$u_l = S_l \frac{\rho b}{\rho u} \quad (3.22)$$

3.9 Calibration

The term calibration is defined as "a test during which the known measurement values are applied to the energy transformer and corresponding release readings are recorded under specific circumstances". To ensure that all data is read from meters and sensors, calibration has been conducted for all the measuring devices and sensors.

3.9.1 Pressure Gauge Calibration (QYB102 Pressure Transmitter)

The calibrating operation for this device is to be tested by Central Organization for Standardization and Quality Control (COSQC) as shown in appendix (A).

3.9.2 Ammonia Gauge Pressure

The calibrating operation for this device is to be tested by Central Organization for Standardization and Quality Control (COSQC) as shown in appendix (A).

3.9.3 Camera Calibration: -

The calibrating operation for this device is made by the same company that manufactured the device as shown in appendix **(A).**

CHAPTER FOUR RESULTS AND DISCUSSION

CHAPTER FOUR

RESULTS AND DISCUSSION

4.1 Introduction

The experimental results regarding laminar flame propagation and laminar burning velocity will be displayed and analyzed in this chapter. The flame is initiated by spark plug and spread in the (LPG - NH_3 - Air) mixture the combustion process is tested using a photographic approach after being ignited by central electrodes. At varied initial pressures ranging (100 , 200 , and 300) kPa, the flame speed and laminar burning velocity were measured. The initial mixture temperature was 298 K Three NH_3 blending ratios (NH_3 10 %, 20%, and 30%) with LPG and with different equivalence ratio were tested.

4.2 Experimental Results

4.2.1 Repeatability Test

Experimental apparatus is specifically designed and built for this study. A repeatability test of one case study is used to confirm the rig validity and measurement accuracy. Previously mentioned, the mixture is prepared inside the CVC. The mixing process is based on the partial pressure blending method. Seven experiments for the CC. the repeatability results are reasonable.

4.3 Validation

Figures (4.1a,4.1b,4.1c) show a comparison between the results obtained from present work with results obtained of other researchers. Figure (4.1a) display the relation between equivalence ratio and burring velocity for pure NH_3 with the initial pressure at 100kPa and temperature 298K. it shows a comparison between the results of present work and the results by **([66]** Hayakawa).

The Figure shows that when the equivalence ratio is unity the burning velocity is maximum. Figure (4.1b) shows the behavior of the result obtained by Okafor [83] , for mixtures of 10%NH_3 and 90% CH_4,20%NH_3 and 80% CH_4 and 30% NH_3 and 70% CH_4 at initial pressure of (100kPa) The figure shows that as the equivalence ratio increases.

The burring velocity increases When the closer to the stoichiometric mixture ,and Figure (4.1c) shows clearly a good match between the present work and result of Akihiro Hayakawa **[66]** .

It shows the equivalence ratio and Markistne Length for mixture of pure N H_3 and Air with initial pressure 100 kPa .

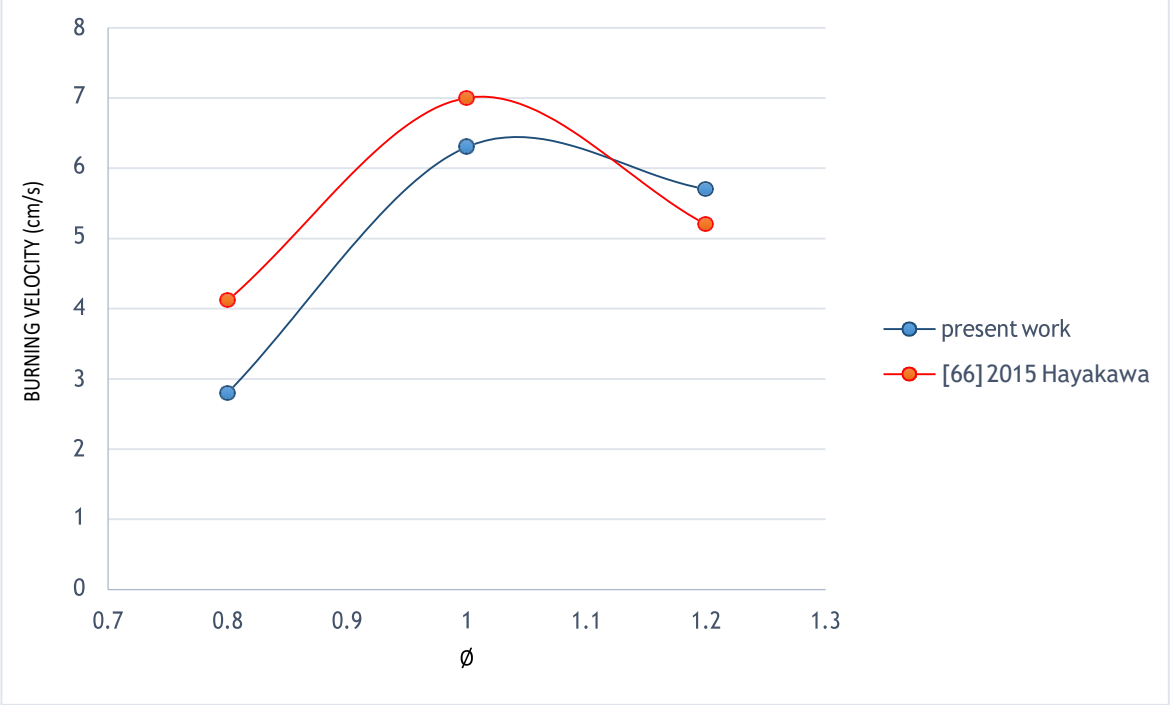

Figure (4.1a) displays the relation between equivalence ratio and burring velocity for pure NH_3

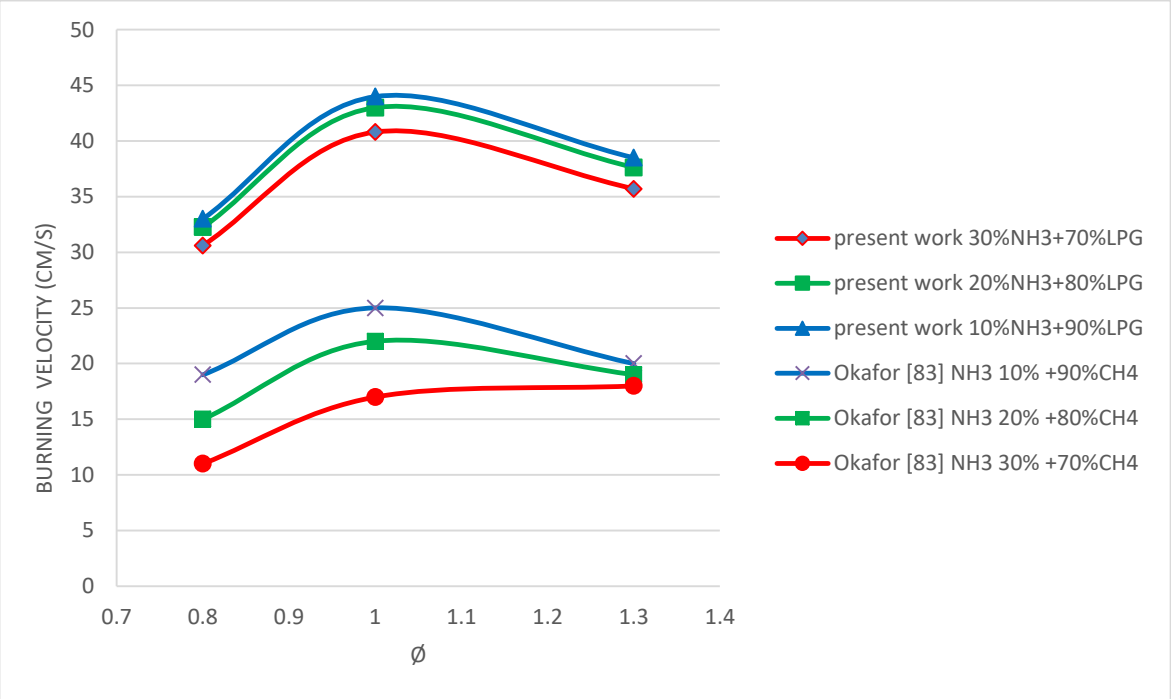

Figure (4.1b) behavior of the result obtained by Okafor [83]

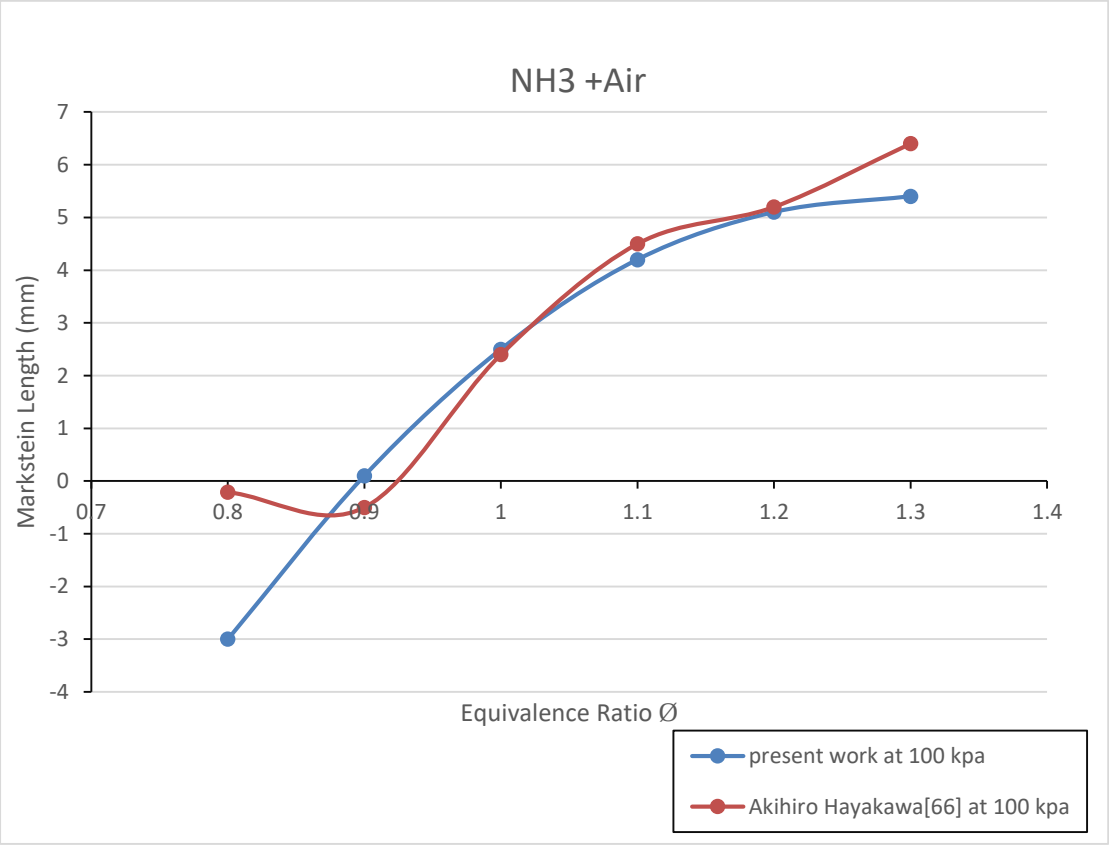

Figure (4.1c) Comparison between the present work and result of Akihiro Hayakawa [66]

4.2.2 Flame Speed Analysis

The results of the expanding spherical flame experiments are presented in this section. After the spark occurs, ignition takes place in the center of the chamber, and the propagates spherically to the whole mixture.

As a typical case of flame propagation, Figure (4.2)shows a sequence of frames of an expanding spherical flame of ammonia / LPG /air mixture for different equivalence ratios. It can be seen that the Schlieren flame images show a disk whose diameter increases with time. The flame image analysis can then be performed to deduce the evolution of flame radius versus, hence the spatial flame speed is evaluated as the rate of variation.

The data obtained from photographs is the radius of expanding flame as a function of time for each run. However, consideration of figures (4.3) shows a plot of the experimental values of flame radius against time for the NH_3 /LPG/air fuel at the stoichiometric mixture for different initial pressure

These figures indicate that the increase of initial pressure flame radius decreased.

The stretched flame speed is calculated using software (Tracker version 4.87) to collect the Cartesian coordinates , by observing the front of the flame for each subsequent frame, then the film is recorded by the high-speed camera and the output data would be (S_n, r, and t).

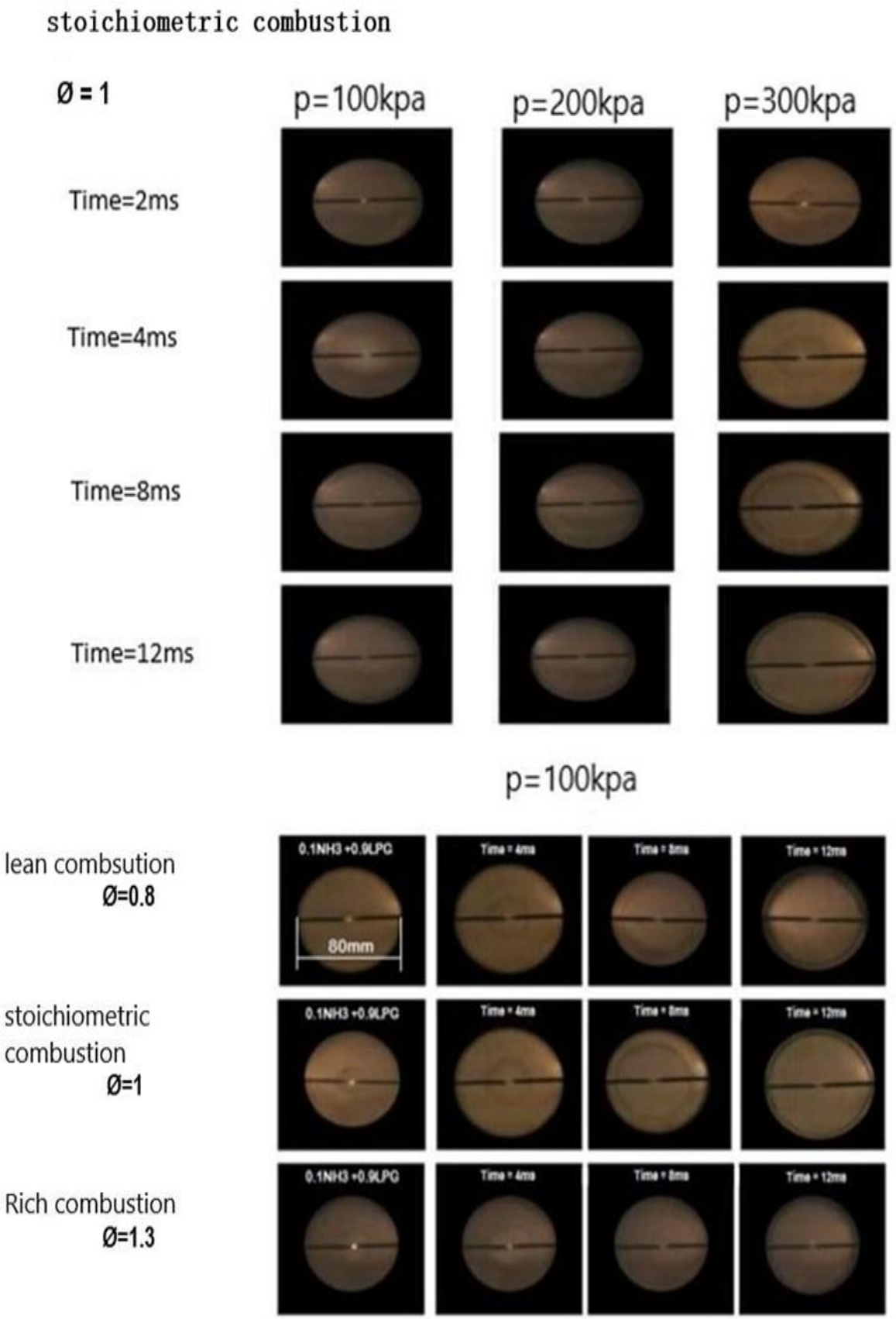

Figure (4.2): Shows a sequence of frames of an expanding spherical flame of (NH_3 and LPG) for different equivalence ratios .

The flame spread area was classified into three regions according to the value of the flame radius, as the first region starts from a radius of value starting from 0-5 mm, and this area is outside the results as it is within the effect of the ignition spark.

As for the second region, it starts from the values of a radius of 5-20 mm, as this region is considered the most important region in the study, where the effect of adding ammonia concentrations is clear.

The third region, which has a flame radius exceeds 35 mm, where this region is where the flame is stable, but outside these values, it is outside the study. It is impossible to measure because of the dimensions of the combustion chamber. The first and third region are to be out of the calculation as shown in table (4.1)

Table (4.1) Flame propagation regions

Region r (mm)	0-5	5-20	20-35	35-	note
Initiation region	Out of study	The effect increases 15mm at 30% NH3			Spark energy causes increases in flame speed
Pre-pressure region		Study region			Stable flame at 20 mm
Cellularity region				Out of study	Out of pre-pressure period

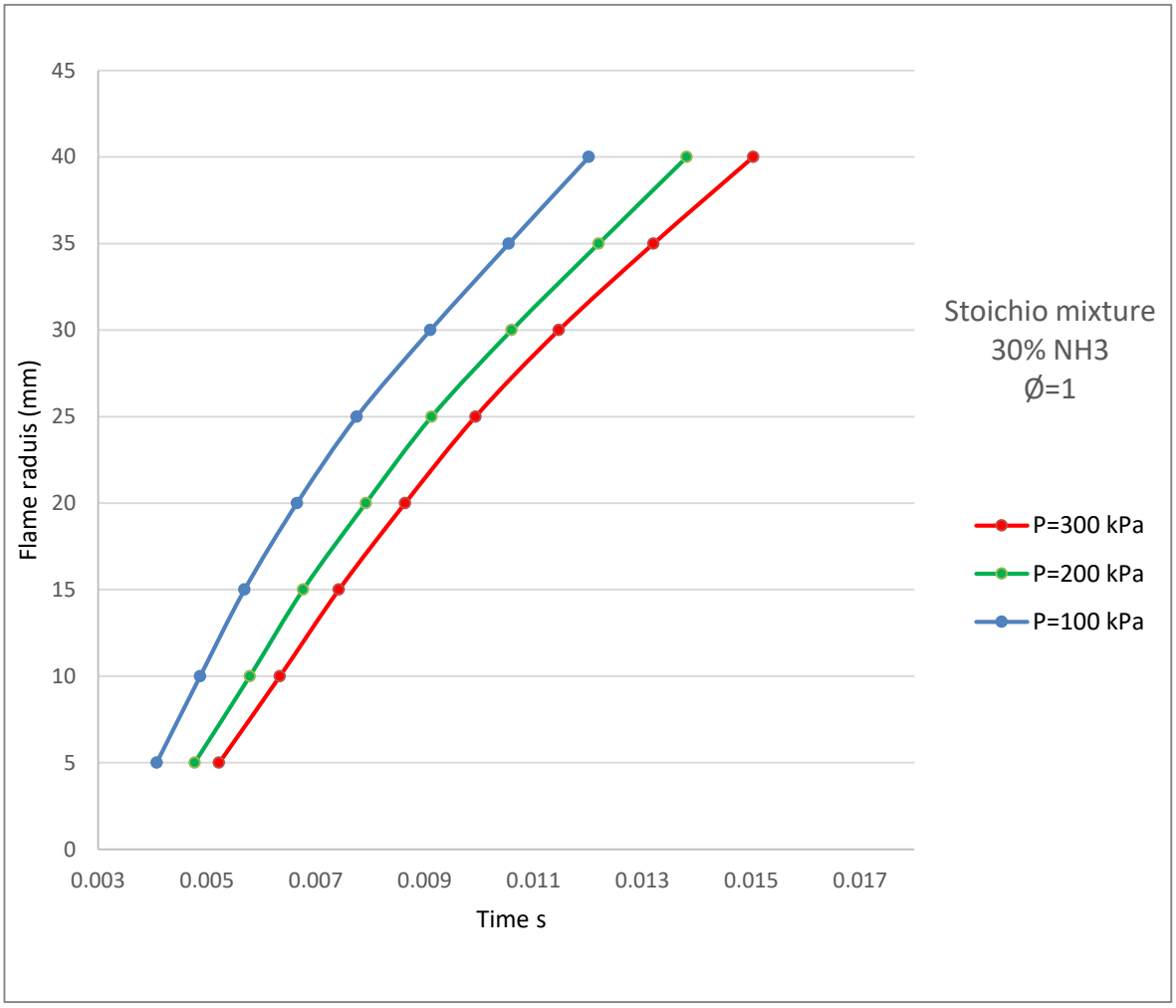

Figure (4.3) Flame radius and Time for 70%LPG + 30%NH_3 at equivalence ratio Ø=1 with initial pressure (100 , 200 and 300) kPa

Figure (4.3) it's clearly shown as increase of the initial pressure flame radius decreased, this is due to the increase in density which more chemical reaction. The experimental flame speed for versus equivalence ratios limits is illustrated in Fig (4.6) , (4.14) and (4.22) for NH3 with many LPG blending ratios at a multi initial pressure. The figure shows that the flame speed increases as the mixtures go from the lean limits (Ø = 0.8) towards the stoichiometric mixture, and then decreases as approaches for rich mixtures (Ø =1.2). Figure (4.14), (4.15), and (4.16) show that the stoichiometric mixture for any blend of NH3 has a higher flame speed than lean or rich mixtures.

4.2.3 Stretched Laminar Flame Speed

Stretched flame speed (Sn) has been measured experimentally inside the combustion chamber. The effects of combustion chamber size, initial pressure, fuel type, ammonia / LPG / air blending ratio at different equivalence ratios upon the Sn have been investigated.

To summarize, for each set of conditions the Sn is plotted versus radius for varying stoichiometry, fuel types, initial pressures, and ammonia blending ratios Generally, the flame propagation speed increases gradually with the increase in the spherical flame radius.

The results show that flame speed decreases as the initial pressure increases. To identify the cause of the initial pressure effect, the flame temperature is insensitive to changes in initial pressure. The initial and final temperature change hence the branching reactions. The effects of initial pressure on the laminar flame speed of NH_3-air mixture blends with LPG for different equivalence ratios are demonstrated in Fig (4.8) and (4.16). Fig (4.24) presents the flame speed for the difference between NH_3 blends and initial pressure. The effect of NH_3 on flame speed becomes more obvious at a blending ratio higher than (30%). The results also show that the flame speed decreases with increasing pressure for any stoichiometry.

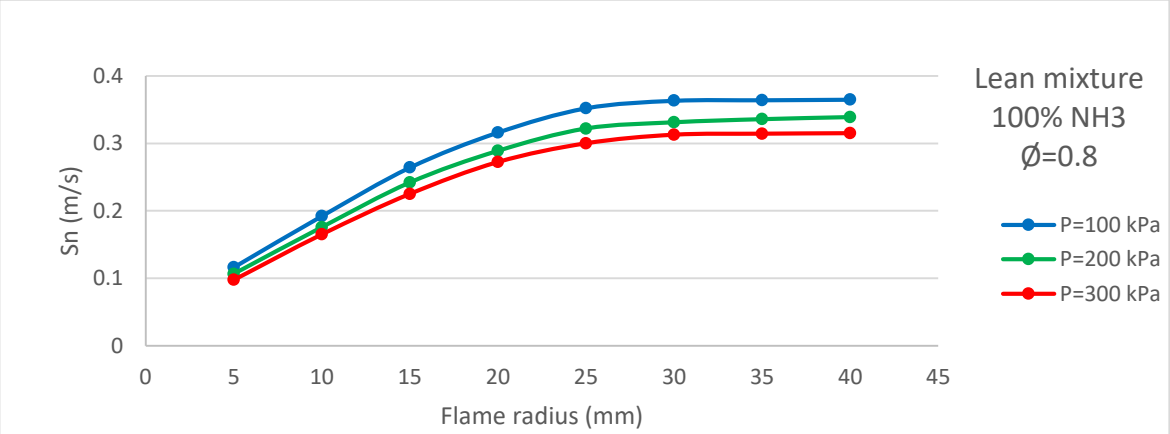

Figure (4.4) laminar flame speed S_n with a flame radius for 100% NH_3 at Ø=0.8

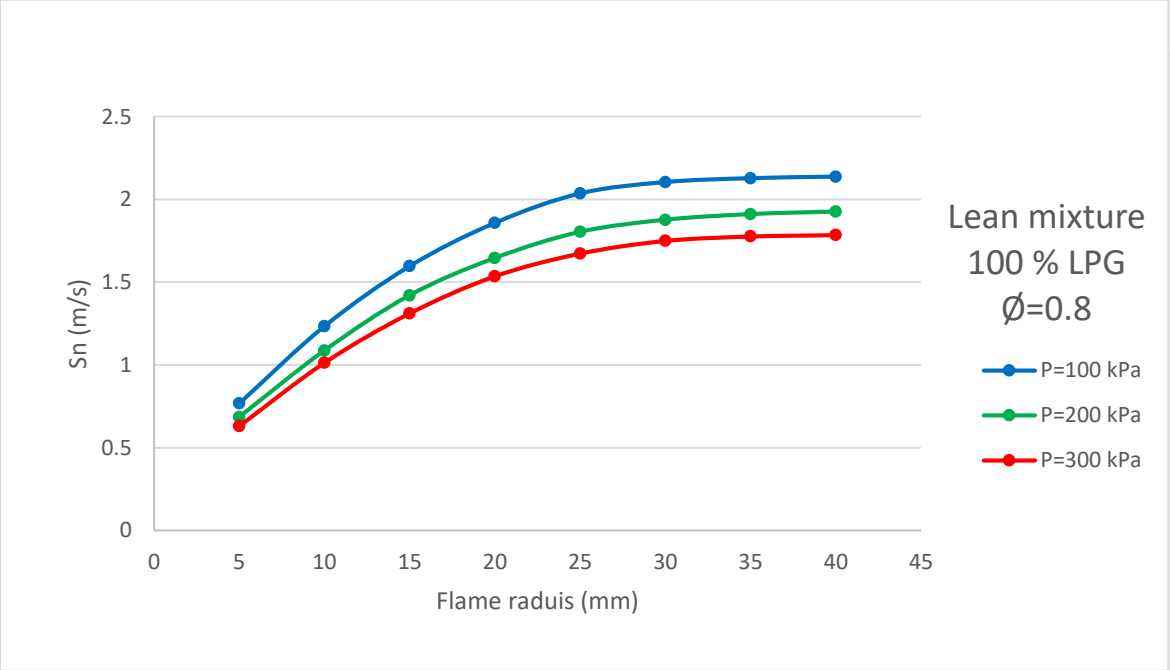

Figure (4.5) laminar flame speed S_n with a flame radius for 100% LPG at Ø = 0.8

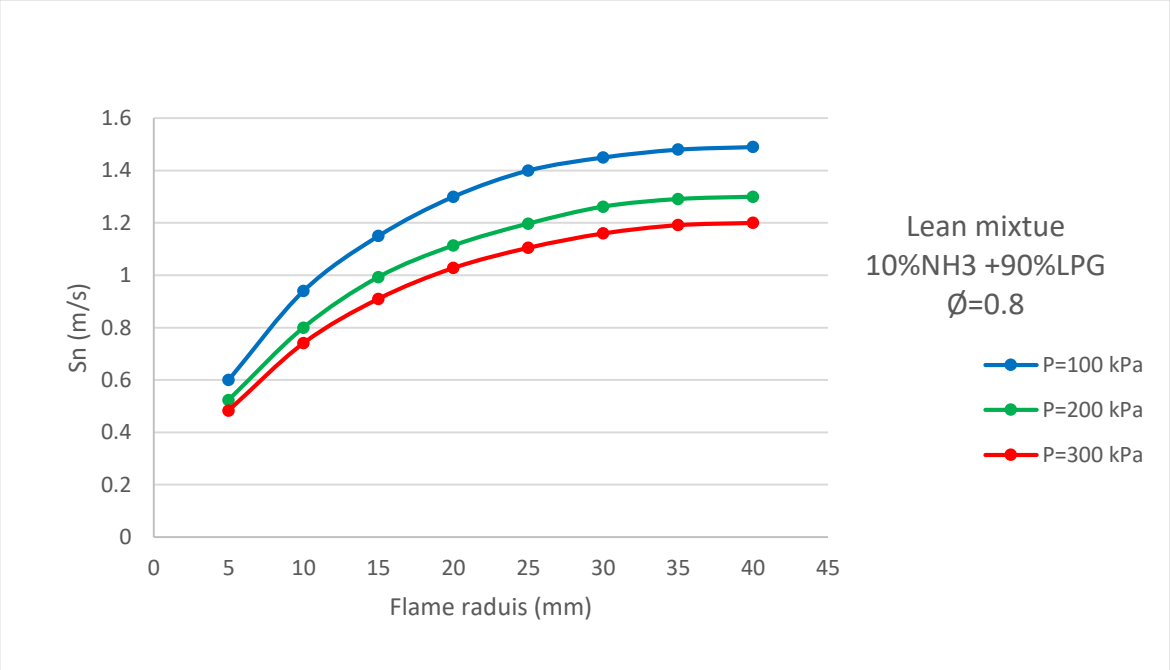

Figure (4.6) laminar flame speed S_n with a flame radius for 10% NH_3 and 90% LPG at Ø = 0.8

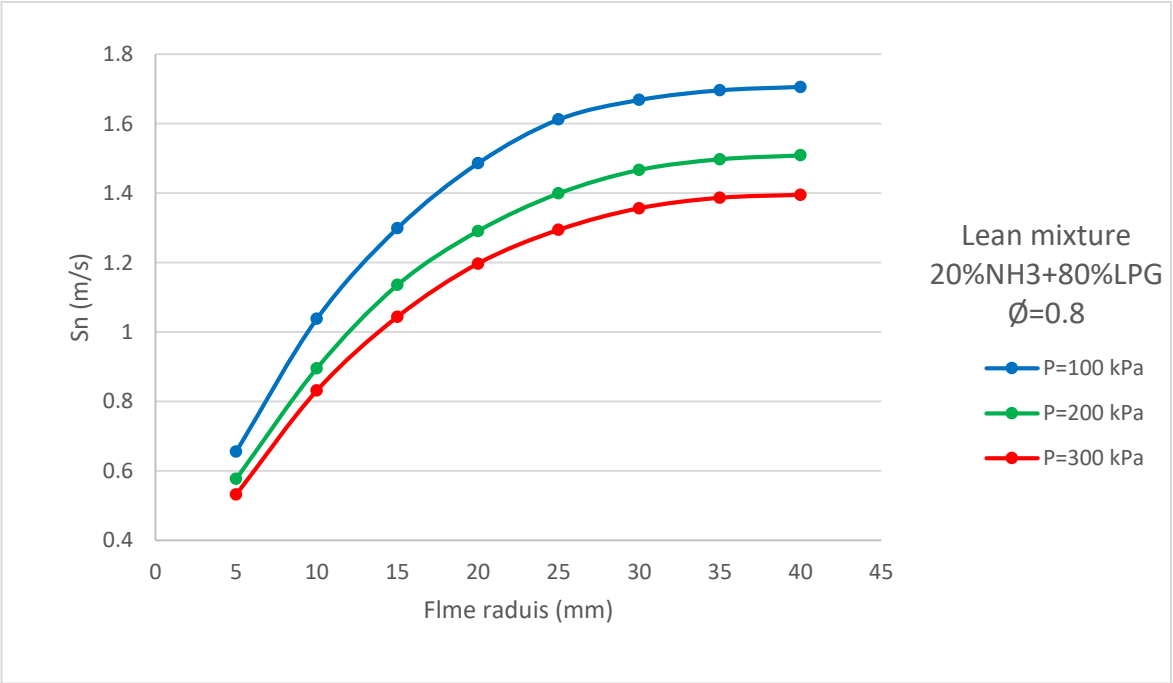

Figure (4.7) laminar flame speed S_n with a flame radius for 20% NH_3 and 80% LPG at Ø = 0.8

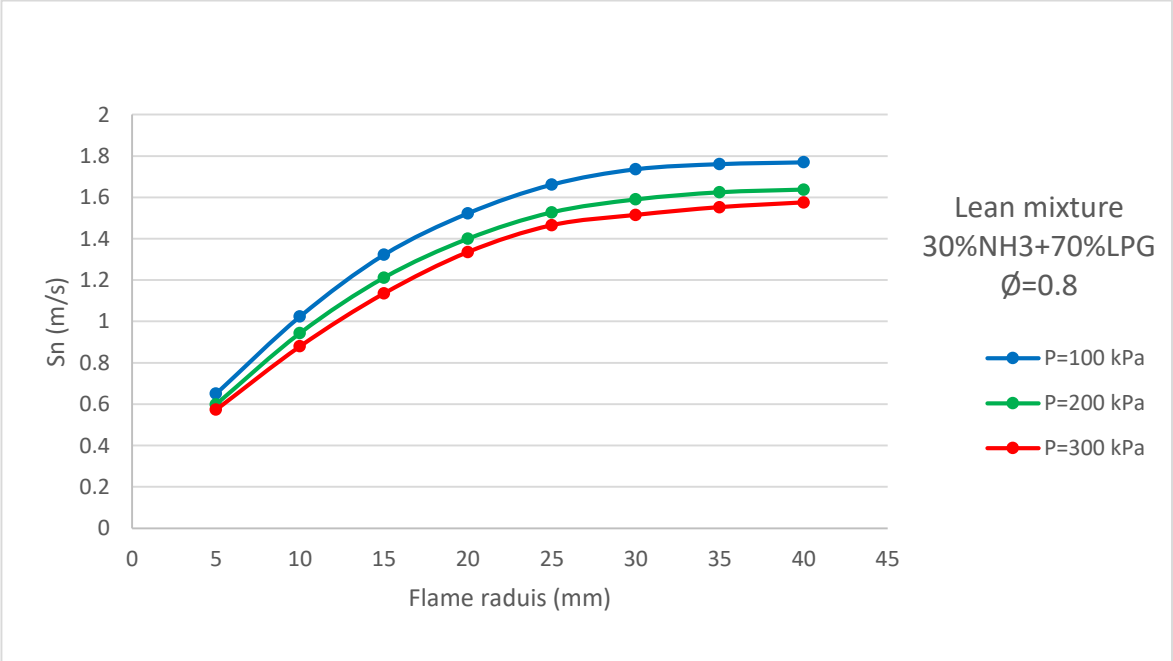

Figure (4.8) laminar flame speed S_n with a flame radius for 30% NH_3 and 70% LPG at Ø = 0.8

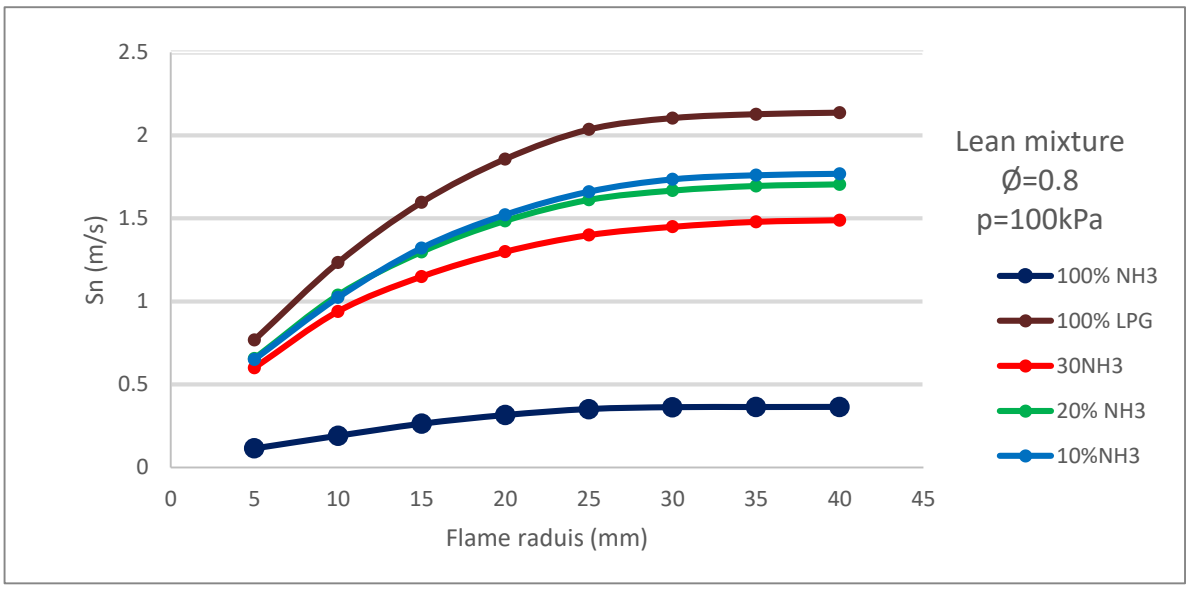

Figure (4.9) laminar flame speed S_n with a flame radius for Lean mixture at Ø = 0.8 and initial pressure 100 kPa

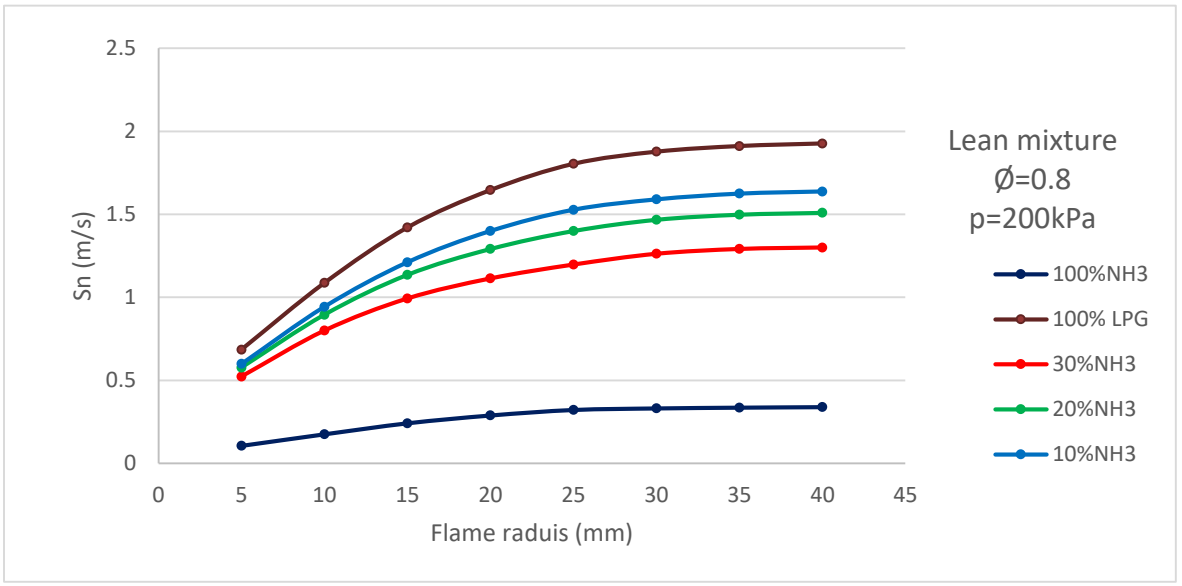

Figure (4.10) laminar flame speed S_n with a flame radius for Lean mixture at Ø =0.8 and initial pressure 200 kPa

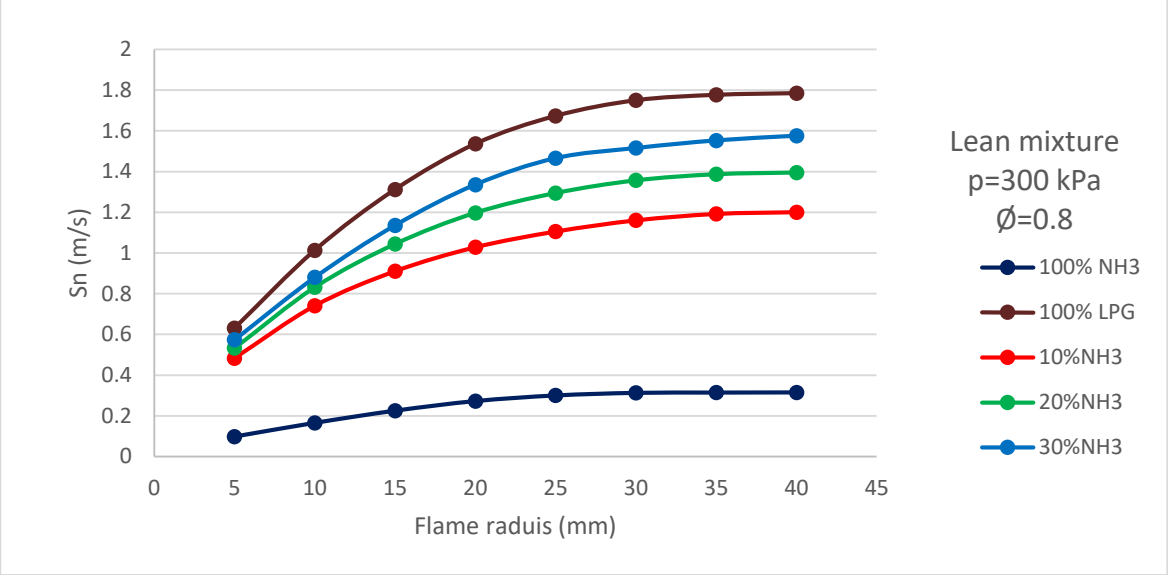

Figure (4.11) laminar flame speed S_n with a flame radius for Lean mixture at Ø = 0.8 and initial pressure 300 kPa

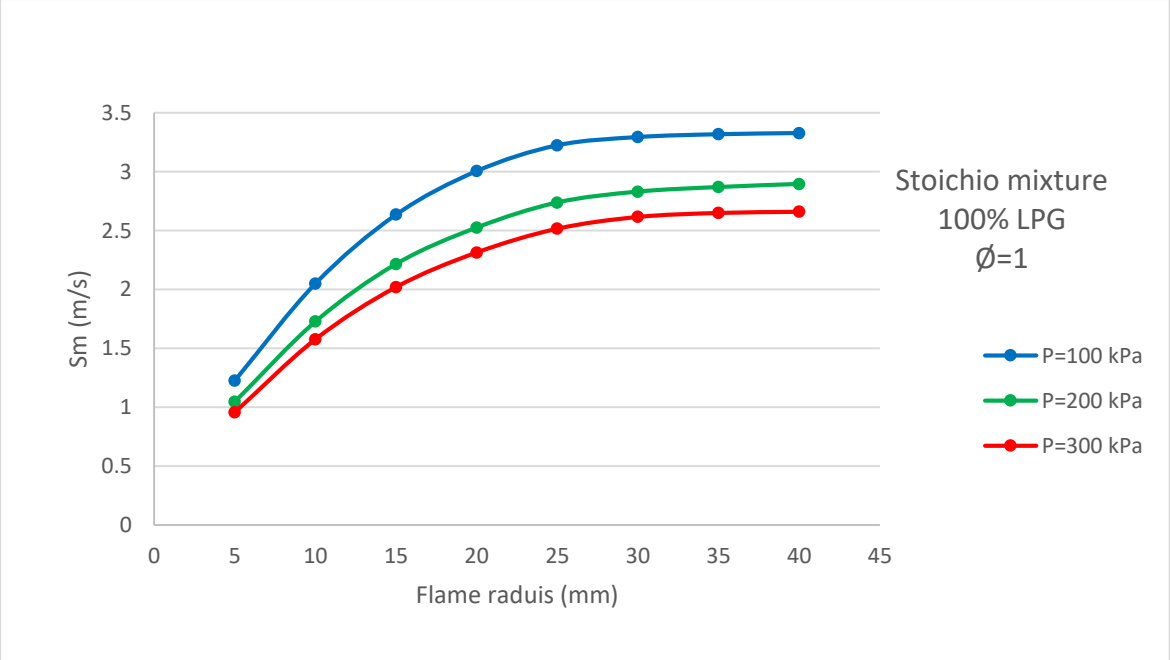

Figure (4.12) laminar flame speed S_n with a flame radius for 100% LPG at Ø=1

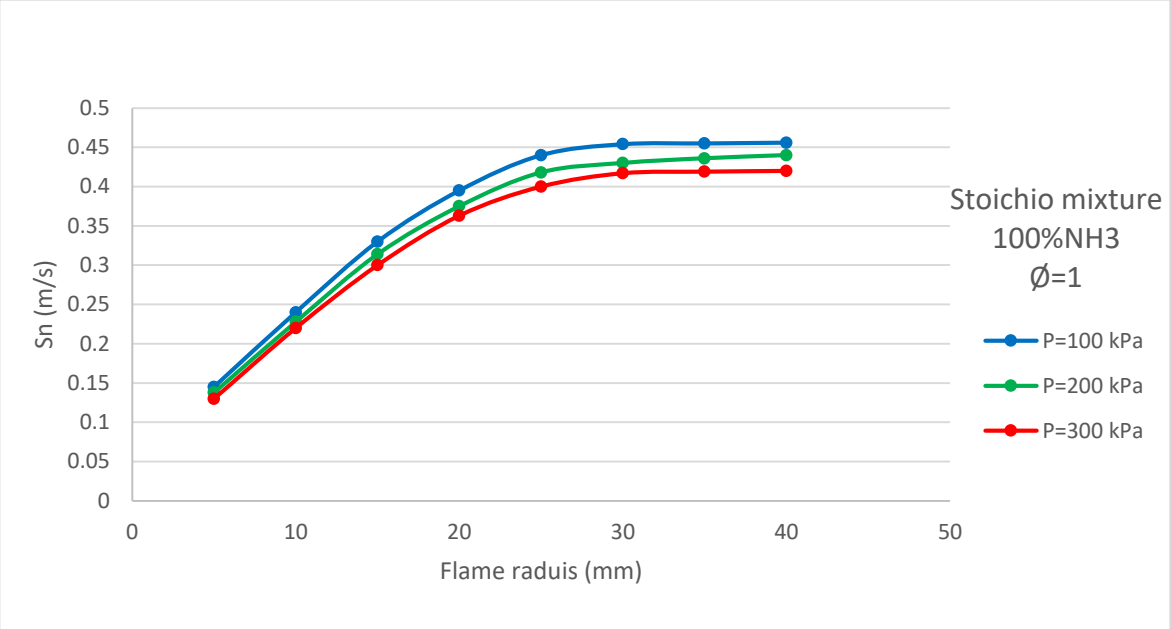

Figure (4.13) laminar flame speed S_n with a flame radius for 100% NH_3 at Ø=1

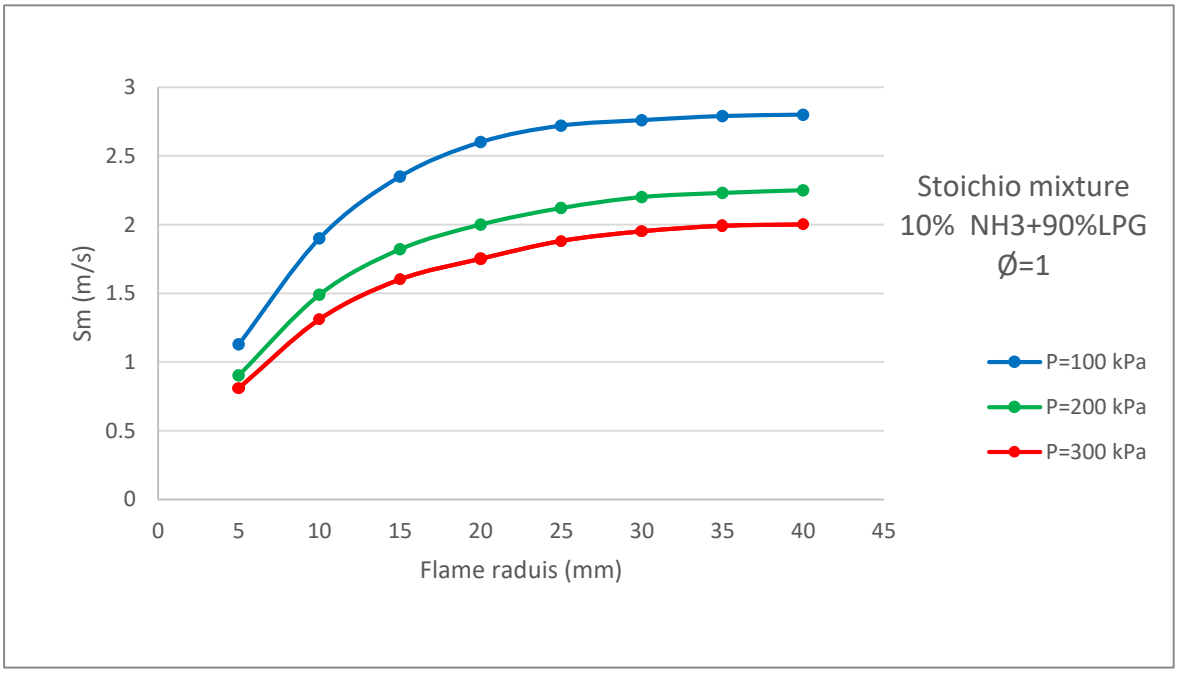

Figure (4.14) laminar flame speed S_n with a flame radius for 10% NH_3 and 90% LPG at Ø = 1

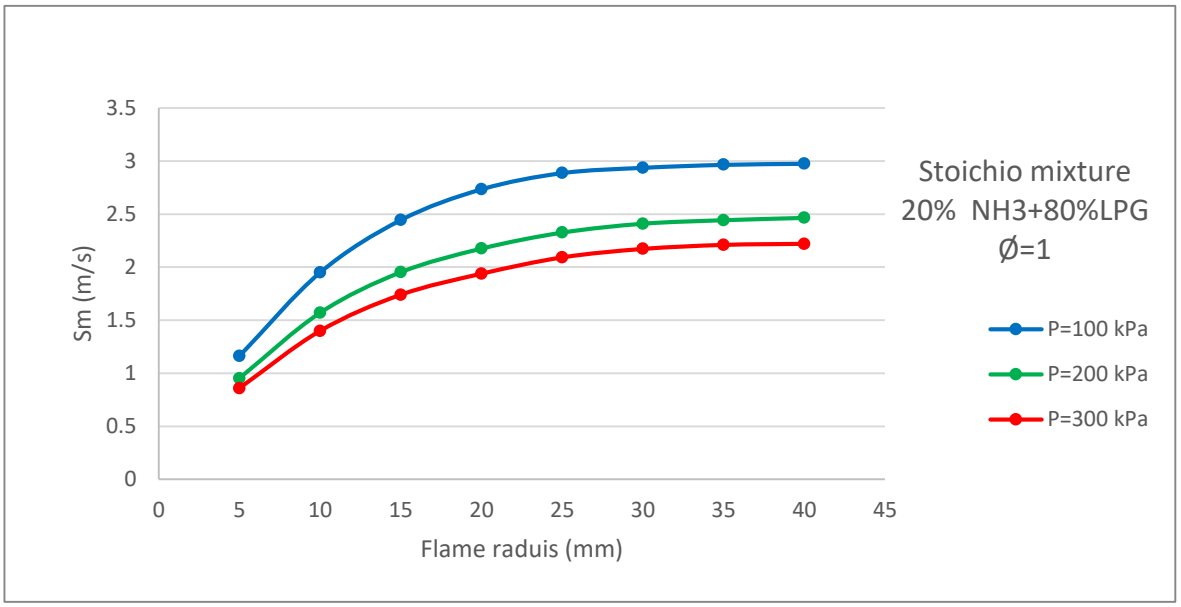

Figure (4.15) laminar flame speed S_n with a flame radius for 20% NH_3 and 80% LPG at Ø = 1

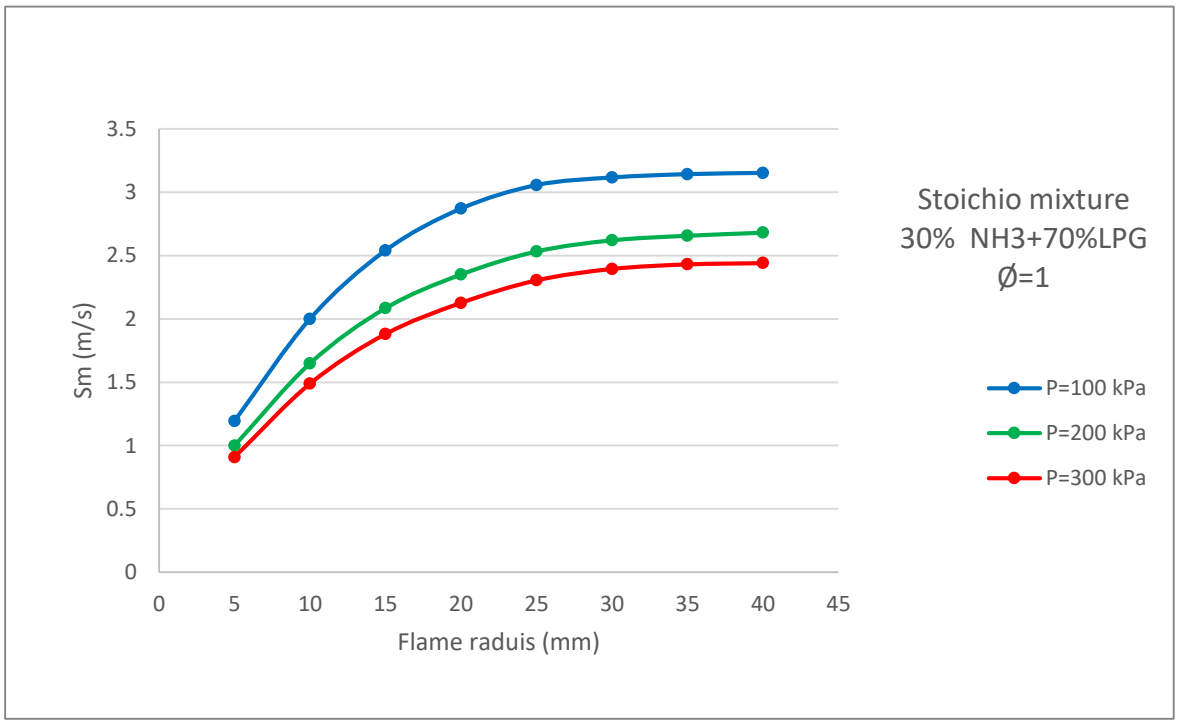

Figure (4.16) laminar flame speed S_n with a flame radius for 30% NH_3 and 70% LPG at Ø = 1

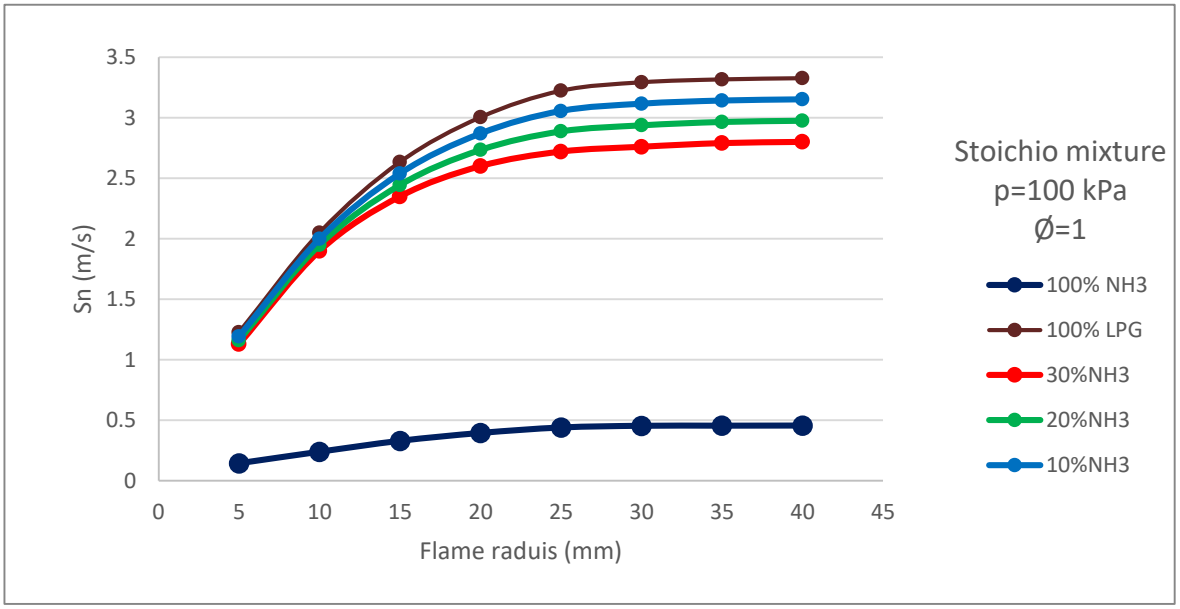

Figure (4.17) laminar flame speed S_n with a flame radius for Stoichio mixture at Ø = 1 and initial pressure 100 kPa

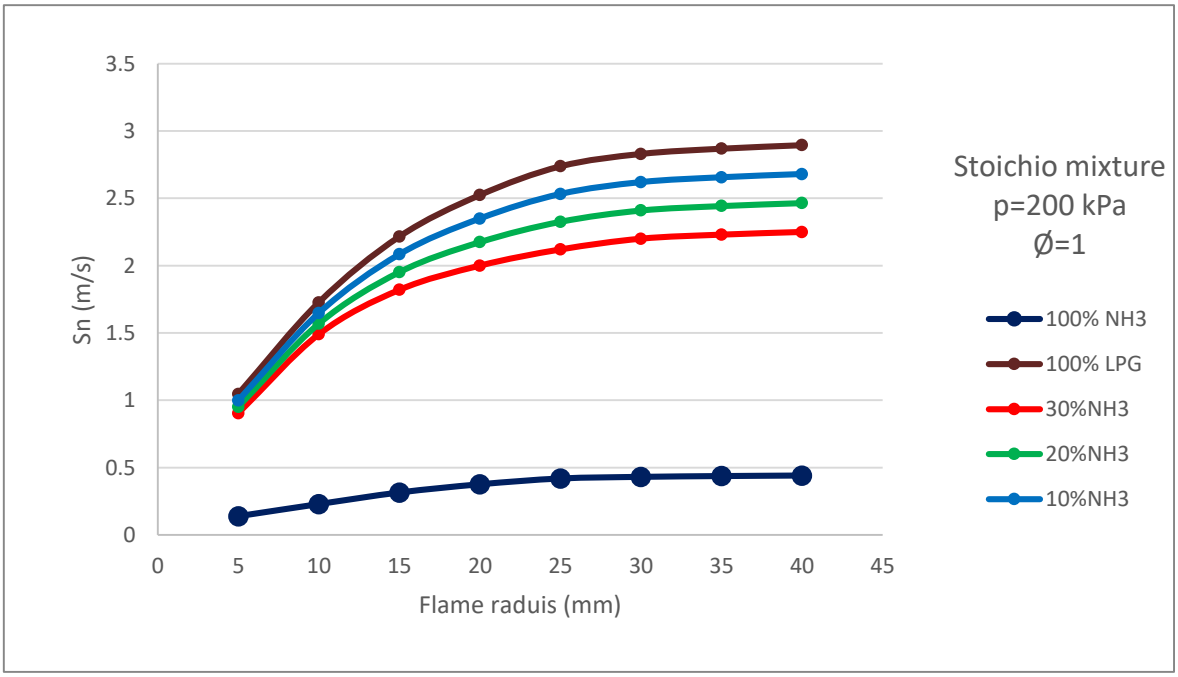

Figure (4.18) laminar flame speed S_n with a flame radius for Stoichio mixture at Ø = 1 and initial pressure 200 kPa

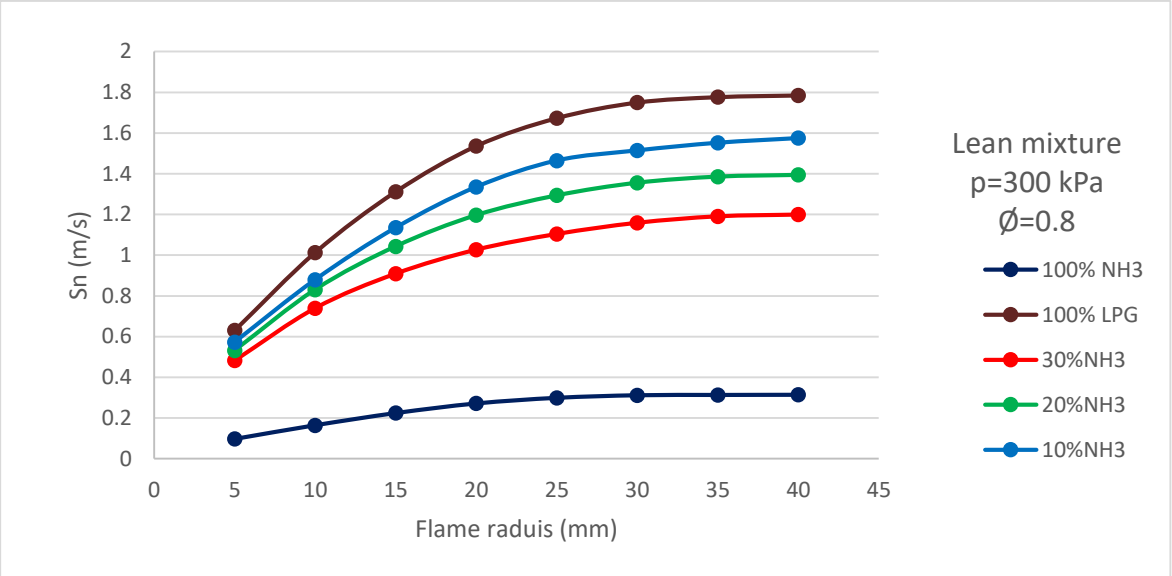

Figure (4.19) laminar flame speed S_n with a flame radius for Stoichio mixture at Ø = 1 and initial pressure 300 kPa

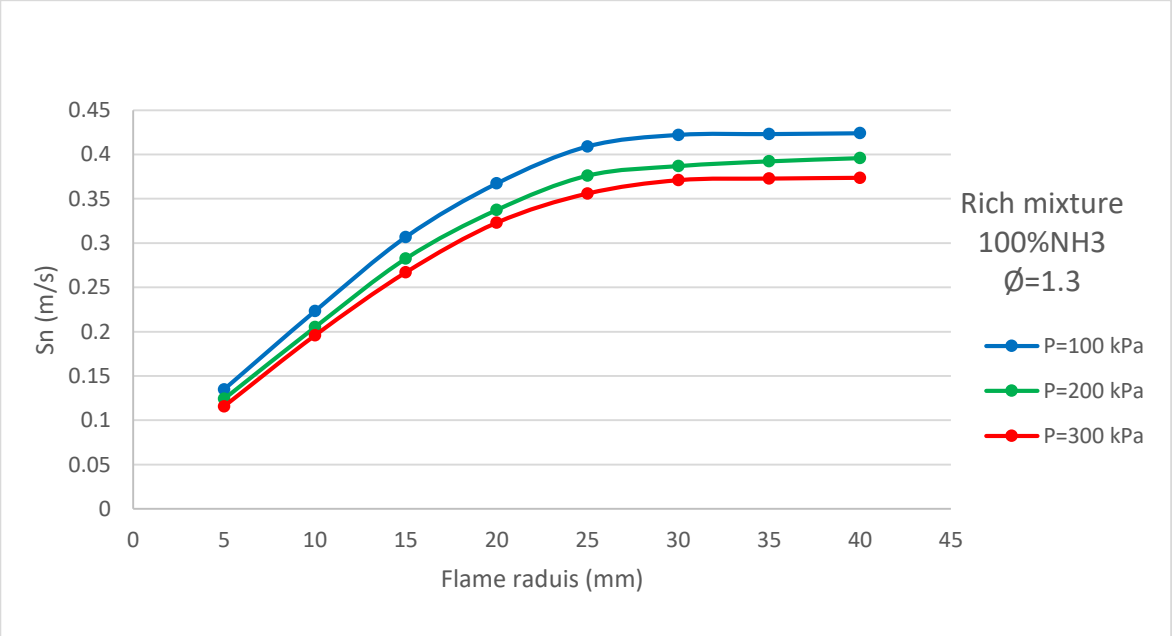

Figure (4.20) laminar flame speed S_n with a flame radius for 100% NH_3 at Ø = 1.3

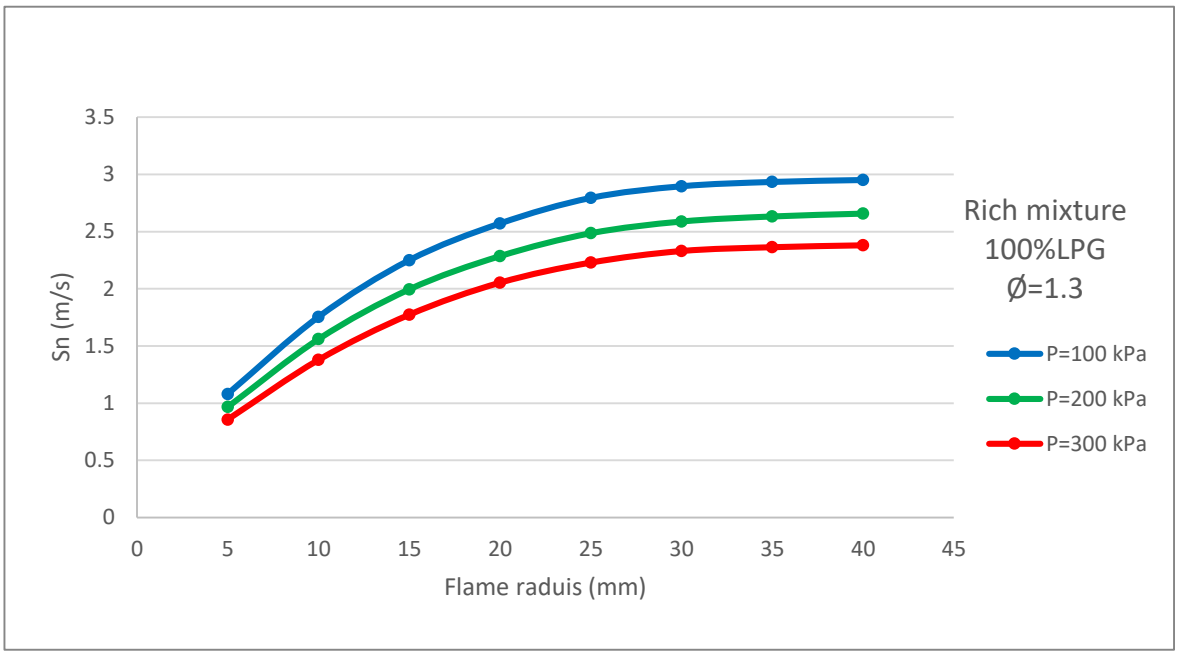

Figure (4.21) laminar flame speed S_n with a flame radius for 100% LPG at Ø = 1.3

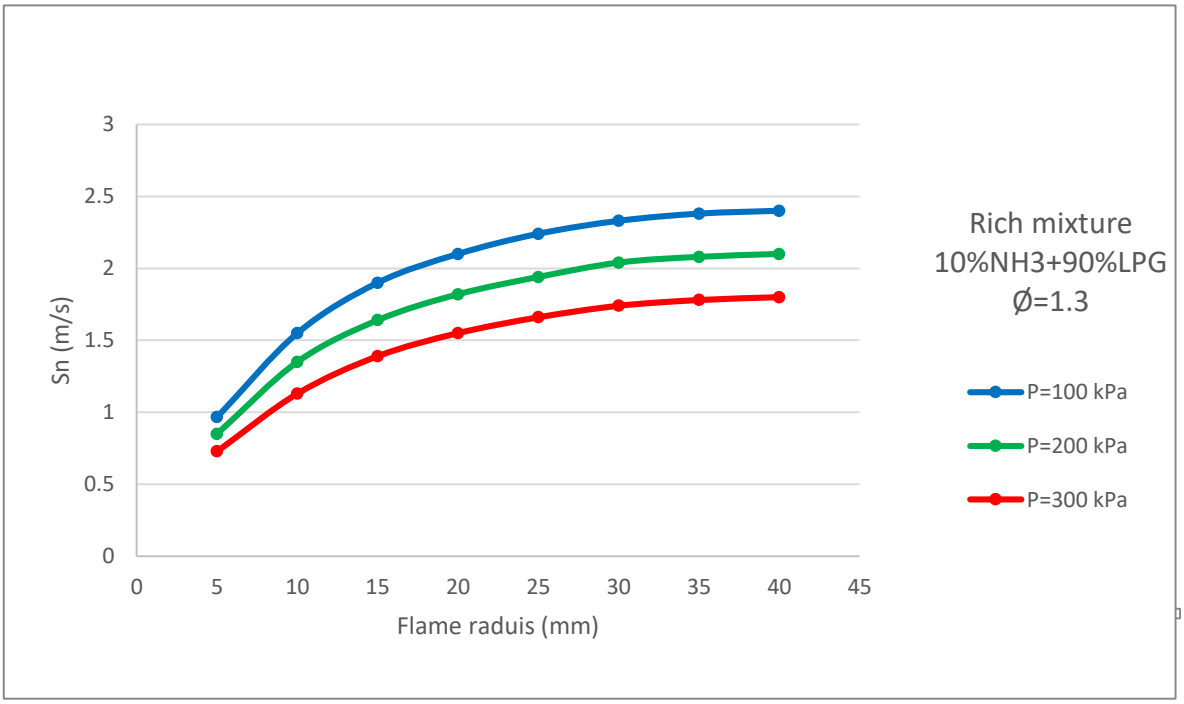

Figure (4.22) laminar flame speed S_n with a flame radius for 10% NH_3 and 90% LPG at Ø = 1.3

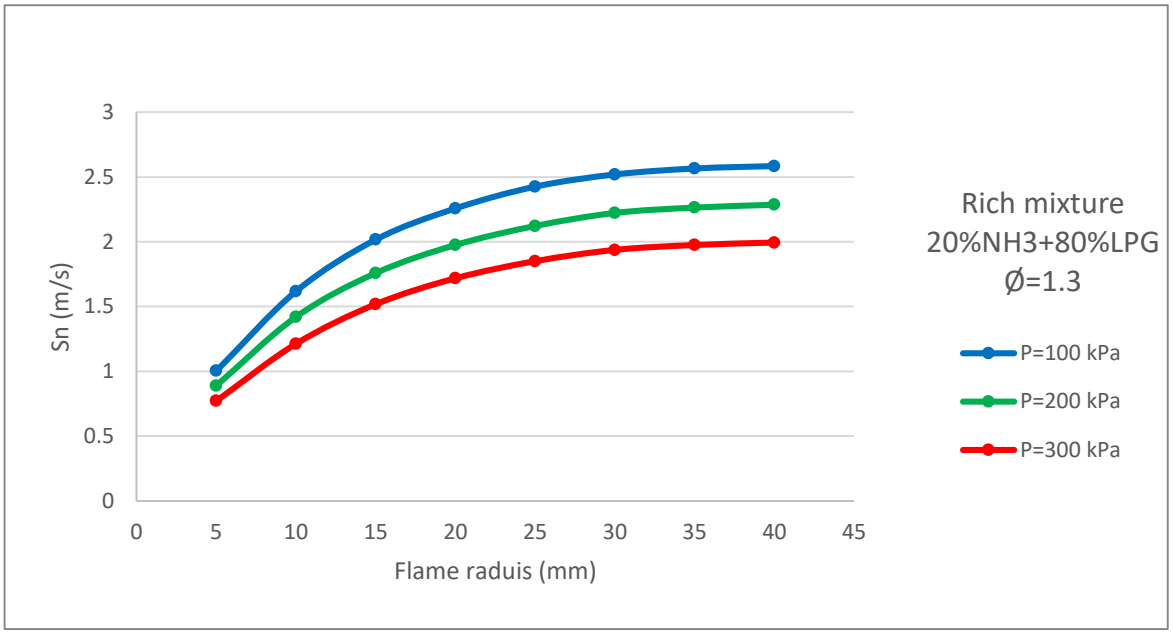

Figure (4.23) laminar flame speed S_n with a flame radius for 20% NH_3 and 80% LPG at Ø = 1.3

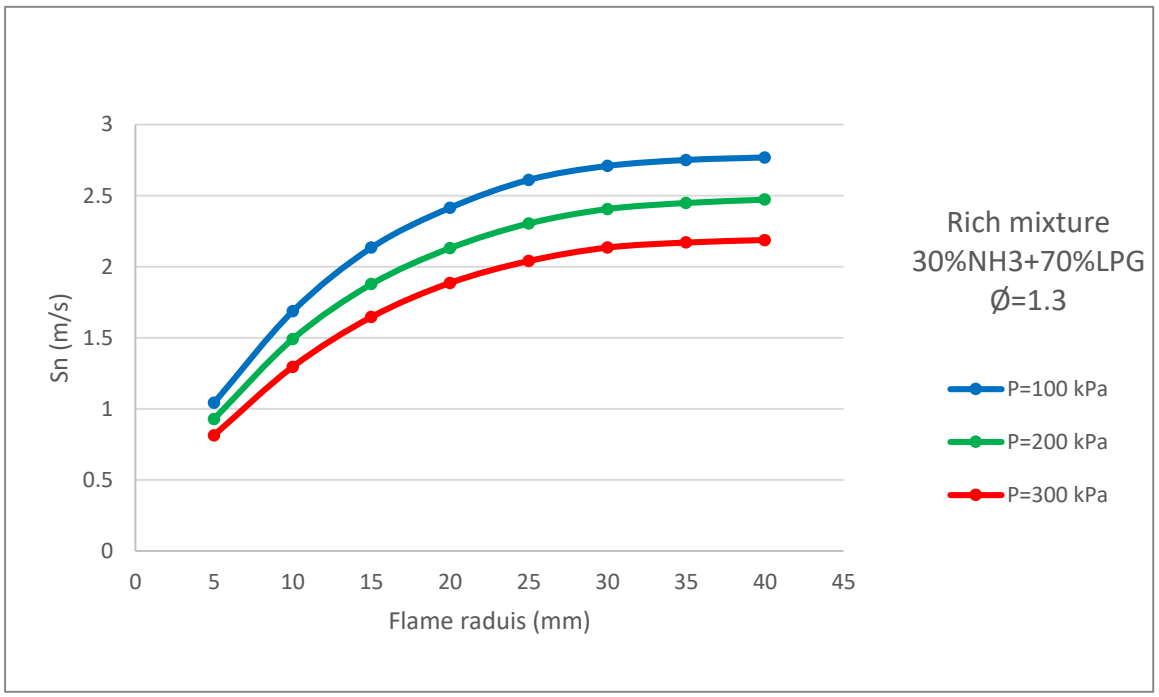

Figure (4.24) laminar flame speed S_n with a flame radius for 30% NH_3 and 70% LPG at Ø = 1.3

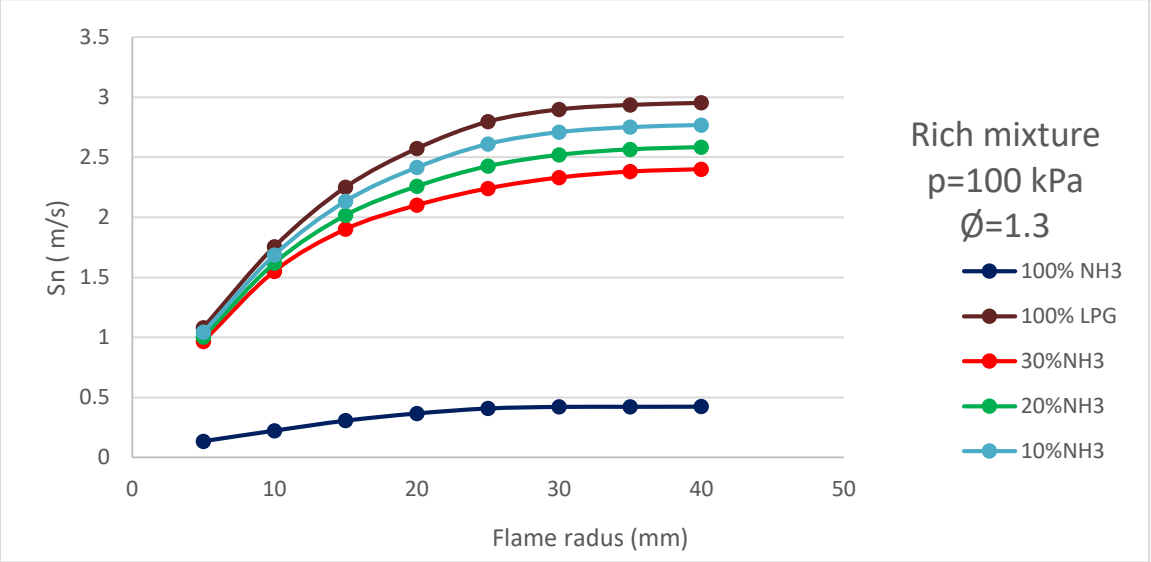

Figure (4.25) laminar flame speed S_n with a flame radius for Rich mixture at Ø = 1.3 and initial pressure 100 kPa

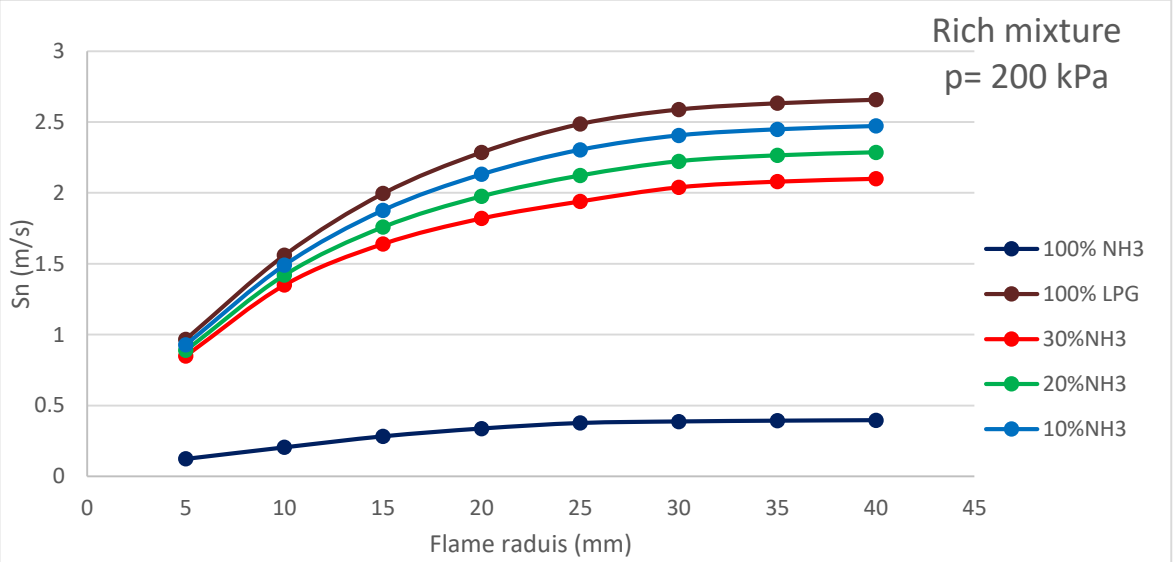

Figure (4.26) laminar flame speed S_n with a flame radius for Rich mixture at Ø = 1.3 and initial pressure 200 kPa

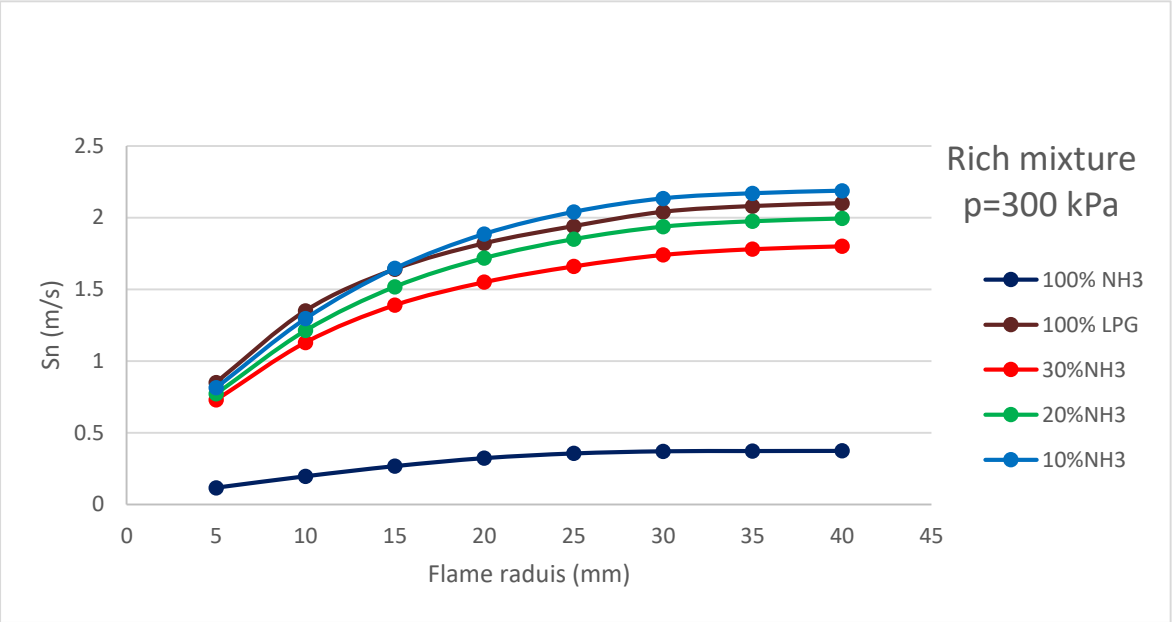

Figure (4.27) laminar flame speed S_n with a flame radius for Rich mixture at Ø =1.3 and initial pressure 300 kPa

4.2.4 Stretched Rate and Markstein Length

When the flame radius is small which happened at an early stage of flame propagation, the stretch rate of the flame front surface is too high since the relation is directly proportional with the flame speed and inversely proportional with flame radius. Eliminating the data of the first region disturbed by the ignition energy and also eliminating data of large radius of the third region of high pressure, linear and nonlinear relations between the flame stretch rate and the stretched flame propagation speed are used in this study.

The stretch rate is inversely proportional to the radius; thus, its effect decreases as the flame propagates because of increases the flame radius. This would be expected on very general grounds as increasing the flame radius, the flame shape becomes less curved and it seems as a planar, one- dimensional and hence, un-stretched flame. The stretch rate (α) has excessive values during the initial stages of flame propagation due to the significant curvature related to a

small spherical surface. Flame speed is affected by flame stretch; it can be accurately determined when the stretch is negligible i.e. when $r \rightarrow \infty$.

Markstein length (L_b) is a parameter representing the response of the flame speed to flame stretch, it is an important parameter to characterize the effect of stretch on global flame instability. Markstein length is related to the diffusional-thermal instability of flame, while the flame thickness and density ratio are related to the hydrodynamic instability of flame. A positive value of Markstein length indicates stable flame front while the negative value indicates unstable flame front [66]. The evolution of flame speed as a function of flame stretch is presented in figure (4.41) for the stoichiometric ammonia - LPG - air blend. the figure shows that the linearly extrapolated speed.

The Markstein length L_b of an ammonia-LPG-air flame is measured in this work utilizing the connection between displacement speed and stretch rate, which indicates the displacement speed reaction to flame stretch. The lengths of Markstein in ammonia/LPG/air with various equivalent ratio have been investigated. When the equivalency ratio increase from 0.8 to 1.3, the Markstein length decreased ammonia-LPG-air mixtures at varying initial pressures. The Markstein length is negative when the lean mixture (Ø=0.8), at different initial pressure, which indicates the flame speeds faster as it is extended. As a result, the flame is unstable, and cellular structures can be seen on the flame surface.

The Markstine length L_b is decreased based on the thermal-diffusion process, the flame is unstable, the corresponding Markstein length is negative, the flame is unstable, and cellular structure can be seen. the Markstein length L_b decreases when the equivalence ratio increases at the initial pressure. and the flame Should be steady owing to equivalency ratio being improved.

As a result, the flame is steady, and no cellular structure can be seen on the

ammonia-LPG-air flame surface in Figure. (4.30), (4.31), and (4.32), respectively. That corresponds to what was observed in an ammonia-LPG-air flame at a different initial pressure. At varied pressures, the Merkstein lengths of ammonia-LPG-air is also investigated.

When the equivalency ratio increases and the initial pressure increases, the Markstein lengths decreases, indicating that flame instability changes from stable to unstable. The flame surface evolved from a smooth surface to a cellular structure that is dispersed across the flame Surface.

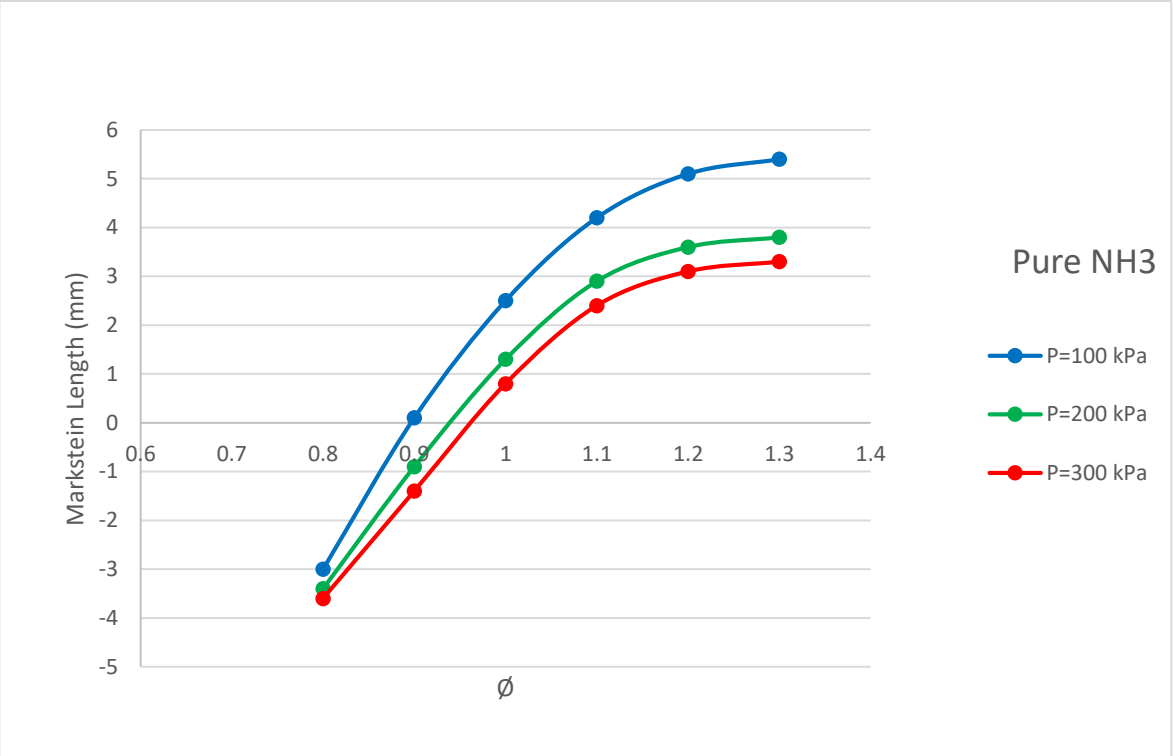

Figure (4.28) Markstein length with equivalence ratio of pure Ammonia at the initial pressures 100, 200, 300 kPa

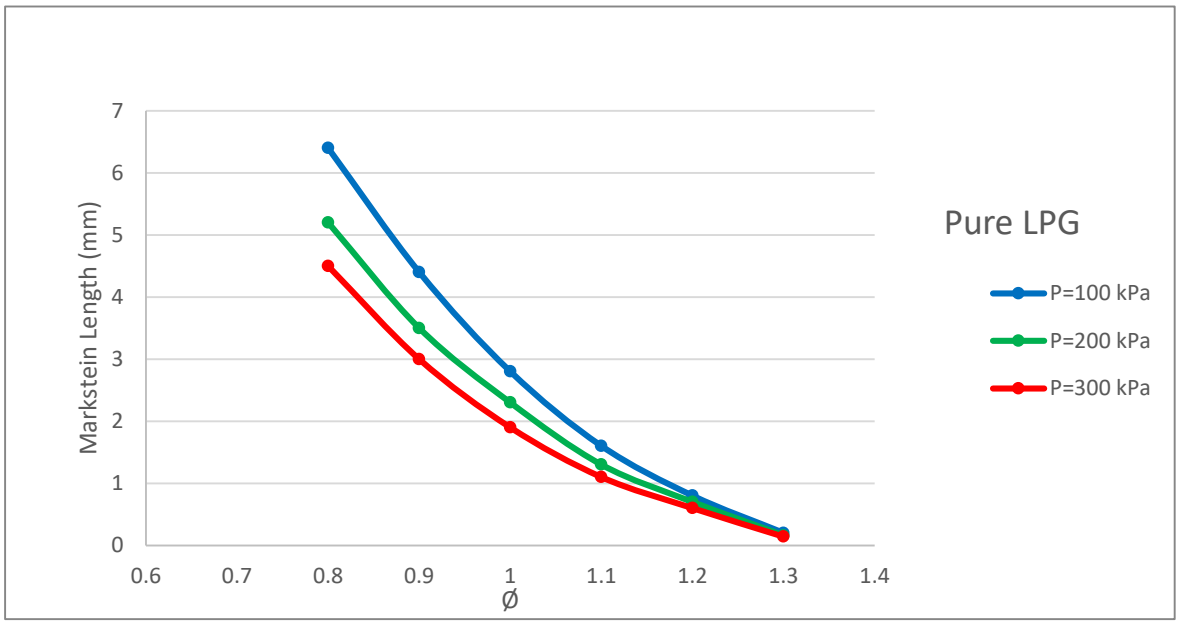

Figure (4.29) Markstein length with equivalence ratio of pure LPG at the initial pressures 100, 200 , 300 kPa

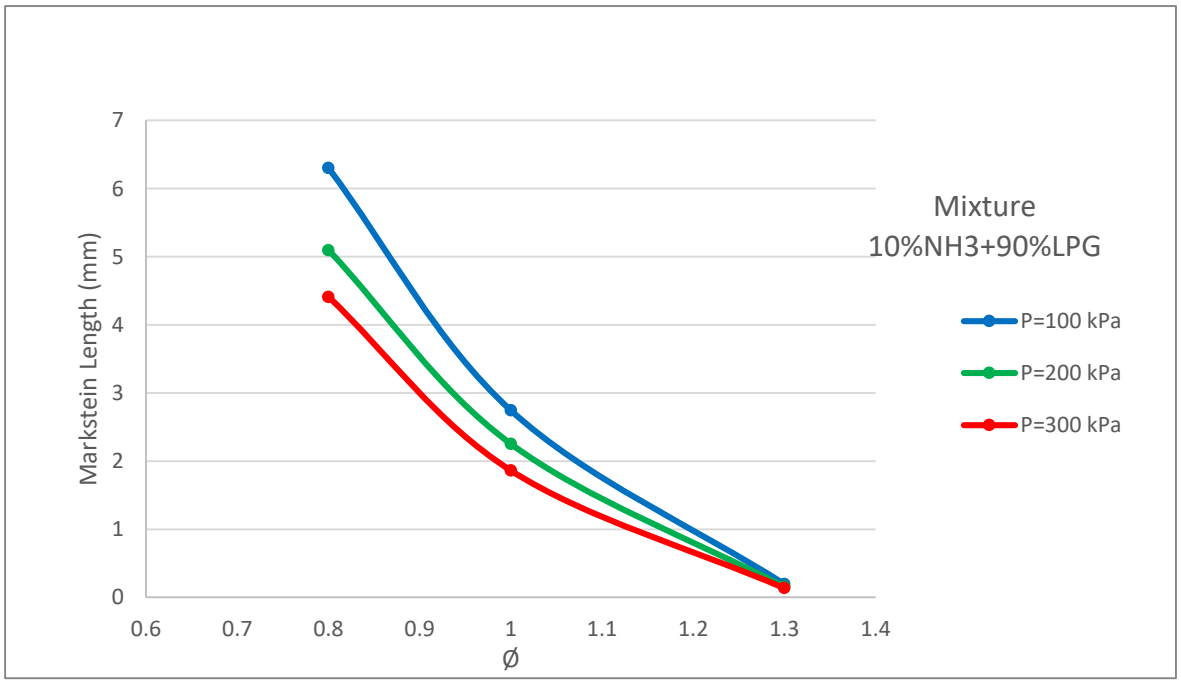

Figure (4.30) Markstein length with equivalence ratio of 10%NH_3+90% LPG at the initial pressures 100, 200 , 300 kPa

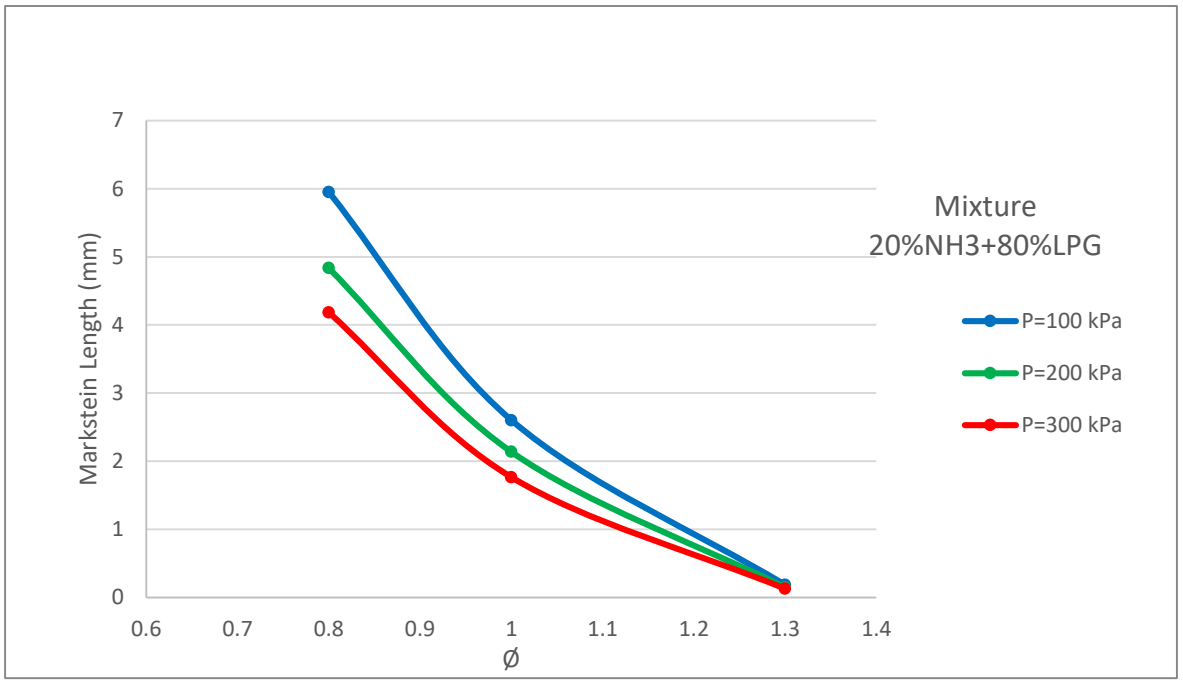

Figure (4.31) Markstein length with equivalence ratio of 20%NH_3+80% LPG at the initial pressures 100, 200, 300 kPa

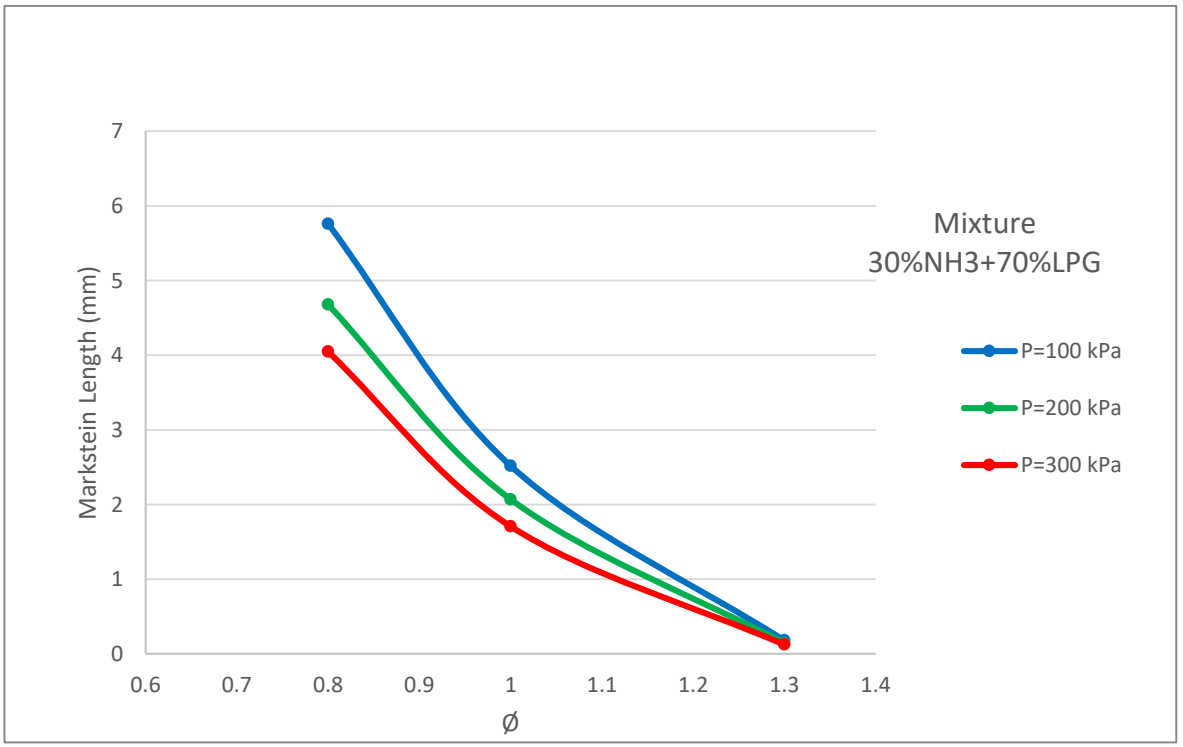

Figure (4.32) Markstein length with an equivalence ratio of 30%NH_3+70% LPG at the initial pressures 100, 200, 300 kPa

4.2.5 Laminar Burning Velocity

It is the fundamental physico-chemical information in evaluating the flame propagation process, which includes information about the reactivity, exothermicity, and diffusivity of the fuel. The laminar burning velocity is also used to validate the chemical kinetic mechanisms, and to estimate the turbulent burning velocities and flame structure studies. It depends on the initial temperature and pressure of the combustible mixture, fuel type, and equivalence ratio.

Flame propagation is caused by heat transmitter from the front of the flame to unburned gasses by ratio active, convection, and conductivity. Figure (4.34), (4.35) and (3.36) depict the experimental investigation that is carried out to determine the velocity of the laminar flame of an NH_3 percent mixture at various equivalency ratios and pressures. With increasing starting pressure, the laminar burning velocity falls and increases with Ø until it achieves its maximum value of (Ø= 1.1).

In addition, while looking at the LPG percent, the laminar burning velocity falls as pressure rises, reaching its maximum value at =1.1. The laminar burning velocity versus equivalency ratio, as well as varying concentrations of Ammonia and LPG, are shown in Figure (4.37).

The fig demonstrates that the highest value of laminar burning occurs at a 10% ammonia concentration or a 90% LPG concentration, shown by the curve (4.34)

When the ammonia concentration is increased to 30% and the LPG concentration is decreased to 70%, the highest value of the laminar burning velocity u_l is at (Ø = 1). Pure Ammonia fuel and pure LPG fuel both show a significant improvement in laminar burning velocity.

4.2.5.1 Effect of Initial Pressure on Laminar Burning Velocity

Laminar burning velocities for NH3 – LPG – air mixture with the temperature of 298 K, at 0.1, 0.2 and 0.3 MPa. The results show that Laminar burning velocity decreases as the initial pressure increases. This is due to the decrease of thermal diffusivity of the fuel mixture with the increase of initial pressure.

Figure (4.35), (4.36) and (4.37) Show when initial pressure increases**,** Laminar burning velocity decrea ses The effect of initial pressure increases, density and comical combustion increase which in turn increases combustion reactions leading to a decrease in laminar burring velocity.

4.2.5.2 Effect with Equivalence Ratio and effect of Ammonia Gas Percentage

Figure (4.33), (4.34) ,(4.38) ,(4.39) and (4.40) show that when the E_{LPG} =0 and E_{NH3} = 100%, the lowest value of the laminar burning velocities is on the lean mixture, and the highest value when it reaches the stoichiometric mixture and begins to decrease on the rich mixture. Figure (4.34) shows that when the E_{LPG} = 100 % and E_{NH3} = 0 %, the lowest value of the laminar burning velocity is on the lean mixture, and the highest value when it reaches the stoichiometric mixture and begins to decrease on the rich mixture.

Whenever the concentration of ammonia exceeds 10% the increase in the laminar burning velocity value begins. Figure (4.35),(4.36) and (4.37) that when the concentration of ammonia gas increases , the laminar burning velocity begins to decrease clearly. That is the higher value of u_l and its highest value at a concentration of 10% of ammonia. The stoichiometric mixture has the highest value for the laminar burning velocity.

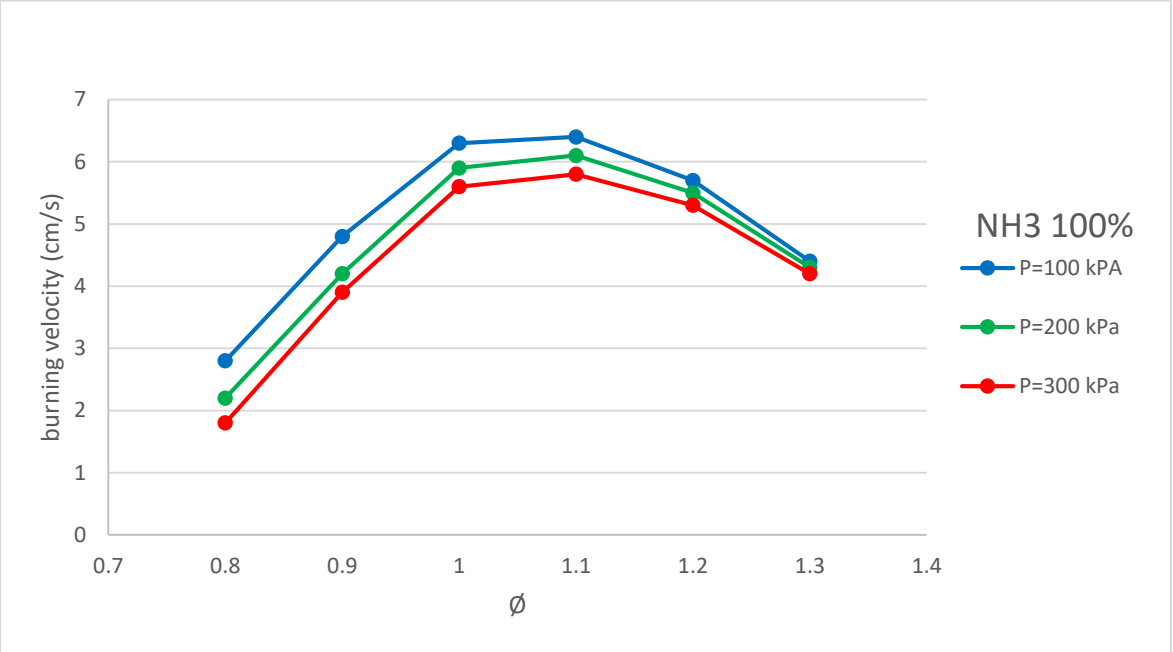

Figure (4.33) burning velocity with equivalence ratio of pure Ammonia at initial pressures 100, 200, 300 kPa

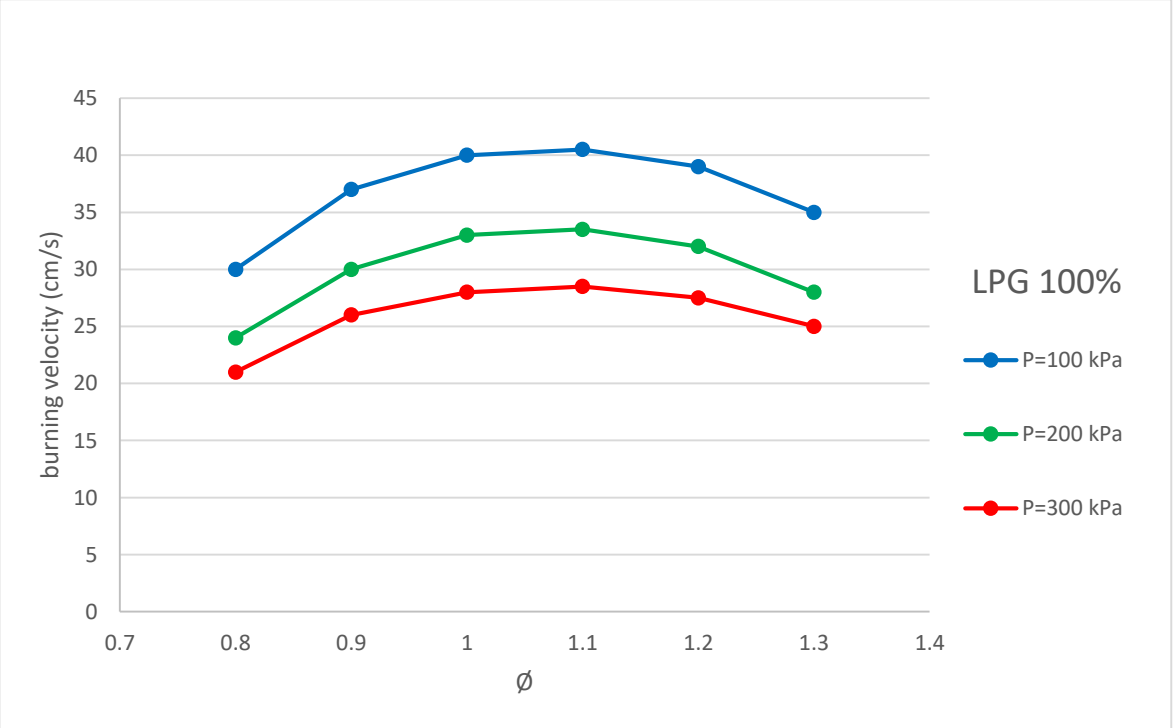

Figure (4.34) burning velocity with an equivalence ratio of pure LPG at initial pressures 100, 200, 300 kPa

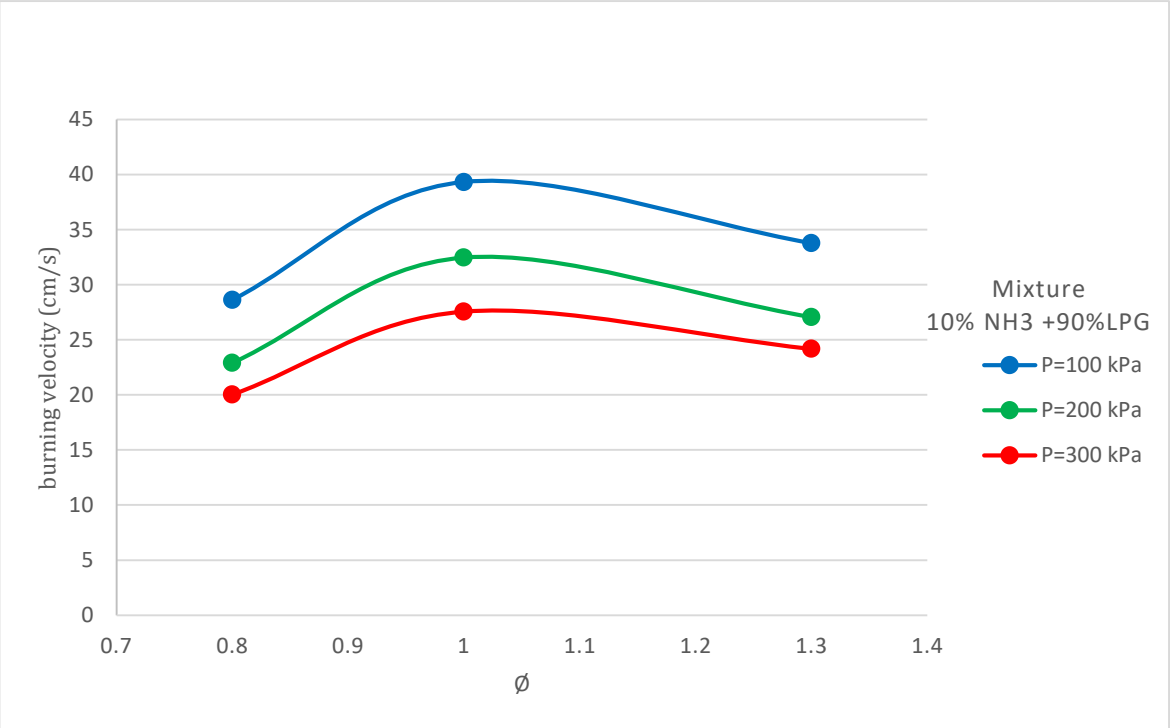

Figure (4.35) shows burning velocity with equivalence ratio of mixture 10% NH_3 and 90% LPG at initial pressures 100, 200, 300 kPa

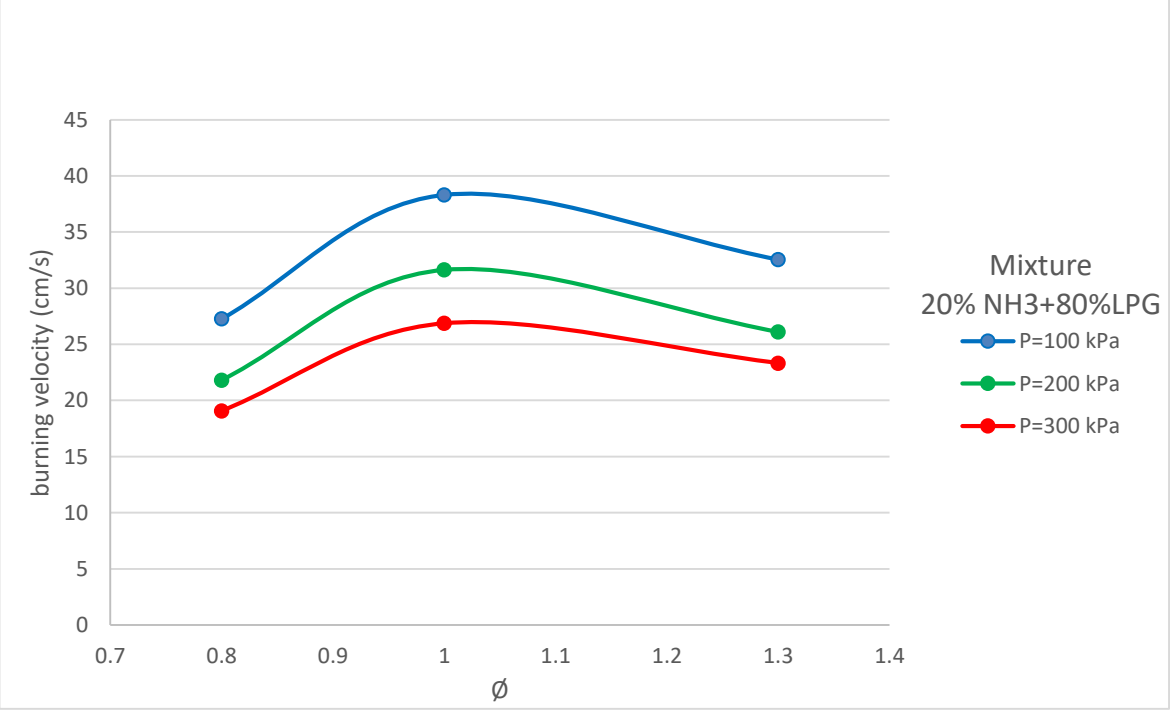

Figure (4.36) burning velocity with equivalence ratio of mixture 20% NH_3 and 80% LPG at initial pressures 100, 200, 300 kPa

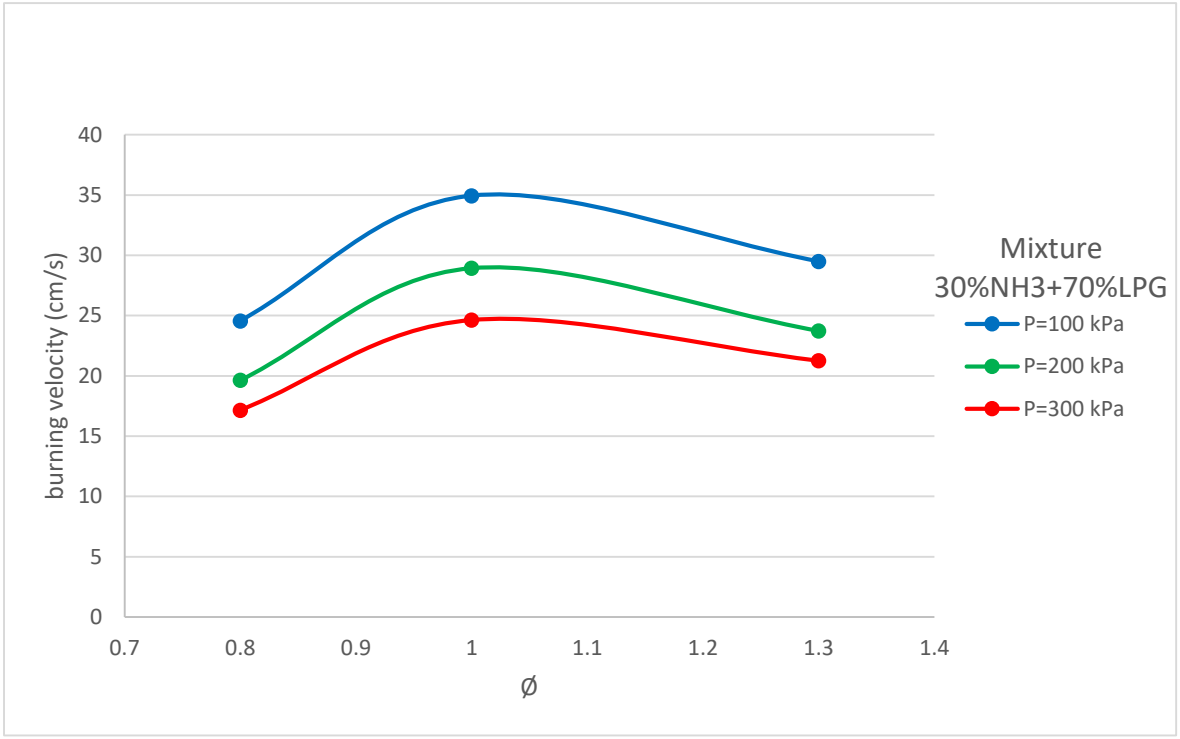

Figure (4.37) burning velocity with an equivalence ratio of mixture 30% NH_3 and 70% LPG at initial pressures 100, 200, 300 kPa

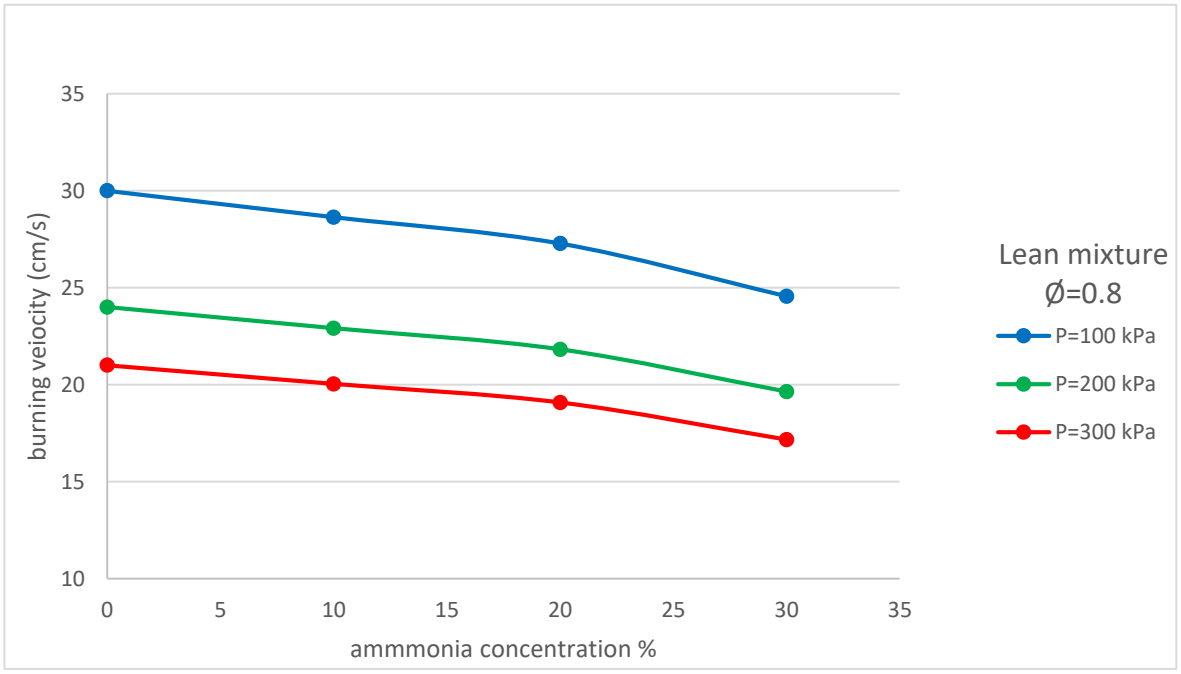

Figure (4.38) laminar burning velocity with ammonia concentration 0 , 10 , 20 and 30% at Lean mixture initial pressures 100 , 200 and 300 kPa

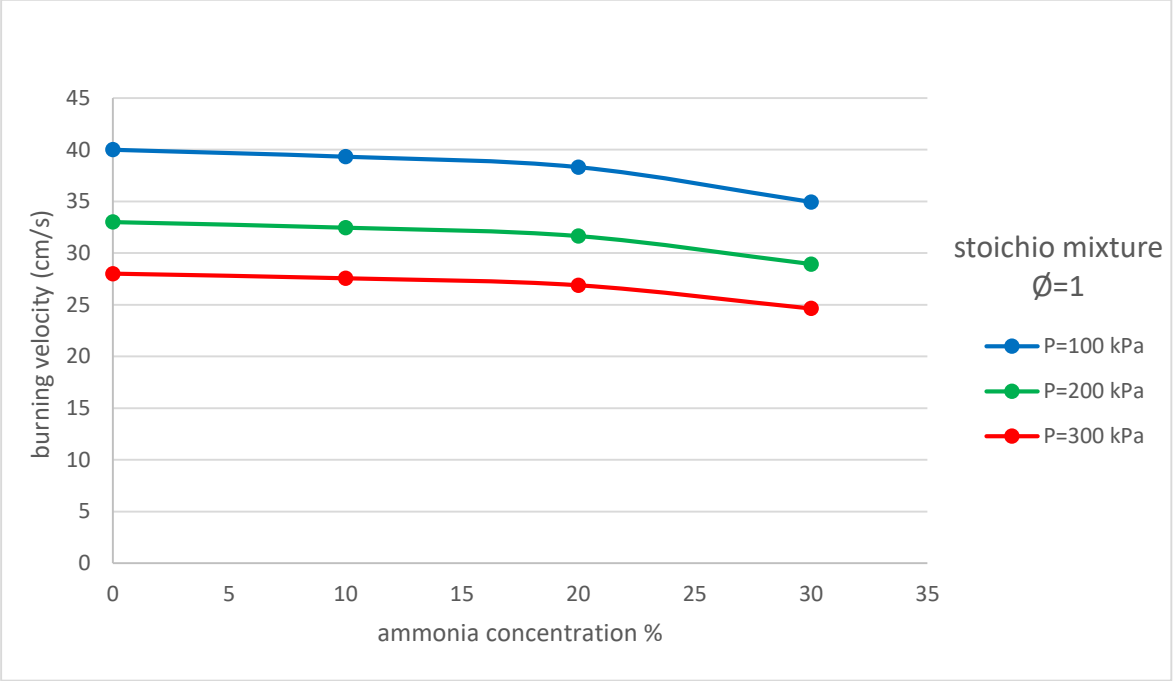

Figure (4.39) burning velocity with ammonia concentrations 0 , 10 , 20 and 30 % at Stoichio mixture initial pressures 100 , 200 and 300 kPa at Ø = 1

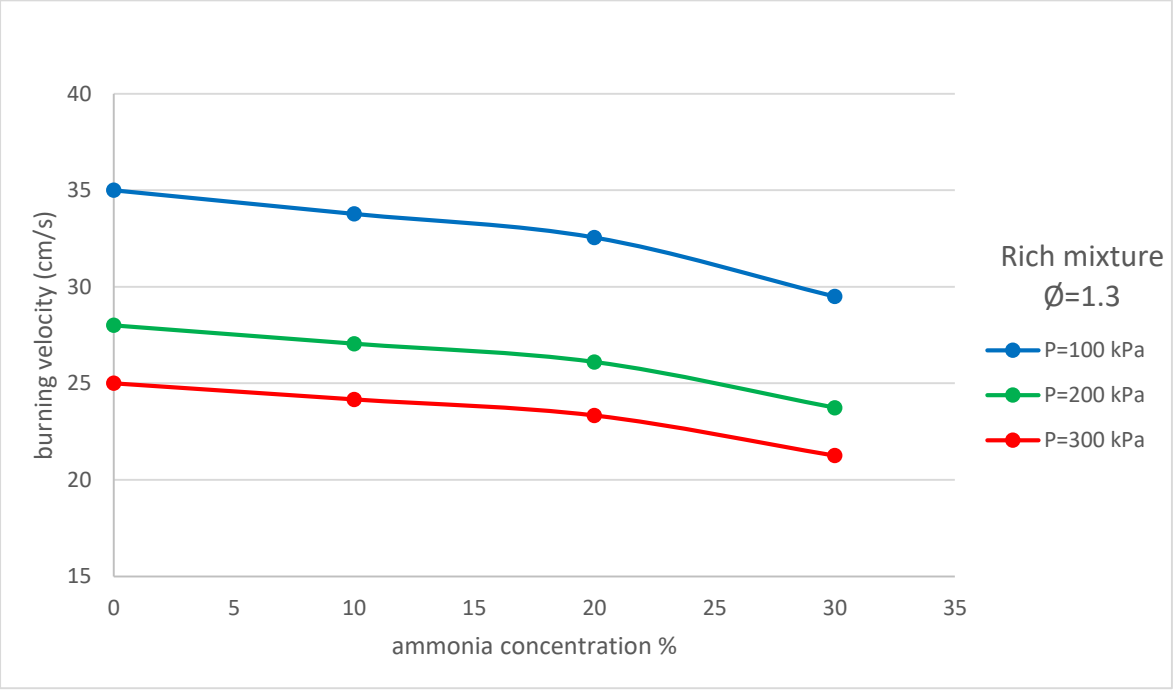

Figure (4.40) burning velocity with ammonia concentrations 0 , 10 , 20 and 30 % at Rich mixture initial pressures 100 , 200 and 300 kPa at Ø=1.3

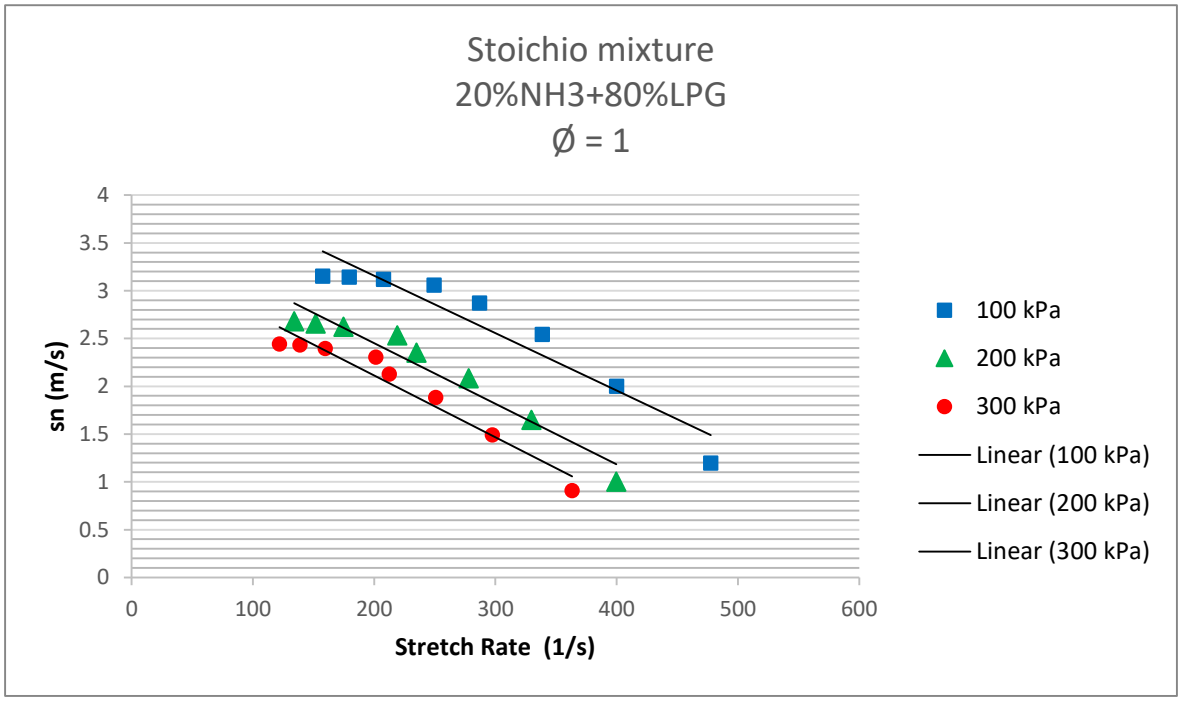

Figure (4.41) Relationship between stretched flame speed S_n and flame stretch rate α

CHAPTER FIVE
CONCLUSION AND RECOMMENDATION

CHAPTER FIVE

CONCLUSIONS AND RECOMMENDATIONS

In the following section, the major conclusions from this study

5.1 Conclusion

Throughout the experimental study of the mixture of (NH_3 – air) mixture and (LPG – air) mixture and (NH_3 –LPG - air) obtaining the properties of each mixture the following conclusions were obtained: -

1- The Value of the Laminar flame speed of a mixture of (NH_3 – air) with different initial pressures and with different radius of the formed flame. The laminar flame speed decreases with increasing the pressure. But the flame speed has a peak higher than the Value of the flame speed formed where mixing (LPG – air) under the same conditions. As for the effect of adding ammonia to the mixture of (LPG – air) at different initial pressures, the value of the laminar flame speed increasing clearly and reaches the highest value when the mixture is stoichiometric.

2- The value related to the laminar burning velocity of a mix (LPG-air) and (NH_3-air) at various equivalence ratio values and initial pressures reduces with increasing the value of the initial pressure, which indicates that the higher the initial pressure, the lower the value regarding the laminar burning velocity, which reaches its maximum value in the case when the mixture is stoichiometric. The (NH_3 – air) mixture's laminar burning velocity is higher than the (LPG – air) mixture laminar burning velocity.

But when ammonia gas is added to the mixture of (LPG – air) in different equivalence ratios and at different initial pressures, its effect is to maintain the laminar burning velocity value with a slight decrease which means that the laminar burning velocity increases by decreasing the initial pressure and by proportion of

added ammonia gas to 10% and reaching the highest value when the mixture is stoichiometric.

3- When studying the properties of LPG-air the Markstein length has the highest value when the mixture is lean and the initial pressure is the lowest and the highest value is the Markstein length when the mixture is rich, contrasting to the properties of ammonia and air.

When ammonia gas is added to the mixture, its effect is limited to reduce the value of the Markstein length, which mean that as the concentration of ammonia increases, the Markstein length decrease and reaches its maximum value when the ammonia concentration is less than 20%

5.2 Recommendations

1- Using a proportion of ammonia gas more than 30% to mix with liquefied petroleum gas, provided that the combustion chamber is larger, with a stronger external structure, and larger dimensions, because the heat generated during the experiment at a pressure of 300 Kps very high, and the cause of a fire inside the combustion chamber with vibration and a loud explosion sound within Safety measures taken inside the laboratory are stopped at a concentration of ammonia 30% and LPG 70%.

2- Re-experiment using turbulent combustion instead of Laminar combustion and calculating the effect of ammonia gas when mixed with liquefied petroleum gas and studying the properties.

3- Investigation the effect of ignition energy on flame speed and stage of flame formation.

REFERENCES

Reference

[1] Wang, Y., Zheng, S., Chen, J., Wang, Z., & He, S. (2018). Ammonia (NH3) storage for massive PV electricity. *Energy Procedia*, *150*, 99–105.

[2] Synák, F., Čulík, K., Rievaj, V., & Gaňa, J. (2019). Liquefied petroleum gas as an alternative fuel. *Transportation Research Procedia*, *40*, 527–534.

[3] Liu, Q., Chen, X., Huang, J., Shen, Y., Zhang, Y., & Liu, Z. (2019). The characteristics of flame propagation in ammonia/oxygen mixtures. *Journal of Hazardous Materials*, *363*, 187–196.

[4] Goldmann, A., & Dinkelacker, F. (2018). Approximation of laminar flame characteristics on premixed ammonia/hydrogen/nitrogen/air mixtures at elevated temperatures and pressures. *Fuel*, *224*, 366–378.

[5] Okafor, E. C., Naito, Y., Colson, S., Ichikawa, A., Kudo, T., Hayakawa, A., & Kobayashi, H. (2019). Measurement and modelling of the laminar burning velocity of methane-ammonia-air flames at high pressures using a reduced reaction mechanism. *Combustion and Flame*, *204*, 162–175

[6] Yang, S. J., Jung, H., Kim, T., & Park, C. R. (2012). Recent advances in hydrogen storage technologies based on nanoporous carbon materials. *Progress in Natural Science: Materials International*, *22*(6), 631–638.

[7] Xu, C., Wang, H., Oppong, F., Li, X., Zhou, K., Zhou, W., Wu, S., & Wang, C. (2020). Determination of laminar burning characteristics of a surrogate for a pyrolysis fuel using constant volume method. *Energy*, *190*, 116315.

[8] Giddey, S., Badwal, S. P. S., Munnings, C., & Dolan, M. (2017). Ammonia as a renewable energy transportation media. *ACS Sustainable Chemistry & Engineering*, *5*(11), 10231–10239.

[9] F. Li, L. Xu, Z. Cao, and M. Du, “A chemi-ionization processing approach for characterizing flame flickering behavior,” Conference Record - IEEE Instrumentation and Measurement Technology Conference, vol. 2015-July, pp. 325–329, 2015, doi: 10.1109/I2MTC.2015.7151288.

[10] Jonatan, J. (2012). *Liquefied Petroleum Gas (LPG) Storage Design*. UMP.

[11] Valera-Medina, A., Xiao, H., Owen-Jones, M., David, W. I. F., & Bowen, P. J. (2018). Ammonia for power. *Progress in Energy and Combustion Science*, *69*, 63–102.

[12] Monteiro, J. O. D. (2015). *Laminar flame speed of fuel mixtures applied to spark-ignition internal combustion engines*.

[13] Turns, S. R. (1996). *Introduction to combustion* McGraw-Hill Companies New York, NY, USA.

[14] Law, C. K. (2006). Combustion physics Cambridge University Press. *New York, USA*, 89–96.

[15] Faghih, M., & Chen, Z. (2016). The constant-volume propagating spherical flame method for laminar flame speed measurement. *Science Bulletin*, *61*(16), 1296–1310.

[16] Bradley, D., Gaskell, P. H., & Gu, X.-J. (1996). Burning velocities, Markstein lengths, and flame quenching for spherical methane-air flames: a computational study. *Combustion and Flame*, *104*(1–2), 176–198.

[17] Marshall, S. P. (2010). *Measuring laminar burning velocities*. Oxford University, UK

[18] Almarcha, C., Denet, B., & Quinard, J. (2015). Premixed flames propagating freely in tubes. *Combustion and Flame*, *162*(4), 1225–1233.

[19] Konnov, A. A., Mohammad, A., Kishore, V. R., Kim, N. Il, Prathap, C., & Kumar, S. (2018). A comprehensive review of measurements and data analysis of laminar burning velocities for various fuel+ air mixtures. *Progress in Energy and Combustion Science*, *68*, 197–267.

[20] Rallis, C. J., & Garforth, A. M. (1980). The determination of laminar burning velocity. *Progress in Energy and Combustion Science*, *6*(4), 303–329.

[21] Kwon, O. C., Rozenchan, G., & Law, C. K. (2002). Cellular instabilities and self-acceleration of outwardly propagating spherical flames. *Proceedings of the Combustion Institute*, *29*(2), 1775–1783.

[22] Hopkinson, B. (1906). Explosions of coal-gas and air. *Proceedings of the Royal Society of London. Series A, Containing Papers of a Mathematical and Physical Character*, *77*(518), 387–413.

[23] Flamm, L., & Mache, H. (1917). Die Verbrennung eines explosiven Gasgemisches in geschlossenem Gefäß. *Sitzungsberichte Der Kaiserlichen Academie Der Wissenschaften in Wien, Klasse IIa*, *126*, 9–44.

[24] Fiock, E. F., Marvin Jr, C. F., Caldwell, F. R., & Roeder, C. H. (1940). *Flame speeds and energy considerations for explosions in a spherical bomb*.

[25] Johnston, R. J., & Farrell, J. T. (2005). Laminar burning velocities and Markstein lengths of aromatics at elevated temperature and pressure. *Proceedings of the Combustion Institute*, *30*(1), 217–224.

[26] Tang, C., He, J., Huang, Z., Jin, C., Wang, J., Wang, X., & Miao, H. (2008). Measurements of laminar burning velocities and Markstein lengths of propane–hydrogen-air mixtures at elevated pressures and temperatures. *International Journal of Hydrogen Energy*, *33*(23), 7274–7285.

[27] Hu, E., Huang, Z., He, J., & Miao, H. (2009). Experimental and numerical study on laminar burning velocities and flame instabilities of hydrogen-air mixtures at elevated pressures and temperatures. *International Journal of Hydrogen Energy*, *34*(20), 8741–8755.

[28] Egolfopoulos, F. N., Hansen, N., Ju, Y., Kohse-Höinghaus, K., Law, C. K., & Qi, F. (2014). Advances and challenges in laminar flame experiments and implications for combustion chemistry. *Progress in Energy and Combustion Science*, *43*, 36–67.

[29] Chan, Y. L., Zhu, M. M., Zhang, Z. Z., Liu, P. F., & Zhang, D. K. (2015). The effect of CO2 dilution on the laminar burning velocity of premixed methane/air flames. *Energy Procedia*, *75*, 3048–3053.

[30] Lipatnikov, A. N., Shy, S. S., & Li, W. (2015). Experimental assessment of various methods of determination of laminar flame speed in experiments with expanding spherical flames with positive Markstein lengths. *Combustion and Flame*, *162*(7), 2840–2854.

[31] Saleh, A. M., & Dr Mohammed, N. H. A.-F. (2006). Effect of initial pressure upon laminar burning velocity of paraffins gaseous fuel in closed vessel. Ph. D. Thesis, University of Technology.

[32] Galmiche, B., Togbe, C., Dagaut, P., Halter, F., & Foucher, F. (2011). Experimental and detailed kinetic modeling study of the oxidation of 1-propanol in a pressurized jet-stirred reactor (JSR) and a combustion bomb. *Energy & Fuels*, *25*(5), 2013–2021.

[33] Hinton, N., & Stone, R. (2014). Laminar burning velocity measurements of methane and carbon dioxide mixtures (biogas) over wide ranging temperatures and pressures. *Fuel*, *116*, 743–750.

[34] Mannaa, O., Mansour, M. S., Roberts, W. L., & Chung, S. H. (2015). Laminar burning velocities at elevated pressures for gasoline and gasoline surrogates associated with RON. *Combustion and Flame*, *162*(6), 2311–2321.

[35] Yasiry, A. S., & Shahad, H. A. K. (2016). An experimental study of the effect of hydrogen blending on burning velocity of LPG at elevated pressure. *International Journal of Hydrogen Energy*, *41*(42), 19269–19277.

[36] Bao, X., Jiang, Y., Xu, H., Wang, C., Lattimore, T., & Tang, L. (2017). Laminar flame characteristics of cyclopentanone at elevated temperatures. *Applied Energy*, *195*, 671–680.

[37] Duva, B. C., Chance, L. E., & Toulson, E. (2020). Dilution effect of different combustion residuals on laminar burning velocities and burned gas Markstein lengths of premixed methane/air mixtures at elevated temperature. *Fuel*, *267*, 117153.

[38] Ellis, O. C. de C. (1928). Flame movement in gaseous explosive mixtures. *J. Fuel Sci.*, *7*, 502–508.

[39] Lewis, B., & Von Elbe, G. (1934). Determination of the speed of flames and the temperature distribution in a spherical bomb from time-pressure explosion records. *The Journal of Chemical Physics*, *2*(5), 283–290.

[40] Halter, F., Tahtouh, T., & Mounaïm-Rousselle, C. (2010). Nonlinear effects of stretch on the flame front propagation. *Combustion and Flame*, *157*(10), 1825–1832.

[41] Chen, Z. (2011). On the extraction of laminar flame speed and Markstein length from outwardly propagating spherical flames. *Combustion and Flame*, *158*(2), 291–300.

[42] Xu, C., Wang, H., Oppong, F., Li, X., Zhou, K., Zhou, W., Wu, S., & Wang, C. (2020). Determination of laminar burning characteristics of a surrogate for a pyrolysis fuel using constant volume method. *Energy*, *190*, 116315.

[43] Kuo, K. K. (1986). *Principles of combustion*.

[44] Zaid, A. K. (1982). *Study of Combustion Behavior of the Commercial Liquefied Gases*. MSc Thesis University of Technology Iraq.

[45] Odgers, J., Kretschmer, D., & Halpin, J. (1985). *Weak limits of premixed gases*.

[46] Tahtouh, T., Halter, F., & Mounaïm-Rousselle, C. (2009). Measurement of laminar burning speeds and Markstein lengths using a novel methodology. *Combustion and Flame*, *156*(9), 1735–1743.

[47] Zhang, X., Tang, C., Yu, H., Li, Q., Gong, J., & Huang, Z. (2013). Laminar flame characteristics of iso-octane/n-butanol blend–air mixtures at elevated temperatures. *Energy & Fuels*, *27*(4), 2327–2335.

[48] Sreeni vasan, R., Raghavan, V., & Sundararajan, T. (2012). An investigation of flame zones and burning velocities of laminar unconfined methane-oxygen premixed flames. *Combustion Theory and Modelling*, *16*(2), 199–219.

[49] Abdul Raheem, A. A., Saleh, A. M., & Shahad, H. A. K. (2021). Measurements and Data Analysis Review of Laminar Burning Velocity and Flame Speed for Biofuel/Air Mixtures. *IOP Conference Series: Materials Science and Engineering*, *1094*(1), 12029.

[50] Kuo, K. K. (2005). Gaseous diffusion flames and combustion of a single liquid fuel droplet. *Principles of Combustion*.

[51] Marshall, S. P., Taylor, S., Stone, C. R., Davies, T. J., & Cracknell, R. F.

(2011). Laminar burning velocity measurements of liquid fuels at elevated pressures and temperatures with combustion residuals. *Combustion and Flame*, *158*(10), 1920–1932

[52] Sharma, S. P., Agrawal, D. D., & Gupta, C. P. (1981). The pressure and temperature dependence of burning velocity in a spherical combustion bomb. *Symposium (International) on Combustion*, *18*(1), 493–501.

[53] Metghalchi, M., & Keck, J. C. (1982). Burning velocities of mixtures of air with methanol, isooctane, and indolene at high pressure and temperature. *Combustion and Flame*, *48*, 191–210.

[54] Ubbelohde, L., & Koelliker, E. (1916). Information about the inner cone of the bunsen flame. *Journal Fur Gasbeluchtung Und Wasserversorgung*, *59*, 49–57.

[55] Mallard, & Chatelier, L. (1883). *Recherches expérimentales et théoriques sur la combustion des mélanges gazeux explosifs*. Dunod.

[56] Daniell, P. J. (1930). The theory of flame motion. *Proceedings of the Royal Society of London. Series A, Containing Papers of a Mathematical and Physical Character*, *126*(802), 393–405.

[57] Nusselt, W. (1915). Die Zundgeschwindigkeit brennbarer gasgemische. *Deut Ing*, *59*, 872–878.

[58] Zeldovich, Y. B., & Frank-Kamenetskii, D. A. (1938). The theory of thermal propagation of flames. *Zh. Fiz. Khim*, *12*, 100–105.

[59] Agnew, J. T., & Graiff, L. B. (1961). The pressure dependence of laminar burning velocity by the spherical bomb method. *Combustion and Flame*, *5*, 209–219.

[60] Huzayyin, A. S., Moneib, H. A., Shehatta, M. S., & Attia, A. M. A. (2008).

Laminar burning velocity and explosion index of LPG–air and propane–air mixtures. Fuel, 87(1), 39–57.

[61] Liao, S. Y., Jiang, D. M., Gao, J., & Huang, Z. H. (2004). Measurements of Markstein numbers and laminar burning velocities for natural gas− air mixtures. *Energy & Fuels*, *18*(2), 316–326.

[62] Huang, Z., Zhang, Y., Zeng, K., Liu, B., Wang, Q., & Jiang, D. (2006). Measurements of laminar burning velocities for natural gas–hydrogen–air mixtures. *Combustion and Flame*, *146*(1–2), 302–311.

[63] Bradley, D., Hicks, R. A., Lawes, M., Sheppard, C. G. W., & Woolley, R. (1998). The measurement of laminar burning velocities and Markstein numbers for iso-octane–air and iso-octane–n-heptane–air mixtures at elevated temperatures and pressures in an explosion bomb. *Combustion and Flame*, *115*(1–2), 126–144.

[64] Burke, M. P., Chen, Z., Ju, Y., & Dryer, F. L. (2009). Effect of cylindrical confinement on the determination of laminar flame speeds using outwardly propagating flames. *Combustion and Flame*, *156*(4), 771–779

[65] Andrews, G. E., & Bradley, D. (1972). Determination of burning velocities: a critical review. *Combustion and Flame*, *18*(1), 133–153.

[66] Hayakawa, A., Goto, T., Mimoto, R., Arakawa, Y., Kudo, T., & Kobayashi, H. (2015). Laminar burning velocity and Markstein length of ammonia/air premixed flames at various pressures. *Fuel*, *159*, 98–106.

[67] Kumar, R., Singhal, A., Katoch, A., & Kumar, S. (2020). Experimental investigations on laminar burning velocities of n-heptane+ air mixtures at higher mixture temperatures using externally heated diverging channel method. *Energy & Fuels*, *34*(2), 2405–2416

[68] Kim, G., Terracciano, A. C., & Vasu, S. (2020). Laminar burning velocity measurements of high-performance jet fuel/air mixtures. *AIAA Scitech 2020*

Forum, 639.

[69] Alekseev, V. A., Christensen, M., & Konnov, A. A. (2015). The effect of temperature on the adiabatic burning velocities of diluted hydrogen flames: A kinetic study using an updated mechanism. *Combustion and Flame*, *162*(5), 1884–1898.

[70] Qiao, L., Gan, Y., Nishiie, T., Dahm, W. J. A., & Oran, E. S. (2010). Extinction of premixed methane/air flames in microgravity by diluents: Effects of radiation and Lewis number. *Combustion and Flame*, *157*(8), 1446–1455.

[71] Wu, X., Huang, Z., Wang, X., Jin, C., Tang, C., Wei, L., & Law, C. K. (2011). Laminar burning velocities and flame instabilities of 2, 5-dimethylfuran–air mixtures at elevated pressures. *Combustion and Flame*, *158*(3), 539–546

[72] Yumlu, V. S. (1967). Prediction of burning velocities of carbon monoxide-hydrogen-air flames. *Combustion and Flame*, *11*(3), 190–194.

[73] Spalding, D. B. (1956). A mixing rule for laminar flame speed. *Fuel*, *35*(3), 347–351.

[74] Ichikawa, A., Hayakawa, A., Kitagawa, Y., Somarathne, K. D. K. A., Kudo, T., & Kobayashi, H. (2015). Laminar burning velocity and Markstein length of ammonia/hydrogen/air premixed flames at elevated pressures. *International Journal of Hydrogen Energy*, *40*(30), 9570–9578.

[75] Lowry, W. B., Serinyel, Z., Krejci, M. C., Curran, H. J., Bourque, G., & Petersen, E. L. (2011). Effect of methane-dimethyl ether fuel blends on flame stability, laminar flame speed, and Markstein length. *Proceedings of the Combustion Institute*, *33*(1), 929–937.

[76] Flamm, L., & Mache, H. (1917). Die Verbrennung eines explosiven Gasgemisches in geschlossenem Gefäß. *Sitzungsberichte Der Kaiserlichen Academie Der Wissenschaften in Wien, Klasse IIa*, *126*, 9–44.

[77] Galmiche, B., Halter, F., & Foucher, F. (2012). Effects of high pressure, high

temperature and dilution on laminar burning velocities and Markstein lengths of iso-octane/air mixtures. *Combustion and Flame*, *159*(11), 3286–3299.

[78] Varea, E., Modica, V., Renou, B., & Boukhalfa, A. M. (2013). Pressure effects on laminar burning velocities and Markstein lengths for isooctane–ethanol–air mixtures. *Proceedings of the Combustion Institute*, *34*(1), 735–744

[79] Wu, F., & Law, C. K. (2013). An experimental and mechanistic study on the laminar flame speed, Markstein length and flame chemistry of the butanol isomers. *Combustion and Flame*, *160*(12), 2744–2756.

[80] Bunjong, D., Pussadee, N., & Wattanakasiwich, P. (2018). Optimized conditions of Schlieren photography. *Journal of Physics: Conference Series*, *1144*(1), 1209

[81] Winterbone , Desmond E., Advanced Thermodynamics for Engineers, Wiley 1997.

[82] Miao, J., Leung, C. W., Huang, Z., Cheung, C. S., Yu, H., & Xie, Y. (2014). Laminar burning velocities, Markstein lengths, and flame thickness of liquefied petroleum gas with hydrogen enrichment. *International Journal of Hydrogen Energy*, *39*(24), 13020–13030.

[83] Okafor, E. C., Naito, Y., Colson, S., Ichikawa, A., Kudo, T., Hayakawa, A., & Kobayashi, H. (2018). Experimental and numerical study of the laminar burning velocity of CH4–NH3–air premixed flames. *Combustion and Flame*, *187*, 185–198.

APPENDIXES

APPENDIXES

APPENDEX (A)

Pressure Transmitter

Manufacturer / FIELD TERMINALS

Model Baoji Xing Measure and Control Instruments,

Range – 100 to 900 kPa, d = 0.1 kPa, Accuracy = 0.5 % F S

COSQC
Central Organization For Standardization and Quality Calibration
Cert. No : PRE/506
Date : 3/11/2021
Due to (if applicable) :

C.O.S.Q.C IRAQ

Accredited CABs IQAS Accreditation no. C.L 009

Calibration Certificate

FOR-TC-012

Central Organization for Standardization and Quality Control (COSQC)
Metrology Department/Mass & Pressure Section/Pressure Lab.
P.O. Box13032 Algeria street, Baghdad ,Tel:7765180 E-Mail : cosqc@cosqc.gov.iq

Certificate No: PRE/ 506 /2021
Date of issue : 4/ 11 /2021

Customer			
Name:	الطالبة رويدة كاصد عيسى		
Address:	بابل		
Item under calibration			
Description:	Pressure Transmitter		
Manufacturer:	FIELD TERMINALS		
Model:	Baoji Xing Measure and Control Instruments		
Serial number:	210924001		
Other identification:	Range = - 100 to 900 KPa	d = 0.1 KPa	Accuracy= 0.5 % of F.S
Date of reception:	31 / 10 /2021	Oredr No.=175	
Condition of reception	As found		
Standard(s) used in the calibration			
Description:	Portable Pressure Calibrator		
Manufacturer:	AMETEK		
Model:	IP1300CBXXANDG		
Serial number:	9894005		
Other identification:	Range = 2000 Kpa	d = 0.01 KPa	
Calibration information			
Date of calibration:	3 / 11 /2021		
Place of calibration:	Pressure Lab.		
Method(s) of calibration:	Calibration method are based on (PROC-TC-012)		
Calibrated quantity:	Pressure		
Results of calibration:	Attached a complete result in Annex 1 of this certificate		
Measurement uncertainty:	The reported expanded uncertainty is DKD-6-1:2014the standard Uncertainty multiplied by coverage factor k=2 to give confidence level of 95% .		
Metrological traceability:	The traceability of measurement to the SI units issued by the National Standard maintained at centeral organization for standardization and quality control through calibration certificat issued (UME) of certificate NO. = G2BA-0080		
Environmental conditions of calibration:	Temp. (23˚C)		R. H.(41%)
Observations, opinions or Recommendations:	**The results are within the tolerance according to DKD-6-1:2014**		

COSQC

Ref.:PROC-TC-012

Approved by:

Saif Ali
Head of Mass & Pressure Section

APPENDIX (A)

Ammonia Gauge Pressure

Model A Bourdon tube, other identification: Range 12 kg /cm^2 , d – 0.1 kg / cm ^{2} and Accuracy =1.7 % of F S

COSQC
Central Organization For Standardization and Quality
Calibrated
Cert. No : PRE/ 505
Date : 3/11/2021
Due to (if applicable)

Accredited CAB
IQAS
Accreditation no. CL 007

C.O.S.Q.C
IRAQ

Calibration Certificate

FOR-TC-012

Central Organization for Standardization and Quality Control (COSQC)

Metrology Department/Mass & Pressure Section/Pressure Lab.

P.O. Box13032 Algeria street, Baghdad ,Tel:7765180

E-Mail : cosqc@cosqc.gov.iq

Certificate No: PRE/ 505 /2021

Date of issue : 4/ 11 /2021

Customer			
Name:	الطالبة رويدة كاصد عيسى		
Address:	بابل		
Item under calibration			
Description:	Pressure gauge		
Manufacturer:	AMMONIA		
Model:	Bourdon Tube		
Serial number:	1-175		
Other identification:	Range = 12 kg/cm²	d = 0.1 kg/cm²	Accuracy= 1.7 % of F.S
Date of reception:	31 / 10 /2021	Oredr No.= 175	
Condition of reception:	As found		
Standard(s) used in the calibration			
Description:	Digital Pressure Gauge		
Manufacturer:	GE Druck		
Model:	DPI104		
Serial number:	5239240		
Other identification:	Range = 20 kg/cm²	d = 0.001 kg/cm²	
Calibration information			
Date of calibration:	3 / 11 /2021		
Place of calibration:	Pressure Lab		
Method(s) of calibration:	Calibration method are based on (PROC-TC-012)		
Calibrated quantity:	Pressure		
Results of calibration:	Attached a complete result in Annex 1 of this certificate		
Measurement uncertainty:	The reported expanded uncertainty is DKD-6-1:2014 and the standard Uncertainty multiplied by coverage factor k=2 to give confidence level of 95% .		
Metrological traceability:	The traceability of measurement to the SI units issued by the National Standard maintained at centeral organization for standardization and quality control through calibration certificat issued (GE Druk) of certificate NO. = 0073039		
Environmental conditions of calibration:	Temp.(23°C)		R.H(43%)
Observations, opinions or Recommendations:	**The results are within the tolerance according to DKD-R 6-1:2014**		

Ref.PROC-TC-012

Approved by:

Saif Ali

Head of Mass & Pressure Section

page 1 of 2

APPENDIX (A)

Calibration of Pressure Transmitters

Calibration Certificate

FOR-TC-012

Central Organization for Standardization and Quality Control (COSQC)
Metrology Department/Mass & Pressure Section/Pressure Lab.

P.O. Box13032 Algeria street, Baghdad ,Tel:7765180 E-Mail : cosqc@cosqc.gov.iq

Certificate No: PRE/ 506 /2021
Date of issue : 4/ 11 /2021

Annex 1/ Results

APP.Pressure	Reading		Mean Reading	Deviation (M-A)	Error
	Upward	Downward	KPa	KPa	% of F.S
KPa	KPa	KPa			
-50	-49.8	-49.6	-49.70	0.30	0.30
0	0.0	0.0	0.00	0.00	0.00
100	99.7	100.1	99.90	-0.10	0.01
200	199.8	200.1	199.95	-0.05	0.01
500	499.7	499.7	499.70	-0.30	0.03
700	699.7	699.7	699.70	-0.30	0.03

Max. Expanded Uncertainty =	± 0.27	KPa

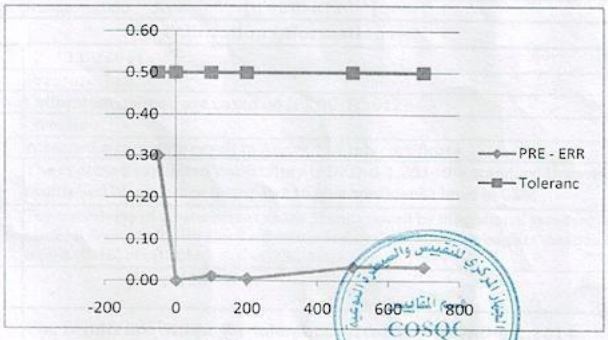

Calibrated by:
Nabeel Lateef

Revisid by :
Saif Ali

Approved by:
Saif Ali
Head of Maas & Pressure Section

APPENDEX (A)

Calibration of Pressure Gauge Ammonia

Calibration Certificate

Central Organization for Standardization and Quality Control (COSQC)
Metrology Department/Mass & Pressure Section /Pressure Lab.

P.O. Box13032 Al jadria street, Baghdad ,Tel:7765180
E-Mail : cosqc@cosqc.gov.iq

Certificate No: PRE/ 505 /2021
Date of issue : 4/ 11 /2021

Annex 1/ Results

APP.Pressure	Reading		Mean Reading	Deviation (M-A)	Error
	Upward	Downward			
kg/cm²	kg/cm²	kg/cm²	kg/cm²	kg/cm²	% of F.S
0	0.0	0.0	0.00	0.00	0.00
2	2.0	2.1	2.05	0.05	0.42
4	4.1	4.2	4.15	0.15	1.25
6	6.1	6.2	6.15	0.15	1.25
8	8.2	8.2	8.20	0.20	1.67
10	10.2	10.2	10.20	0.20	1.67

Max. Expanded Uncertainty =	± 0.13 kg/cm²

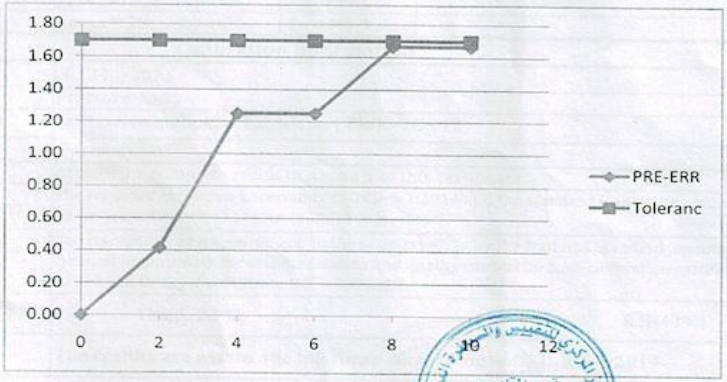

Calibrated by:
Nabeel Lateef

Revisid by :
Saif Ali

Approved by:
Saif Ali
Head of Maas & Pressure Section

APPENDEX (A)

Calibration of Camera High - Speed

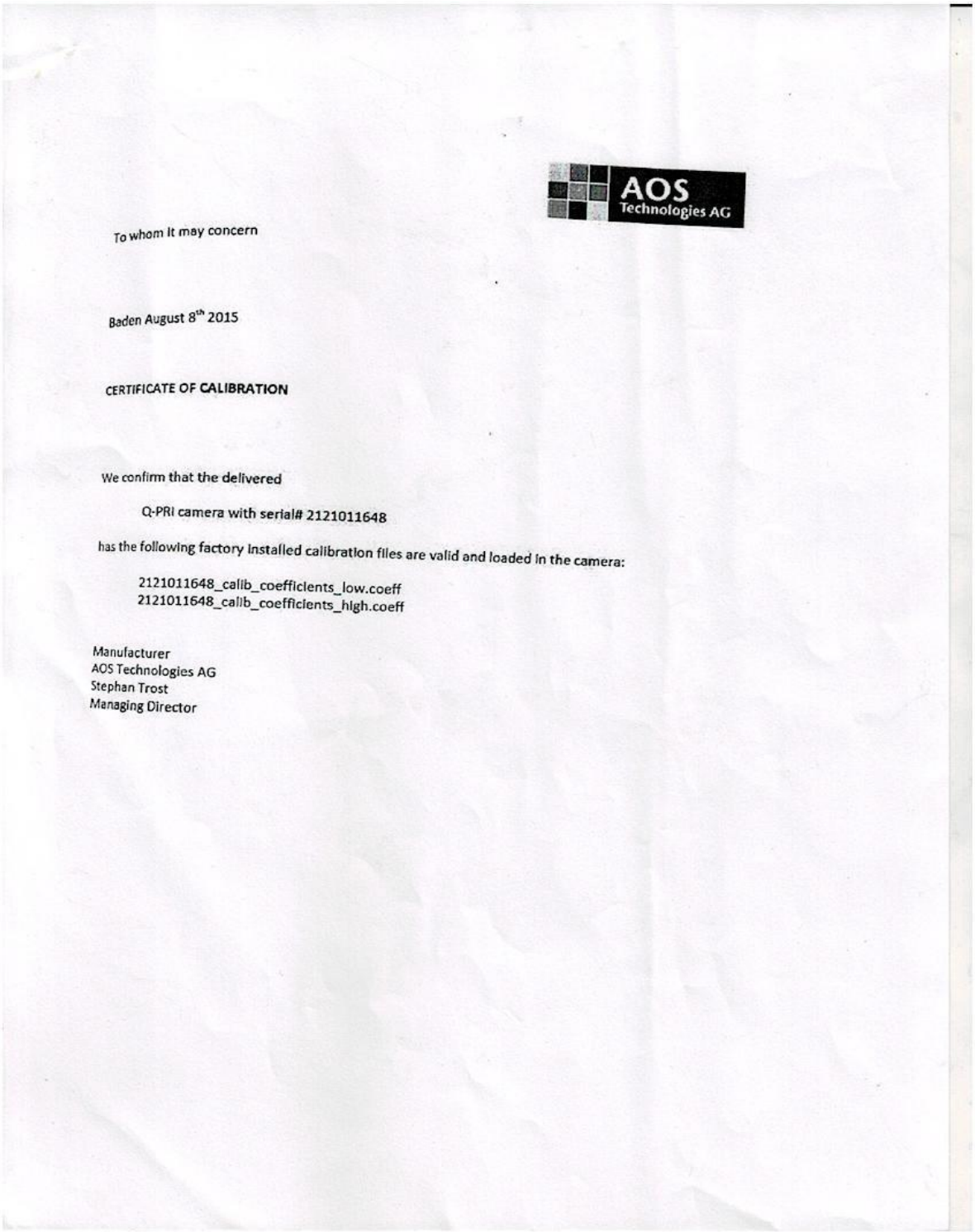

AOS Technologies AG

To whom it may concern

Baden August 8th 2015

CERTIFICATE OF CALIBRATION

We confirm that the delivered

Q-PRI camera with serial# 2121011648

has the following factory installed calibration files are valid and loaded in the camera:

2121011648_calib_coefficients_low.coeff
2121011648_calib_coefficients_high.coeff

Manufacturer
AOS Technologies AG
Stephan Trost
Managing Director

APPENDIX (A)

Camera Calibration High-Speed

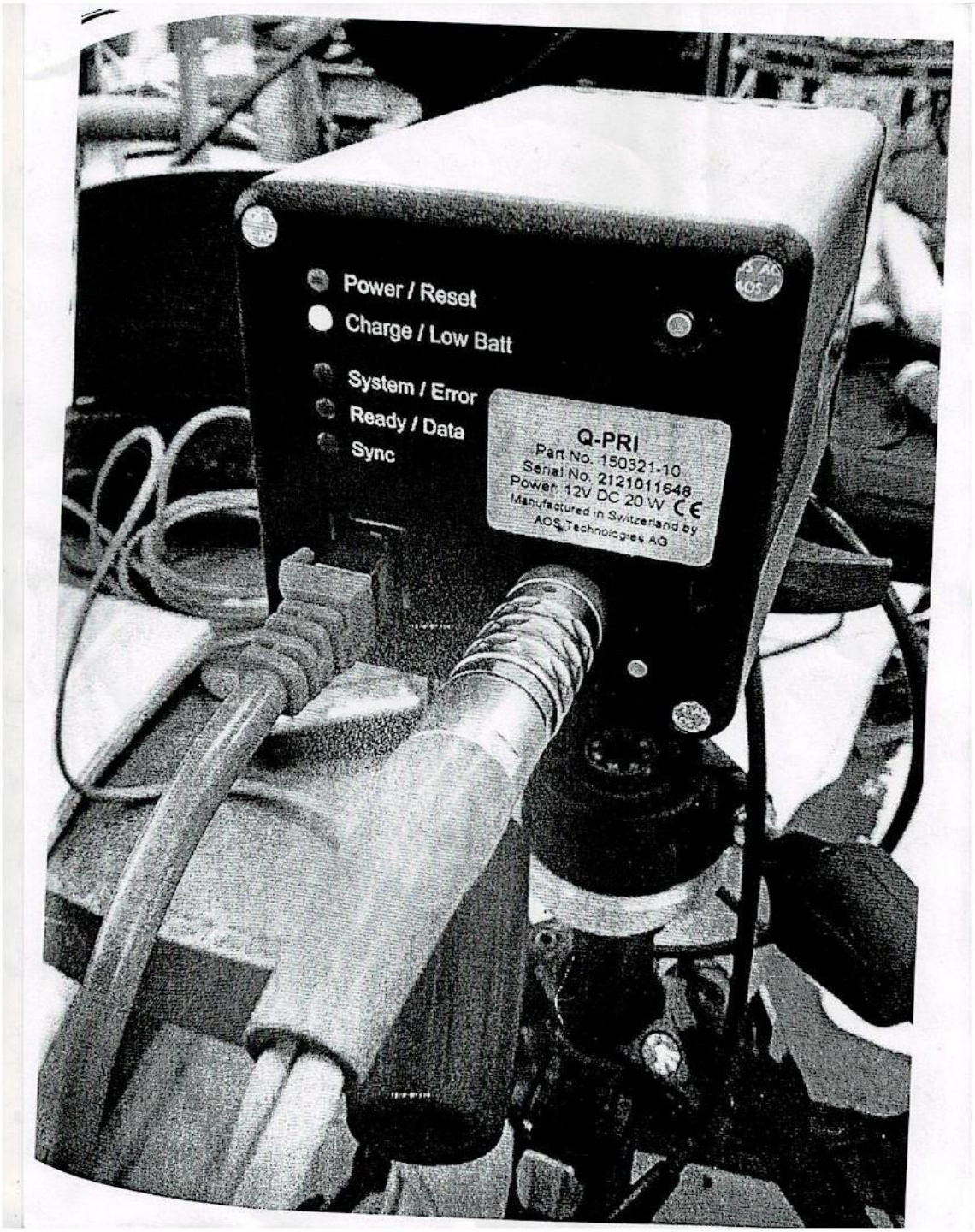

APPENDIX (B)
Analysis of LPG components provided from Hilla Plant

State Company for Gas Filling and Services
GAS Analysis Dept

الشركة العامة لتعبئة وخدمات الغاز
فرع بابل
وحدة المختبر

مواصفات الغاز السائل المستلم من شركة غاز الجنوب الى مستودع غاز الحلة للفترة من ٢٠٢١/٢/١١ الى ٢٠٢١/٢/٢٠

composition	11/2	12/2	13/2	14/2	15/2	16/2	17/2	18/2	19/2	20/2	الملاحظات
C2MOL %	0.89	0.61	0.72	0.79	0.95	0.73	0.72	0.86	0.65	0.66	
C3MOL %	64.34	58.27	60.02	60.24	66.01	56.60	59.18	59.49	57.47	58.34	
C4MOL %	32.50	39.76	37.41	37.77	32.42	42.38	39.83	39.18	40.70	39.64	
C5MOL %	2.27	1.36	1.85	1.2	0.62	0.29	0.27	0.47	1.18	1.36	
Density at 15.6C°	0.538	0.540	0.544	0.535	0.534	0.539	0.540	0.539	0.539	0.544	
Vapor Pressure(Kg\cm²)at(37.8C°)	8.5	8.7	8.5	8.4	8.6	8.5	8.1	8.3	8.1	8.4	
Corrosion copper strip	1b	1b	1b	1b	1b	1b	1b	1b	1b	1b	
Evaporated Temp at(95%)	+2	+3	+2	+3	+2	+2	+2	+2	+2	+2	

ملاحظات

- النسب القياسية لل (C_3) هي (0.6) و(C_5) (2.0).

زاهد مجيد كاظم

م. وحدة المختبر

الخلاصة

تبحث هذه الدراسة تجريبيا" في سرعة اللهب الرقائقي وسرعة الاحتراق الصفيحي المخلوط مسبقا" لانواع وقود مختلفة . تم تصميم غرفة الحجم الثابت المشتعلة مركزيا" وبناؤها للتحقيق تجريبا" في سرعة الله الممتدة وسرعة الاحتراق الصفيحي وطول ماركشتاين . يتم تسجيل عملية الاحتراق بواسطة كاميرا عالية السرعة تم خلط غازالامونيا وغاز البترول المسال في غرفة الاحتراق ذات حجم ثابت اسطوانية الشكل وحجمها (0.04899 م^3) وقطر داخلي 395 ملم وطول 400 ملم تحتوي غرفة الاحتراق على اطواق مثقبة بسمك 12 ملم تربط مع بليت بشكل دائري قطره 407 ملم و570 ملم على التوالي ولكلا الجانبين وكل الحديد المستخدم هو الفولاذ المقاوم للصدا لمقاومة الظروف الخارجية اي داخل غرفة الاحتراق حيث صممت هذه غرفة الاحتراق لغرض اجراء التجربة تمت الدراسة بخلط الغازات (غاز الامونيا –غاز البترول المسال – الهواء) وبنسب محددة (10 % –20 % –30 %) وباستخدام منظم اشتعال مركزي ,ونظام تصوير باستخدام كاميرا عالية السرعة وضغوط اولية (100 – 200 – 300) كيلو باسكال ونسب تكافؤ (0.8 – 1 – 1.3) ودرجة حرارة 298 كلفن اظهرت الدراسة التجريبة باستخدام غرفة الاحتراق ثابتة الحجم والاشتعال المركزي انه كلما زاد الضغط الاولي انخفضت سرعة اللهب وطول ماركشتاين وسرعة الاحتراق وكلما زاد تركيز غاز الامونيا في الخليط زادت سرعة الهب و انخفض طول ماركشتاين وسرعة الاحتراق . اظهرت الدراسة التجريبة عند نسبة تكافؤ 0.8 وضغط اولي 100 كيلو باسكال وتركيز الامونيا 10% ونصف قطر اللهب 20ملم اذا بلغت سرعة اللهب 1.3 م \ ثا وعند نفس الضغط الاولي 100 كيلو باسكال وتركيز الامونيا 30% بلغت سرعة اللهب 1.52288 م \ ثا تبين النتائج الزيادة التدريجة لغاز الامونيا للخليط عند نسبة تكافؤ 0.8 تزيد من سرعة اللهب وحصلنا من النتائج العملية على قيم سرعة اللهب عند نسبة تكافؤ 0.8 وضغط اولي مقداره 100 كيلو باسكال وتركيز غاز الامونيا 30% وقطر لهب 25 ملم فان قيمة سرعة اللهب 1.19712 م \ ثا وعند نفس الظروف وتركيز 30% وضغط اولي 200 كيلو باسكال كانت سرعة اللهب 1.104653 م \ ثا اظهرت النتائج ان زيادة الضغط الاولي يقلل من قيمة سرعة اللهب وان تاثير الزيادة التدريجية لغاز الامونيا على قيم طول ماركشتاين عند قيم ضغط اولي 100 كيلو باسكال ونسبة تكافؤ 0.8 وتركيز غاز الامونيا 10% وصلت قيمة طول ماركشتاين 6.3 وعند نفس الظروف وضغط اولي 100 كيلو باسكال وتركيز الامونيا 30% وصلت قيمته 5.67 اظهرت النتائج زيادة الضغط الاولي يقلل من قيمة طول ماركشتاين عند ضغط اولي 100 كيلو باسكال ونسبة تكافؤ 0.8 وتركيز الامونيا 30% وصلت قيمته 5.67 وعند نفس الظروف وضغط اولي 200 كيلو باسكال وصلت قيمته 4.68 كما اظهرت النتائج تاثير الضغط الاولي على سرعة الاحتراق حيث تقل سرعة الاحتراق مع زيادة الضغط

الاولي فعند ضغط 100 كيلو باسكال ونسبة تكافؤ 0.8 وتركيز الامونيا 30% اصبحت قيمة 24.56 سم \ ثا وعند نفس الظروف وضغط ابتدائي 200 كيلو باسكال وصلت قيمة سرعة الاحتراق 19.64 سم \ ثا واظهرت النتائج ان الزيادة التدريجية لغاز الامونيا تخفض سرعة الاحتراق فعند ضغط اولي 100كيلو باسكال ونسبة تكافؤ 1 وتركيز غاز الامونيا 10% اصبحت سرعة الاحتراق 39.32 سم \ ثا وعند نفس الظروف وضغط اولي 100 كيلو باسكال وتركيز الامونيا 30% وصلت سرعة الاحتراق 34.945 سم \ ثا

.

جمهورية العراق
وزارة التعليم العالي والبحث العلمي
جامعة بابل /كلية الهندسة
قسم الهندسة الميكانيكية

دراسة عملية لخواص اللهب لخلائط مختلفة من الغاز البترولي المسال والأمونيا

رسالة

مقدمة الى جامعة بابل /كلية الهندسة وهي جزء من متطلبات نيل شهادة الماجستير في الهندسة /قسم الهندسة الميكانيكية / قدرة

اعدت من قبل

رويدة كاصد عيسى دفار

بأشراف

أ . د سامر محمد عبد الحليم

1443 هـ

2022 م